THE NORWEGIAN UNIVERSITY OF SCIENCE AND TECHNOLOGY
DEPARTMENT OF ENERGY AND PROCESS ENGINEERING

COMBUSTION MODELING IN TURBULENT BOUNDARY-LAYER FLOWS

BY
TORE MYHRVOLD

THESIS FOR THE DR. ING. DEGREE
APRIL 2003

URN:NBN:no-7265

URN:NBN:no-7265

Abstract

This thesis presents an investigation of turbulence modeling and chemical-kinetics effects, including local extinction, for turbulent reacting boundary-layer flows by using Favre-averaged Navier-Stokes equations.

Local extinction effects with detailed chemistry calculations were investigated using the Eddy Dissipation Concept (EDC) by Magnussen for turbulent combustion. In this case, turbulent jet flames were used for validation, since it appears that there is no data for the detailed chemistry of turbulent reacting boundary-layer flows near walls. The predictions of a lifted jet flame by EDC were in reasonable accordance with measured data. Both k-ε- and Reynolds-stress-equation (RSE) turbulence models that were developed for constant and variable density were employed. These turbulence models predicted different residence times in the EDC reactor model, and therefore, local extinction was predicted differently.

Turbulence modeling was investigated by employing a full low-Reynolds-number RSE model, which was validated against DNS data for turbulent boundary-layer flow. The model was in reasonable agreement with the data, but more work is needed on certain parts of it, since better agreement for some of the terms was expected.

The behavior of EDC close to walls was discussed and a low-Reynolds-number version of EDC was proposed. When employing the proposed modification of EDC, and using a single-step (laminar) expression for the reactor reaction rate, it was shown that the mean chemical reaction term approaches the laminar expression at the wall.

The modeling of chemical reactions for a low-Reynolds-number turbulent premixed flame in a Couette flow (including a wall flame) with EDC was presented and the results were compared to DNS data. Finite-rate chemistry was used with a single-step mechanism. Both the standard version, and the proposed modification of EDC were tested and discussed. The predictions show that by introducing limits to the EDC mass fraction variable of fine-structures regions, or by using the proposed low-Reynolds-number version, EDC predicted a reasonable flame picture compared to the DNS flame. These predictions indicate that the proposed low-Reynolds-number version of EDC could be a useful way to extend the model to turbulent reacting flows near walls.

URN:NBN:no-7265

Preface

The Research Council of Norway financially supported this work for three years, including an eight-month stay at University of California at Berkeley (USA). I am very grateful for their support.

During my work, Professor Ivar Ertesvåg has guided me and been my best source of knowledge. He deserves my greatest thanks. I will also thank Professor Inge Gran and Professor Bjørn F. Magnussen for encouraging discussions throughout my study. I also appreciated the support from Ole Martin Hansen and Robert Olsen.

Finally, I would like to thank Department of Mechanical Engineering and Professor J.-Y. Chen at UC Berkeley for letting me participate in the work at their combustion group, and Ricardo Cabra for the very interesting collaborative work.

This thesis will be submitted for the degree:

Doktor Ingeniør (Dr. ing.)
Doctor of Engineering

at the Norwegian University of Science and Technology (NTNU).

Trondheim, April 2003

Tore Myhrvold

URN:NBN:no-7265

Contents

URN:NBN:no-7265

URN:NBN:no-7265

Nomenclature

Latin letters

A	Lumley's "stress flatness" invariant
A_2, A_3	second and third invariants of stress anisotropy
A_i	chemical symbol of species i
A_l	pre-exponential factor in Arrhenius expression
a_0, a_1, a_2	coefficients in series expanisions of velocity fluctuations
a_f	coefficient in the discretized equation
a_{ij}	dimensionless stress anisotropy, $\overline{u_i' u_j'}/k - 2\delta_{ij}/3$
a_nb, a_P	coefficients in the discretized equation
b	source term in the discretized equation
b_0, b_1, b_2	coefficients in series expansions of velocity fluctuations
b_i	body forces in x_i direction
C_1',C_2'	constants in RSE model
$C_i, i = 1, \ldots, 8$	constants in RSE models
C_{ij}	transient and convective terms in RSE models
C_k	transient and convective terms in the exact k equation
C_l, C_s	constants in RSE model
$C_{p\mathrm{d}1}$, $C_{p\mathrm{d}2}$	constants in RSE model
$C_{\varepsilon 1}$, $C_{\varepsilon 2}$	constants in the k-ε model
C_μ, C_μ'	constants in turbulence models
c_0, c_1, c_2	coefficients in series expanisions of velocity fluctuations
c_i	concentration of species i in the mixture
c_p	constant pressure specific heat capacity
$c_{p,i}$	constant pressure specific heat capacity for species i
D, d	diameter
D	diffusion coefficient
Da	Damköhler number
D_{ij}, D_k, D_ε	diffusion terms in turbulence equations
d_i, d_i^A	indicators of length-scale gradient direction

URN:NBN:no-7265

d_i^P	pressure diffusion of k in RSE model
E_{al}	activation energy in Arrhenius expression
e	specific internal energy
e_t	total specific internal energy
f	mixture fraction
f_1, f_2, f_i, f_{ii}	Reynolds-number functions in modified EDC variable
f_A, f'_A	functions of flatness parameter and turbulence Reynolds number
f_n	wall-damping function in RSE model
$f_{R_T}, f'_{R_T}, f''_{R_T}$	Reynolds-number functions
f_{w1}, f_{w2}, f_{w3}	Reynolds-number functions in "wall-damping" terms
f_ε	near-wall function in ε equation
f_μ	Reynolds-number function
f'_μ	Reynolds-number function in modified EDC variable
H	lift-off height, half channel width (m)
h	specific enthalpy
h_i°	specific enthalpy of formation of species i
h_t	total specific enthalpy
$\boldsymbol{J}$	convective and diffusive flux vector
k	turbulence kinetic energy (or turbulence energy)
Le	$= Sc/Pr$; Lewis number
l, l_0, l_t	turbulence length scale
M	molecular weight of mixture
M_i	molecular weight of species i
Ma	Mach number
m	mass
m_i	mass of species i
N_i, N_i^A	length-scale gradient vectors
N_R	number of chemical reactions
N_S	number of species
n	total number of moles of mixture
n	number of scalars in general transport equation
n_i	number of moles of species i
n_k	directional cosines
P_{ij}, P_k, P_ε	production rate of $\overline{u'_i u'_j}$, k, and ε, respectively
Pr	$= \nu/\alpha$; Prandtl number
p	static pressure: $\overline{p}$ is the mean, p' is the fluctuation
p'	pressure correction
Q, q	heat flux
Q	volumetric flow rate

Re	Reynolds number
R_k	reaction rate of species k
R_T	$= k^2/\nu\varepsilon$; turbulence Reynolds number
R_u	$= 8.314\,\mathrm{kJ/kmolK}$; universal gas constant
R_λ	$= u'\lambda/\nu$; turbulence Reynolds number
r	radius
r_F	air-to-fuel ratio on mass basis
S	source term
$\left(\overline{S}_1\right)_P$	constant part of source term in point P
$\left(\overline{S}_2\right)_P$	coefficient in variable part of source term in point P
S_h	source term in enthalpy equation
S_T	turbulence flame speed
S_φ	source term in general scalar transport equation
Sc	$= \nu/D$; Schmidt number
s_{ij}	deformation tensor
T	temperature
T^1	reference temperature
T^*	reactor temperature in EDC combustion model
$\widehat{T}$	reduced temperature
T_ε	transport term in ε equation
t	time
$\boldsymbol{U}$	velocity vector
u	Cartesian velocity component in the x direction
u_1	Cartesian velocity component in the x_1 direction
u_1^+	dimensionless mean velocity in the x_1 direction
$u_1'^+, u_2'^+, u_3'^+$	$= \sqrt{\overline{u_1'u_1'}}, \sqrt{\overline{u_2'u_2'}}, \sqrt{\overline{u_3'u_3'}}$, respectively; RMS of normal stresses
u_i	Cartesian velocity component: $\overline{u}_i$ is the Reynolds-averaged mean, u_i' is its fluctuation. $\widetilde{u}_i$ is the Favre-averaged mean, u_i'' is its fluctuation
V	volume
v	Cartesian velocity component in the y direction
X	mole fraction
X_i	mole fraction of species i
x	x_1
x_2^+	dimensionless wall distance
x_i	Cartesian coordinates, $i = 1, 2, 3$
Y	mass fraction
Y_i	mass fraction of species i
Y_F, Y_O, Y_P	mass fractions of fuel, oxidizer and product, respectively

y	x_2

Greek letters

α	heat-release factor in Arrhenius expression
α	$= \lambda/(c_p\rho)$; thermal diffusivity
β, β_l	temperature exponent (Zel'dovich number)
Γ_i	general diffusion coefficient
γ	dimensionless pre-exponential factor in Arrhenius expression
γ	fraction of the fluid occupied by turbulence fine structures
Δ	interval
δ_{ik}	Kronecker delta
δ_{l0}	unstrained laminar flame thickness
ε	dissipation rate of k
ε_{ij}	dissipation rate of $\overline{u_i' u_j'}$
η	Kolmogorov length scale
θ	turbulence time scale
κ	von Karmans constant
λ	thermal conductivity
λ	Taylor length scale
μ	dynamic viscosity
μ_i	dynamic viscosity of species i
μ_t	dynamic turbulence viscosity
ν	$= \mu/\rho$; kinematic molecular viscosity
ν_{il}', ν_{il}''	stoichiometric coefficients of species i in reaction l
ν_r	homogeneous reactor mixing rate
ν_t	kinematic turbulence viscosity
Π_{ij}	pressure-correlation term in RSE model
ρ	density
σ	Prandtl number or Schmidt number (Prandtl-Schmidt number)
σ_k, σ_ε	turbulence Prandtl-Schmidt number in k and ε equation
σ_t	turbulence Prandtl-Schmidt number
τ	Kolmogorov time scale
τ^*	turbulence fine-structure time scale
τ_c	chemical time scale
τ_{ik}	viscous stress tensor
τ_t	turbulence time scale
τ_w	wall shear stress
Φ	equivalence ratio

Φ_{ij}	redistribution term in RSE models
φ_i	general scalar variable
χ	fraction of reacting turbulence fine structures
ω_i	chemical production rate of species i on mass basis
ω_{ij}	rotation tensor

Subscripts

a	adiabatic
b	bottom cell face
e	east cell face
F	fuel
L	laminar
max	maximum value
min	minimum value
NO	non-orthogonal
n	north cell face
nb	neighboring grid point
nn	general indicator for the cell face subscript
O	oxidizer
P	product
P	main node point
s	south cell face
t	top cell face
w	west cell face
t, T	turbulence (or turbulent)
u	universal
v	viscous
w	wall

Superscripts

$'$	fluctuating value, Reynolds averaging
$''$	fluctuating value, Favre averaging
$-$	mean
$\sim$	mass-weighted mean
$+$	dimensionless variable
$*$	fine structure state in EDC
$\circ$	surrounding fluid state

$\circ$	last time step

Abbreviations

2D, 3D	two dimensional, three dimensional
CFD	computational fluid dynamics
DNS	direct numerical simulation
EDC	Eddy Dissipation Concept
inh	inhomogeneous
PDE	partial differential equation
PDF	probability density function
POW	power-law scheme
ppm	parts per million
PSR	perfectly stirred reactor
RMS	root-mean square
RSE	Reynolds-stress-equation
RSM	Reynolds-stress-equation model
slm	standard liter per minute
SOU	second-order upwind scheme
STD	standard
TDMA	tri-diagonal matrix algorithm

Chapter 1

Introduction

1.1 Motivation for the thesis

Turbulent combustion plays an important role in the increasing amount of energy consumption all over the world. Most energy consumption involves combustion, and nearly all flames are turbulent. Since energy resources are limited, efficient use of these resources will be more and more important in the future. Improved knowledge about turbulent combustion will allow better control of combustion processes and be a guide to more efficient use of energy. Combustion normally takes place in a vessel where chemical reactions occur in the vicinity of, and in interactions with, the surrounding walls. This flame-wall interaction is of great importance in turbulent combustion. Several effects that are relevant to combustion are introduced by the presence of a wall. For example, a wall may quench the flame, which may lead to undesired effects such as unburned hydrocarbons.

There are numerous practical applications where more knowledge about turbulent combustion near walls is important. These include internal combustion engines, gas turbines, furnaces, reactors, and rocket motors. More specific practical situations can be the undesired ignition of a combustible mixture by a hot surface, pre-ignition of a fuel-air mixture by hot spots in an engine, and catalytic combustion over a hot surface. Despite the practical relevance of flame-wall interactions, little is known about turbulent combustion near walls. Experimental work is difficult to do and expensive, and numerical modeling is hampered by the lack of results from experimental work or the development of computer resources. For this reason, combustion models are seldom developed to account for near-wall phenomena in turbulent reacting flows. More knowledge on boundary-layer and near-wall phenomena in turbulent combusting flows is needed to develop such models.

1.2 Turbulent combustion modeling near walls

Turbulent reacting flows can be modeled in several ways. One approach is probability-density-function (PDF) methods. In this approach a single modeled equation for the joint PDF of velocity, dissipation, and composition provides a closure for turbulent combustion [117]. In the present work, turbulent combustion was studied by using mass-weighted (Favre averaged) conservation equations.

The description of turbulence and combustion near walls is essential for a correct calculation in all engineering computer codes. Combustion is strongly influenced by the presence of walls, which, as mentioned, may cause flame quenching. On the other hand, turbulence is affected by combustion. For example, combustion can change the turbulence length scale. The interaction between the wall and a turbulent flame front was characterized by Poinsot [115] as three effects: "A local thermal effect, by which heat losses to the wall affect the flame structure and results in local quenching, a geometrical effect which limits the spatial extent of the flame-brush and reduces the flame-brush size in the vicinity of the wall, and a laminarization effect, which is a result of the wall affecting the structure of the turbulence." Obviously, turbulence is an important part in the two last effects.

Close to a wall, the turbulent boundary layer needs to be resolved with much higher resolution than for turbulent flow far away from walls. This is due to the steep gradients in mean values that occur in the boundary layer close to the wall surface. In addition, one of the most challenging effects in turbulence modeling for non-reacting flows is the modeling of pressure-velocity fluctuations. These fluctuations result from pressure waves influenced by the presence of walls. The effects from these fluctuations are believed to be just as crucial for combusting flows. In addition, variable-density and buoyancy effects have become important. The need for the best possible turbulence model is obvious. A lot is already known about low-Reynolds-number turbulence models for non-reacting flows. This is not the case for reacting flows, however. Turbulence models for combusting flows are less developed. The practice that is usually adopted is to extend the models developed for constant-density flows to variable-density flows by introducing mass weighting of the turbulence equations.

Modeling the combustion processes will include the calculation of chemical reactions including local extinction. Heat transfer through the wall, change of turbulence scales, and the intermittent nature of turbulent flow may affect the time scale for the chemical reactions in several ways. There may be slow as well as fast reactions. The laminarization and low-Reynolds-number effects mentioned above will also be important in a combustion model.

In summary, some of the features a turbulent combustion model should be able to account for when predicting turbulent reacting near-wall flow are: high and low Reynolds numbers

and the transition between them, variable-density effects, pressure-velocity correlations, local extinction at the flame front, slow and fast chemical reactions, and the "laminarization" effect very close to the wall. The interaction between turbulence and combustion is obviously an important issue regarding turbulent reacting near-wall flows. Other important effects, such as for example catalytic combustion, may also be included in a model for turbulent combustion near walls.

1.3 Previous work

Investigating the interaction between flames and walls by using experimental methods is extremely difficult as most of the interesting phenomena occur in a very thin layer near the wall. For this reason, there are few experimental results [18, 95, 116]. Most of the experimental work has been concerned with measureing heat fluxes through the wall. The impinging jet flame on a flat plate is an example of a configuration that is commonly used to measure heat fluxes through walls. However, engine tests have indicated that flame stretch, local quenching of the flame front, and low-Reynolds-number effects due to the change of turbulent scales when approaching a wall, are important issues in flame-wall interaction [95].

In recent years, Direct Numerical Simulations (DNS) have provided increasingly more information about wall quenching, turbulence structures, and combustion-turbulence interaction towards a wall. DNS are reported for both two- and three-dimensional cases, but only for simple chemistry, and only for low-Reynolds-number flows. These cases have so far provided important data for model validation, but even more detailed information is required. For example, the importance of detailed chemistry versus simple chemistry has only been reported for laminar flames [119]. This observation is likely to be important also for turbulent flames. Some work has been done on designing models for near-wall turbulent reacting flows [18, 76, 77, 115, 131], and some of them take into account several of the aspects discussed in the previous section. However, the validation of most models suffers from the lack of detailed experimental and DNS data, or they are designed for special cases. A more detailed review of the subject will be given in Chapter 4. A discussion of turbulence models for high and low Reynolds numbers and models for constant-density flows versus models developed for variable-density flows will be given in Chapter 3 and 7.

1.4 Present contribution

The present work has concentrated on some of the issues just described. It has been focused on studying turbulence and chemical reactions including local extinction effects. The objective has been to investigate these phenomena by using low-Reynolds-number turbulence models, and by using a combustion model employing finite-rate chemistry including detailed chemical mechanisms. Progress was made on all three subjects, which will create a basis for future work. However, finite-rate chemistry calculations using detailed mechanisms were not performed due to the lack of detailed chemistry data for turbulent reacting near-wall flow. For this reason, only single-step mechanisms were employed for investigating chemical reactions in near-wall flow. Certain phenomenon, that may occur at a wall in a turbulent reacting flow, such as catalytic combustion, was not considered in the present work.

The main contributions of this thesis are:

- The behavior of EDC, in conjunction with a detailed chemical mechanism for a lifted hydrogen flame in a coflow of hot gases, was shown and compared to experimental work and PDF-transport modeling results. The predictions with EDC gave a reasonable flame picture, and show that EDC with detailed chemistry can predict local extinction effects.

- The effects of employing different turbulence models were studied in relation to local extinction effects when using EDC in conjunction with a detailed chemical mechanism for a lifted hydrogen flame in a coflow of hot gases.

- A low-Reynolds-number second-moment closure was implemented into the CFD code SPIDER and validated towards DNS data for turbulent boundary-layer flow.

- The behavior of EDC close to a wall was discussed, and a modification of EDC for low Reynolds numbers was proposed.

- A single-step chemical mechanism for finite-rate chemistry calculations with EDC was implemented in SPIDER and validated against DNS results for a premixed flame

- It was shown that EDC with finite-rate chemistry, using a single-step mechanism, predicted premixed flames for low Reynolds numbers well.

- The proposed low-Reynolds-number version of EDC was tested on a premixed wall flame. These predictions show that the proposal could be a useful way to construct a new model for turbulent reacting near-wall flow.

- Investigation of the proposed low-Reynolds-number version of EDC revealed that the mean chemical reaction rate approaches the reactor reaction rate at the wall. When employing a single-step (laminar) chemical mechanism in conjunction with finite-rate chemistry in EDC, the mean chemical reaction term approaches the laminar expression at the wall.

1.5 Survey of the thesis

Chapter 2 presents the governing equations for reacting fluid flow in Cartesian tensor notation. The nature of turbulent flow is discussed and mass-weighted turbulence equations are presented.

Chapter 3 deals with modeling of turbulent combustion. Both turbulence models developed for constant and variable density as well as Magnussen's Eddy Dissipation Concept (EDC) for turbulent combustion are presented.

Chapter 4 reviews turbulent reacting near-wall flow. Different approaches, such as experimental work, direct numerical simulations, and modeling are discussed.

Chapter 5 gives a brief introduction of the general-purpose CFD code SPIDER used for all calculations in the present work.

Chapter 6 reports on a numerical investigation of a lifted H_2/N_2 turbulent jet flame in a vitiated coflow by using the EDC. Emphasis was placed on how well EDC, in conjunction with a detailed chemical mechanism, can predict local extinction. The effects of employing different turbulence models were investigated. This work has been prepared for submission to Combustion Science and Technology, 2003.

Chapter 7 shows the numerical implementation and test of a low-Reynolds-number second-moment closure in comparison to DNS data for turbulent boundary-layer flow.

Chapter 8 discusses the behavior of EDC close to walls. A proposed low-Reynolds-number version of EDC for turbulent reacting near-wall flows is presented.

Chapter 9 investigates a turbulent premixed reacting Couette flow, which includes a near-wall flame. Both the standard version, and the proposed modification of EDC are used to predict the flow. The behavior of EDC and differences between the models are shown and discussed. The results are compared to a DNS predicted flame.

Concluding remarks are given in Chapter 10.

Numerical modeling results together with experimental work are reported in the paper in

Appendix A. It was presented at the 29th International Symposium on Combustion in Sapporo, Japan 2002.

Appendix B shows the work of predicting an attached jet flame by using EDC with different turbulence models. Local extinction effects in EDC were discussed. This work was presented at the Scandinavian-Nordic Section of the Combustion Institute meeting in Gothenburg, Sweden, 2001.

URN:NBN:no-7265

Chapter 2

Mathematical description of turbulent reacting flows

Turbulent combustion involves chemical reactions of gaseous turbulent fluid flow including heat release and radiation. Therefore, theoretical analysis of turbulent combustion requires understanding of the conservation equations of fluid dynamics including its thermodynamic properties, transport properties, and chemical kinetics. The reacting gaseous mixtures concerned in the present work were assumed to follow the *continuum hypothesis* which defines continuous flow for the multicomponent continuum [60, 141]. The equations in the present context are expressed in Cartesian tensor notation with Einstein's summation convention.

2.1 The conservation equations

2.1.1 Overall mass conservation

Mass can neither be formed nor destroyed in chemical reactive flows. The equation for overall conservation of mass (the continuity equation) can be written [42, 141]

$$\frac{\partial \rho}{\partial t} + \frac{\partial}{\partial x_k}(\rho u_k) = 0. \tag{2.1}$$

The equation expresses how the total mass in a small fluid element changes in time; the total amount of mass stored in a fluid element per time unit equals the mass sum flowing in and out of the element.

2.1.2 Species mass conservation

In chemical reactive flows, species are consumed and formed. For a mixture of N_S species, the conservation equations for the mass fraction of species i can be written [42, 141]

$$\frac{\partial}{\partial t}(\rho Y_i) + \frac{\partial}{\partial x_k}(\rho Y_i u_k) = \frac{\partial}{\partial x_k}\left(\frac{\mu}{\sigma}\frac{\partial Y_i}{\partial x_k}\right) + \rho\omega_i, \qquad i = 1, \ldots, N_S, \tag{2.2}$$

where μ/σ represents mass diffusivity, and σ is the Schmidt number. From left to right, these terms represent local rate of change, convection, diffusion, and production of species i due to chemical reactions. The last term is often called the chemical source term or the chemical production term. The diffusive flux was expressed in a very simplified version. Fick's law of mass diffusion [9, 59] has been applied, whereas effects from pressure diffusion and thermal diffusion (Soret effect) have been neglected. In addition, a single diffusion coefficient, $D = \mu/(\rho\sigma)$, was employed for all species. Hence, differential diffusion effects were neglected.

2.1.3 Momentum conservation

An equation for conservation of momentum follows from *Euler's Law of Motion* for a continuum, which is analogous to Newton's second law and the momentum law for a particle system [42, 60, 140, 141]

$$\frac{\partial}{\partial t}(\rho u_i) + \frac{\partial}{\partial x_k}(\rho u_i u_k) = -\frac{\partial p}{\partial x_i} + \frac{\partial \tau_{ik}}{\partial x_k} + \rho b_i, \qquad i = 1, 2, 3. \tag{2.3}$$

τ_{ik} is the newtonian stress tensor which can be written

$$\tau_{ik} = \mu\left(\frac{\partial u_i}{\partial x_k} + \frac{\partial u_k}{\partial x_i} - \frac{2}{3}\frac{\partial u_l}{\partial x_l}\,\delta_{ik}\right). \tag{2.4}$$

In the expression for τ_{ik}, the coefficient of bulk viscosity has been set to zero (which means applying Stoke's Hypothesis [124]). Equation 2.3 is also called the Navier-Stokes equations [140].

2.1.4 Energy conservation

The energy conservation equation can be derived from the 1st law of thermodynamics in several ways [42, 77, 103, 141]. Total energy in a system is the sum of kinetic, gravitational, and internal energy. Total enthalpy is defined as $\rho h_t = \rho e_t + p$, where $e_t = e + \frac{1}{2}u_i u_i$ is the

sum of specific internal energy and kinetic energy. Static enthalpy is $h = h_t - \frac{1}{2}u_i u_i$. In terms of static enthalpy, the energy conservation equation can be written as [42, 77, 141]

$$\frac{\partial}{\partial t}(\rho h) + \frac{\partial}{\partial x_k}(\rho h u_k) = \frac{\partial}{\partial x_k}\left(\frac{\mu}{\sigma}\frac{\partial h}{\partial x_k}\right) + S_h, \tag{2.5}$$

where μ/σ represents thermal diffusivity and σ is the Prandtl number. Ideal gas behavior was assumed, and hence enthalpy was calculated as $h = h(T)$ [42]. The complexity of the source term, S_h, depends on the assumptions (simplifications), which may vary from case to case, such as e.g. neglecting radiation. In the present work, equality between the Schmidt number ($\sigma = Sc$ in Eq. 2.2) and the Prandtl number ($\sigma = Pr$ in Eq. 2.5), was assumed. This implies unity Lewis number (Le), since $Le = Sc/Pr$. Also, the Dufour effect was neglected. These effects are described in detail elsewhere [9, 42, 77, 141].

2.1.5 General transport equation

The conservation equations, as they appear in Eqs. 2.2–2.5, can all be written on the same general form as

$$\frac{\partial}{\partial t}(\rho\varphi_i) + \frac{\partial}{\partial x_k}(\rho\varphi_i u_k) = \frac{\partial}{\partial x_k}\left(\Gamma_i \frac{\partial \varphi_i}{\partial x_k}\right) + S_i \qquad i = 1, \ldots, n. \tag{2.6}$$

where φ_i represents a scalar variable such as for example Y_i, a Cartesian velocity component u_i, or h.

2.2 The chemical production term

The chemical production term ω_i in Eq. 2.2 may include expressions for the consumption or formation of chemical species. In a reacting gaseous mixture, a system of chemical reactions occurs. For a system of N_R chemical reactions of N_S species, an arbitrary chemical reaction may be written in the form [42, 77, 139, 141]

$$\sum_{i=1}^{N_S} \nu'_{il} A_i \longrightarrow \sum_{i=1}^{N_S} \nu''_{il} A_i \qquad l = 1, \ldots, N_R \tag{2.7}$$

where ν'_{il} and ν''_{il} are the stoichiometric coefficients of species i appearing as a reactant and as a product, respectively, in reaction l. The reaction rate for species i for such a system is [42, 139]

$$\omega_i = \frac{M_i}{\rho} \sum_{l=1}^{N_R} \left(\nu''_{il} - \nu'_{il}\right) k_l \prod_{m=1}^{N_S} c_m^{\nu'_{ml}}, \tag{2.8}$$

where M_i is the molar mass of species i and c_m is the concentration of species m. The rate coefficient k_l for reaction l depends strongly and in a nonlinear way on the temperature and can be described by an Arrhenius expression as [42, 139]

$$k_l = k_l(T) = A_l T^{\beta_l} \exp\left(-\frac{E_{\mathrm{a}l}}{R_{\mathrm{u}} T}\right), \tag{2.9}$$

where A_l is the pre-exponential factor, β_l is the temperature exponent, $E_{\mathrm{a}l}$ is the activation energy, and R_{u} is the universal gas constant.

2.3 Describing mixture composition

The composition of an ideal gas mixture can be described by giving the mass or the number of moles of each component present. The mass fraction of component i is defined as [103]

$$Y_i = \frac{m_i}{m}, \tag{2.10}$$

where m_i is the mass of species i and m is the total mass of the mixture, whereas the mole fraction of component i is defined as [103]

$$X_i = \frac{n_i}{n}, \tag{2.11}$$

where n_i is the number of moles of species i and n is the total number of moles of the mixture. The apparent molecular weight of a mixture, M, is defined as the ratio of the total mass of the mixture, m to the total number of moles of the mixture, n. M can be calculated as a mole-fraction average of the component molecular weights as [103]

$$M = \sum_{k=1}^{N_{\mathrm{s}}} X_k M_k. \tag{2.12}$$

In the present work, the coefficient of viscosity of the mixture was found from the expression [110]

$$\mu = \frac{\sum_{k=1}^{N_{\mathrm{s}}} Y_k \mu_k (M_k)^{1/2}}{\sum_{k=1}^{N_{\mathrm{s}}} Y_k (M_k)^{1/2}}, \tag{2.13}$$

where $\mu_k = \mu_k(T)$ was found from the CHEMKIN II database [71].

The specific enthalpy for an ideal mixture is given as [103]

$$h = \sum_{k=1}^{N_{\mathrm{s}}} h_k Y_k. \tag{2.14}$$

The specification of the state of a mixture requires the composition and the values of two independent intensive properties such as temperature and pressure [103]. This implies that, in that case, determining the change in enthalpy requires temperature and pressure. However, if each species i is assumed to behave as an ideal gas, the specific enthalpy of species i is independent of pressure. Specific enthalpy can then be calculated from temperature-dependent functions only as [42, 103]

$$h_i(T) - h_i^\circ = \int_{T^\circ}^{T} c_{p,i}(T) dT, \tag{2.15}$$

where h_i° is the specific enthalpy at some reference temperature T° and $c_{p,i}$ is the specific heat capacity at constant pressure for species i,

$$c_{p,i} = \left(\frac{\partial h_i}{\partial T} \right)_p. \tag{2.16}$$

In the present work, h_i and $c_{p,i}$ were taken from the CHEMKIN II database [71]. If the expression in Eq. 2.14 is put into the expression for $c_{p,i}$, this leads to [42]

$$c_p = \sum_{k=1}^{N_\mathrm{s}} Y_k c_{p,k} + \left(\sum h_k \frac{\partial Y_k}{\partial T} \right). \tag{2.17}$$

The last term in Eq. 2.17 was neglected in the present work, and hence the approximation

$$c_p = \sum_{k=1}^{N_\mathrm{s}} Y_k c_{p,k}, \tag{2.18}$$

was used for the mixture composition. The last term in Eq. 2.17 is negligible in flows where chemical reactions are assumed to take place infinitely fast, but may be important when reactions are slow [42]. For a mixture of ideal gases, pressure, density, and temperature can be coupled through the equation of state, as [77, 141]

$$p = \rho R_\mathrm{u} T \sum_{k=1}^{N_\mathrm{s}} (Y_k / M_k). \tag{2.19}$$

2.4 The nature of turbulent flow

A flow can be laminar or turbulent or in the transition between them. Laminar flow is characterized by regular, smooth movements. Turbulent flow is characterized by three-dimensional, irregular, fluctuating movement in both time and space [13, 58, 133]. Hinze [58]

defined turbulent fluid motion as "an irregular condition of flow in which the various quantities show a random variation with time and space coordinates, so that statistically distinct average values can be discerned". Launder [79] explained that turbulent in turbulent flow means that the flow velocity at a point is constantly changing in a non-repeating irregular, chaotic way. Velocity fluctuations arise in all directions. When heat transfer takes place across a shear flow in turbulent motion, continual variation in temperature also arise at any point in the flow, and in most cases, the temperature fluctuations exhibit a character similar to that of the turbulent velocity field. One very distinct difference between laminar and turbulent flow, which is extremely important in combusting flow, is the difference in transport mechanisms. Turbulent flow generally mixes fluid at a considerably higher rate than laminar flow, since most of turbulent mixing is determined from the convective transport in the turbulent eddies. Another aspect, important to distinguish in turbulent boundary-layer flows is isotropic and anisotropic turbulence as explained by Hinze [58]. In isotropic turbulence, the turbulence statistical quantities are equal in all directions. Turbulence is called anisotropic when the direction of the statistical quantities matter, like in a wall boundary layer where steep mean velocity gradients, associated with the wall shear stress, arise.

2.5 Favre-averaged conservation equations

Turbulent flow can be described by the same conservation equations as for laminar flow (Eqs. 2.1–2.5). However, computational resources are, today, capable of solving these equations by direct numerical simulation (DNS) only for low or moderate Reynolds numbers. One method, which is less computer expensive, and which can, in principle, be solved for all ranges of Reynolds numbers, is to describe the random nature of turbulent flow through statistical methods. Mathematically, this means to describe turbulence through averaged conservation equations. Averaging means to decompose an instantaneous variable into a mean and a fluctuation. Following Reynolds [121], an instantaneous variable can be written as

$$\varphi = \overline{\varphi} + \varphi', \tag{2.20}$$

where $\overline{\varphi}$ is the mean and φ' its fluctuation. Favre introduced density in the mean values and decomposed an instantaneous variable as [77]

$$\varphi = \widetilde{\varphi} + \varphi'', \tag{2.21}$$

where

$$\widetilde{\varphi} = \frac{\overline{\rho\varphi}}{\overline{\rho}}. \tag{2.22}$$

The present work employed Favre averaging when combusting flows where calculated. This is favorable in computations of variable-density flows such as turbulent combustion [42, 77].

Differences between Reynolds averaging and Favre averaging are described in more detail elsewhere [42, 77].

By introducing Eq. 2.21 into the conservation equations (2.1)–(2.5) and Eq. 2.6, and perform averaging, Favre-averaged conservation equations, (mass-weighted conservation equations or, *turbulence equations*) appear:

Overall mass conservation

$$\frac{\partial \overline{\rho}}{\partial t} + \frac{\partial}{\partial x_k}(\overline{\rho}\widetilde{u}_k) = 0. \tag{2.23}$$

Species mass conservation

$$\frac{\partial}{\partial t}(\overline{\rho}\widetilde{Y}_i) + \frac{\partial}{\partial x_k}(\overline{\rho}\widetilde{Y}_i\widetilde{u}_k) = \frac{\partial}{\partial x_k}\left(\frac{\mu}{\sigma}\frac{\partial \widetilde{Y}_i}{\partial x_k} - \overline{\rho}\widetilde{Y_i''u_k''}\right) + \overline{\rho}\widetilde{\omega}_i. \tag{2.24}$$

Momentum conservation

$$\frac{\partial}{\partial t}(\overline{\rho}\widetilde{u}_i) + \frac{\partial}{\partial x_k}(\overline{\rho}\widetilde{u}_i\widetilde{u}_k) = -\frac{\partial \overline{p}}{\partial x_i} + \frac{\partial}{\partial x_k}\left(\overline{\tau}_{ik} - \overline{\rho}\widetilde{u_i''u_k''}\right) + \overline{\rho}\widetilde{b}_i. \tag{2.25}$$

Energy conservation

$$\frac{\partial}{\partial t}(\overline{\rho}\widetilde{h}) + \frac{\partial}{\partial x_k}(\overline{\rho}\widetilde{h}\widetilde{u}_k) = \frac{\partial}{\partial x_k}\left(\frac{\mu}{\sigma}\frac{\partial \widetilde{h}}{\partial x_k} - \overline{\rho}\widetilde{h''u_k''}\right) + \overline{S}_h. \tag{2.26}$$

General scalar transport equation

$$\frac{\partial}{\partial t}(\overline{\rho}\widetilde{\varphi}_i) + \frac{\partial}{\partial x_k}(\overline{\rho}\widetilde{\varphi}_i\widetilde{u}_k) = \frac{\partial}{\partial x_k}\left(\Gamma_i\frac{\partial \widetilde{\varphi}_i}{\partial x_k} - \overline{\rho}\widetilde{\varphi_i''u_k''}\right) + \overline{S}_i, \qquad i = 1, \ldots, n. \tag{2.27}$$

The terms $-\overline{\rho}\widetilde{u_i''u_k''}$ are called turbulence stresses (or Reynolds stresses), whereas the terms $-\overline{\rho}\widetilde{Y_i''u_k''}$ and $-\overline{\rho}\widetilde{h''u_k''}$ are commonly called turbulence fluxes. The turbulence stresses and fluxes are unknown quantities, and finding their magnitude requires approximation. Describing these unknown quantities in terms of known is called turbulence modeling (see Chapter 3).

2.6 The Reynolds-stress equations

Exact equations for the Reynolds stresses was developed by Chou [27, 28]. For constant-density flows they can, by using Reynolds averaging, be written [42]

$$\underbrace{\frac{\partial}{\partial t}(\overline{\rho}\overline{u_i'u_j'}) + \frac{\partial}{\partial x_k}(\overline{\rho}\overline{u_i'u_j'}\overline{u}_k)}_{\overline{\rho}C_{ij}} = \underbrace{-\overline{\rho}\left(\overline{u_i'u_k'}\frac{\partial \overline{u}_j}{\partial x_k} + \overline{u_j'u_k'}\frac{\partial \overline{u}_i}{\partial x_k}\right)}_{\overline{\rho}P_{ij}} + \underbrace{\frac{\partial}{\partial x_k}\left(\mu\frac{\partial \overline{u_i'u_j'}}{\partial x_k}\right)}_{\overline{\rho}D_{ij,\mathrm{v}}}$$

$$+ \underbrace{\frac{\partial}{\partial x_k}\left(-\overline{\rho}\overline{u_i'u_j'u_k'} - \left(\overline{p'u_i'}\delta_{jk} + \overline{p'u_j'}\delta_{ik}\right)\right)}_{\overline{\rho}D_{ij,\mathrm{t}}}$$

$$+ \underbrace{\overline{p'\left(\frac{\partial u_i'}{\partial x_j} + \frac{\partial u_j'}{\partial x_i}\right)}}_{\overline{\rho}\Phi_{ij}} - \underbrace{2\mu\overline{\frac{\partial u_i'}{\partial x_k}\frac{\partial u_j'}{\partial x_k}}}_{\overline{\rho}\varepsilon_{ij}}. \qquad (2.28)$$

The left side of the equation expresses the total rate of increase of the Reynolds stresses for a small identified packet of fluid, which rate of change arises from an imbalance of the terms on the right-hand side [79]. P_{ij} represents the rate of production. $D_{ij,\mathrm{v}}$ and $D_{ij,\mathrm{t}}$ represents viscous diffusion and turbulence diffusion respectively. The redistribution term Φ_{ij} serves to redistribute energy among the normal stresses. For constant-density flows, this term makes no contribution to the overall level of turbulence energy since, by continuity (see Eq. 2.1), its trace is zero. ε_{ij} represents the destruction rate of $\overline{u_i'u_j'}$ by viscous action. C_{ij}, P_{ij} and $D_{ij,\mathrm{v}}$ are expressed in terms of known quantities, whereas $D_{ij,\mathrm{t}}$, Φ_{ij}, and ε_{ij} are unknown and require modeling (treated in Chapter 3).

The Reynolds-stress equations defines a basis or, the "state of the art", in turbulence modeling, since the modeled versions of these equations are able to describe the anisotropic behavior of turbulence motion, which is difficult with simpler models. Describing the anisotropic behavior of the turbulence stresses is essential in describing turbulent flows close to a solid surface.

This equation (Eq. 2.28) can also be written in terms by introducing Favre averaging [42, 77] for the equations to be used in variable-density flows. Jones [64] wrote the equation for

variable-density flows as

$$\underbrace{\frac{\partial}{\partial t}\left(\overline{\rho}\widetilde{u_i''u_j''}\right)+\frac{\partial}{\partial x_k}\left(\overline{\rho}\widetilde{u_i''u_j''}\widetilde{u}_k\right)}_{C_{ij}}=\underbrace{-\overline{\rho}\left(\widetilde{u_i''u_k''}\frac{\partial\widetilde{u}_j}{\partial x_k}+\widetilde{u_j''u_k''}\frac{\partial\widetilde{u}_i}{\partial x_k}\right)}_{\overline{\rho}P_{ij}}$$

$$+\underbrace{\frac{\partial}{\partial x_k}\left(-\overline{\rho u_i''u_j''u_k''}-\frac{2}{3}\delta_{ij}\overline{u_k''p'}\right)}_{\overline{\rho}D_{ij,\mathrm{t}}}$$

$$\underbrace{-\left(\overline{u_i''\frac{\partial p'}{\partial x_j}}+\overline{u_j''\frac{\partial p'}{\partial x_i}}-\frac{2}{3}\delta_{ij}\overline{u_k''\frac{\partial p'}{\partial x_k}}\right)}_{\overline{\rho}\Phi_{ij}}$$

$$\underbrace{-\left(\overline{u_i''}\frac{\partial\overline{p}}{\partial x_j}+\overline{u_j''}\frac{\partial\overline{p}}{\partial x_i}\right)}_{\overline{\rho}\Phi^1_{ij}}+\underbrace{\frac{2}{3}\delta_{ij}\overline{p'\frac{\partial u_k''}{\partial x_k}}}_{\overline{\rho}\Phi^2_{ij}}$$

$$-\overline{\rho}\varepsilon_{ij}, \tag{2.29}$$

where the viscous terms ($D_{ij,\mathrm{v}}$ in Eq. 2.28) were omitted, since the equation was derived for high-Reynolds-number flows. Jones decomposed the pressure-fluctuating part differently than the conventional way (used in Eq. 2.28) since there are no unique way of decomposing the fluctuating pressure terms as suggested by Lumley [88]. Additional terms (Φ^1_{ij} and Φ^2_{ij}), which can not be neglected when assuming variable density, now appear in the equation. Unfortunately, these terms are difficult to model due to the lack of experimental data for validation (see Sec. 3.3). The terms containing mean values for pressure can be associated with buoyancy effects, whereas all three terms can be related to the Reynolds stresses and scalar fluxes in the case of variable-density mixing of inert gaseous fluids, at least in the situation where the density difference arises from either temperature differences or because the fluid have different molar masses [64].

2.7 Turbulence kinetic energy

The mean turbulent kinetic energy, or turbulence kinetic energy, for a turbulent flow is defined as half the trace of the Reynolds-stress tensor as [5, 42, 118]

$$k = \frac{1}{2}\widetilde{u_k'' u_k''}. \tag{2.30}$$

Turbulence kinetic energy (or just turbulence energy) is the mean kinetic energy of the turbulent fluctuations [13, 133]. The expression in Eq. 2.30 can be obtained when the mean is withdrawn from the kinetic energy per mass unit ($\frac{1}{2}u_k u_k$) for a fluid in motion. A transport equation for k can be written [42]

$$\underbrace{\frac{\partial}{\partial t}(\overline{\rho}k) + \frac{\partial}{\partial x_k}(\overline{\rho}k\widetilde{u}_k)}_{\overline{\rho}C_k} = \underbrace{-\overline{\rho}\overline{u_i'' u_j''}\frac{\partial \widetilde{u}_i}{\partial x_j}}_{\overline{\rho}P_k} + \underbrace{\frac{\partial}{\partial x_j}\left(\overline{\tau_{ij}u_i''} - \frac{1}{2}\overline{\rho u_i'' u_i'' u_j''} - \overline{p'u_j''}\right)}_{\overline{\rho}D_{k,\mathrm{t}}}$$

$$- \overline{u_i''}\frac{\partial \overline{p}}{\partial x_i} + \overline{p'\frac{\partial u_i''}{\partial x_i}} - \underbrace{\overline{\tau_{ij}\frac{\partial u_i''}{\partial x_j}}}_{\overline{\rho}\varepsilon}. \tag{2.31}$$

Here, C_k is transient term and convection of k with the mean flow, P_k is production of k, and $D_{k,\mathrm{t}}$ is turbulence diffusion. ε is dissipation of turbulence kinetic energy. The terms $D_{k,\mathrm{t}}$ and ε are unknown and require modeling. The two additional terms, which are zero for constant density, also need modeling, but are often neglected [42]. This was also done in the present work.

2.8 Dissipation of turbulence kinetic energy

Dissipation of turbulence kinetic energy represents dissipation of mechanical energy into heat due to viscous forces and is defined, by using Reynolds averaging, as [5, 42]

$$\varepsilon = \nu\overline{\frac{\partial u_i'}{\partial x_k}\frac{\partial u_i'}{\partial x_k}}. \tag{2.32}$$

A transport equation for ε can be deduced from the conservation equations [42]. Chou [28] presented an equation for a variable proportional to ε, but current concepts in modeling ε, spring from the work of Davydov [36, 79]. An exact transport equation of ε may be derived from the Navier-Stokes equations [79]. However, this exact equation is seldom

used since most terms consist of small-scale correlations describing the detailed mechanics in the dissipation process [79]. In turbulence modeling, developers are in search for a model connecting the dissipation rate variable to large-scale variables (see Chapter 3).

2.9 Turbulent boundary-layer flow

Boundary-layer flows are flows where viscous forces from a wall nearby are important. Schlichting [124] described the boundary layer as the thin layer the velocity of the fluid increases from zero at the wall (no slip) to its full value which corresponds to external frictionless flow. The boundary-layer concept is due to Prandtl [42, 124].

Boundary-layer flows can be (or must be) described differently than frictionless flows not affected by walls. Often in terms of simplified equations, but in many cases difficulties due to for example wall heat- and mass transfer arise. The turbulent boundary layer itself can be described in terms of an inner and an outer area. For high-Reynolds-number flow, viscous shear stresses dominate in the inner region, whereas turbulence stresses dominate in the outer region. The transition region between them (where both viscous and turbulence stresses have to be considered) is often called the "buffer" region. The region from the wall to the point where viscous forces become negligible in a turbulent near-wall flow can be classified in different ways (see e.g. Pope [118]).

2.9.1 Some basic concepts

In a turbulent boundary-layer, the mean turbulence field can simply be described as functions of a normalized wall shear velocity and a normalized wall distance as [42]

$$u_1^+ = \frac{\overline{u}_1}{u_\tau}, \qquad x_2^+ = \frac{x_2 u_\tau}{\nu}, \tag{2.33}$$

where $u_\tau = (\tau_w/\rho)^{1/2}$ is the wall shear velocity. These functions are commonly used when describing boundary-layer flows. In a turbulent boundary layer, the velocity distribution can be approximately described in terms of these functions as [42]

$$u_1^+ = x_2^+, \tag{2.34}$$

for the viscous sub-layer, and

$$u_1^+ \approx \frac{1}{\kappa} \ln(E x_2^+), \tag{2.35}$$

for the area outside the "buffer" region, where $E = 9$ and $\kappa \approx 0.4$, called von Kármán's universal constant [42, 58], are commonly used values. A dimensionless temperature distribution, similar to the one for the velocity, can be deduced based on using the wall heat flux, the wall shear velocity and wall temperature [42, 70].

2.9.2 Turbulence correlations in the viscous sub-layer

One way to try to explain the phenomena very close to a wall is to develop series expansions of the velocity fluctuations as [57, 79]

$$\begin{aligned} u_1' &= a_0 + a_1 x_2 + a_2 x_2^2 + \cdots \\ u_2' &= b_0 + b_1 x_2 + b_2 x_2^2 + \cdots \\ u_3' &= c_0 + c_1 x_2 + c_2 x_2^2 + \cdots , \end{aligned} \tag{2.36}$$

where a_i, b_i, and c_i are functions in time with their mean equal to zero, since $\overline{u_i'} = 0$. When the gradient in x_1- and x_3 direction is equal to zero, the velocity fluctuations are only dependent of x_2, that is $u_i' = u_i'(x_2)$. For $x_2 = 0$, $u_1' = u_2' = u_3' = 0$, which give $a_0 = b_0 = c_0 = 0$. From continuity, with $u_i = u_i(x_2)$, one obtains $\partial u_2'/\partial x_2 = du_2'/dx_2 = 0$, which gives $b_1 = 0$. Equation (2.36) is then written

$$\begin{aligned} u_1' &= a_1 x_2 + a_2 x_2^2 + \cdots \\ u_2' &= \qquad b_2 x_2^2 + \cdots \\ u_3' &= c_1 x_2 + c_2 x_2^2 + \cdots \end{aligned} \tag{2.37}$$

From (2.37), it follows that

$$\overline{u_1' u_2'} = \overline{a_1 b_2} x_2^3 + \cdots \tag{2.38}$$

From this expression, it can easily be seen that the turbulence shear stresses are small when x_2 approaches zero. In a similar manner, the variation of turbulence energy and the turbulence energy dissipation rate can be expressed as [57]

$$k = \frac{1}{2}\left(\overline{a_1^2} + \overline{c_1^2}\right) x_2^2 + \left(\overline{a_1 a_2} + \overline{c_1 c_2}\right) x_2^3 + \cdots \tag{2.39}$$

$$\varepsilon = \nu\left(\overline{a_1^2} + \overline{c_1^2}\right) + 4\nu\left(\overline{a_1 a_2} + \overline{c_1 c_2}\right) x_2 + \cdots \tag{2.40}$$

From Eqs. (2.39)–(2.40) it can be seen that $k \to 0$ when $x_2 \to 0$, whereas ε is finite at the wall. From Eqs. (2.39)–(2.40), the approximation

$$\varepsilon \approx 2\nu \left(\frac{\partial \sqrt{k}}{\partial x_2}\right)^2 \tag{2.41}$$

can also be deduced [57], which is correct up to terms linear in x_2 [79]. This expression has been used in different ways in modeling the limiting behavior of ε at the wall. According to Ertesvåg [41], the dissipation rate can reach its maximum very close to the wall, whereas k have its maximum value at $x_2^+ \approx 10$.

2.10 Summary

In the present chapter, the governing equations for turbulent combusting flows have been presented. The following simplifications were made:

- Differential diffusion was neglected.
- Pressure diffusion effects, the Dufour-effect, and the Soret-effect were neglected.
- Stoke's hypothesis was used.
- Ideal gas behavior was assumed.
- Equality of Schmidt and Prandtl numbers ($Le = 1$).
- Radiative heat transfer was neglected.
- Low Mach number ($Ma^2 \ll 1$) assumption.
- Gravity effects were neglected.

It is important to keep in mind that several of these effect, such as differential diffusion, pressure diffusion, the Dufour-effect, and the Soret-effect may be of greater importance in boundary-layer flows than in shear-free flows.

URN:NBN:no-7265

Chapter 3

Modeling turbulent reacting flows

Finding approximate solutions to the unknown turbulence stresses, fluxes, and the mean chemical source term, identified in the Favre-averaged Navier-Stokes equations presented in the previous chapter, is commonly called turbulent combustion modeling. Finding the turbulence stresses or fluxes is regarded as turbulence modeling, whereas finding the mean chemical source term is normally regarded as turbulent combustion modeling (or just combustion modeling). In both turbulence and combustion modeling, there are numerous models developed, and finding the optimal one can often be a challenge. In this sense, experience in using a certain model may be more important than using the most complex one. The present work employed two well-known approaches; the k-ε turbulence model and the Reynolds-stress-equation turbulence model (often referred to as second-moment closures). For the chemical source term, Magnussen's Eddy Dissipation Concept (EDC) was employed. These approaches are further described below.

3.1 The k-ε turbulence model

The k-ε model was introduced by Jones and Launder in 1972 [65], whereas Launder and Spalding's version from 1974 [83] has later been known as the "standard" k-ε model. The model was developed for constant density and simple thin shear layer flow, whereas models for variable-density flow have been developed later (see Sec. 3.3). The k-ε model is based on assuming that the turbulent mixing process can be described by introducing an apparent viscosity, an *eddy viscosity*. Boussinesq introduced as early as in 1877 an additional viscosity in turbulent flow [5, 42]. From an analogy with the expression for viscous stresses (see

Eq. 2.4), the turbulence stresses can be modeled by employing Favre averaging, as [42]

$$-\overline{\rho}\widetilde{u_i''u_j''} = \mu_t\left(\frac{\partial\widetilde{u}_i}{\partial x_j} + \frac{\partial\widetilde{u}_j}{\partial x_i}\right) - \frac{2}{3}\left(\overline{\rho}\widetilde{k} + \mu_t\frac{\partial\widetilde{u}_l}{\partial x_l}\right)\delta_{ij}, \tag{3.1}$$

where μ_t is the eddy viscosity and k is the turbulence kinetic energy. For constant density, the last term in this expression gives no contribution since, from continuity, it will be zero. The turbulence kinetic energy must be included for the expression to hold for $i = j$ [5]. The turbulence fluxes can be modeled in analogy with the turbulence stresses as [42]

$$-\overline{\rho}\widetilde{\varphi''u_j''} = \frac{\mu_t}{\sigma_t}\frac{\partial\widetilde{\varphi}}{\partial x_j}, \tag{3.2}$$

where σ_t is the turbulence Prandtl-Schmidt number. An approximate value for σ_t is usually found by assuming that $\sigma_t \approx \sigma$. The exact equations for k and ε were described in Sec. 2.7 and Sec. 2.8. The k-ε model involves modeled transport equations for k and ε and employs a model for the eddy viscosity based on these variables. The exact equation for turbulence kinetic energy k (Eq. 2.31) creates the basis for the modeled k equation, but the exact equation for ε is not used (see Sec. 2.8). The modeled equations for ε essentially results from dimensional analysis and intuition [79]. According to Launder [79], all proposals can be written on the form

$$T_\varepsilon = C_{\varepsilon 1}\frac{P_k\varepsilon}{k} - C_{\varepsilon 2}\frac{\varepsilon^2}{k} + \text{EST}. \tag{3.3}$$

The terms represent, from left to right, net transport of ε, production and destruction of ε, and "Extra Strain Terms". The two first terms on the right-hand side are taken proportional to the production and destruction terms in the k equation and then multiplied by the time scale ε/k. One underlying thought of this procedure may be that it is the same turbulent movements that are responsible for transporting both k and ε [42].

A high-Reynolds-number version

The high-Reynolds-number version of the model employed in the present work was

$$\frac{\partial}{\partial t}(\overline{\rho}\widetilde{k}) + \frac{\partial}{\partial x_j}(\overline{\rho}\widetilde{k}\widetilde{u}_j) = \frac{\partial}{\partial x_j}\left[\left(\mu + \frac{\mu_t}{\sigma_k}\right)\frac{\partial\widetilde{k}}{\partial x_j}\right] + \overline{\rho}P_k - \overline{\rho}\widetilde{\varepsilon}, \tag{3.4}$$

$$\frac{\partial}{\partial t}(\overline{\rho}\widetilde{\varepsilon}) + \frac{\partial}{\partial x_j}(\overline{\rho}\widetilde{\varepsilon}\widetilde{u}_j) = \frac{\partial}{\partial x_j}\left[\left(\mu + \frac{\mu_t}{\sigma_\varepsilon}\right)\frac{\partial\widetilde{\varepsilon}}{\partial x_j}\right] + C_{\varepsilon 1}\frac{\widetilde{\varepsilon}}{\widetilde{k}}\overline{\rho}P_k - C_{\varepsilon 2}\frac{\widetilde{\varepsilon}}{\widetilde{k}}\overline{\rho}\widetilde{\varepsilon}, \tag{3.5}$$

where

$$\overline{\rho}P_k = \mu_t\left(\frac{\partial\widetilde{u}_i}{\partial x_j} + \frac{\partial\widetilde{u}_j}{\partial x_i}\right)\frac{\partial\widetilde{u}_i}{\partial x_j} - \frac{2}{3}\left(\overline{\rho}\widetilde{k} + \mu_t\frac{\partial\widetilde{u}_l}{\partial x_l}\right)\frac{\partial\widetilde{u}_i}{\partial x_i}, \tag{3.6}$$

Table 3.1: Constants in the k-ε model [83].

σ_k	σ_ε	$C_{\varepsilon 1}$	$C_{\varepsilon 2}$	C_μ
1.0	1.3	1.44	1.92	0.09

$$\mu_t = \overline{\rho}\nu_t = C_\mu \overline{\rho}\frac{\widetilde{k}^2}{\widetilde{\varepsilon}}. \tag{3.7}$$

The different terms in Eqs. 3.4 and 3.5 are, from left to right, transient term, convective transport, diffusive transport, production, and destruction of k and ε, respectively. For constant-density flow, the two last terms in P_k (Eq. 3.6) will be zero (from continuity). For high Reynolds numbers, the effects from the molecular viscosity in these equations are negligible. The model constants are shown in Table 3.1, where σ_k and σ_ε are turbulence Prandtl-Schmidt numbers. The solution from solving these equations (Eq. 3.4 and 3.5) are subsequently input to the model expression for the eddy viscosity (Eq. 3.7), and hence, the turbulence stresses in Eq. 3.1 can be found.

The k-ε model is by far the most widely used advanced turbulence model worldwide since it is easy to implement, it is relatively practical in use, and it is more numerically stable compared to for example Reynolds-stress-equation models. The k-ε model have several known shortcomings important in combusting flows. For example, it is incapable of reproducing the stabilizing/destabilizing influences of swirling motions and buoyancy forces, the effects of strong streamline curvature, and variable density-mean pressure gradient influences [64]. Also, the commonly used gradient model for the turbulence stresses (Eq. 3.2) may have some shortcomings. It can not predict counter-gradient diffusion, which is known to take place in some turbulent flames [21, 64]. When counter-gradient diffusion takes place, the turbulence flux and the velocity gradient have the same sign and cannot be described by Eq. 3.2 [21].

A low-Reynolds-number version

There are early examples of turbulence models for low Reynolds numbers. van Driest [135] developed a near-wall turbulence model based on the mixing-length hypothesis. He simply introduced a damping of the mixing length towards the wall. Jones and Launder [65] introduced both a high-Reynolds-number- and a low-Reynolds version of the k-ε model. They extended the high-Reynolds-number k-ε model to low-Reynolds-number flows by introducing viscous diffusion terms, applied Reynolds-number functions into the model constants, and added terms to account for that the dissipation processes are not isotropic in

near-wall flow. Several similar models have been developed since then [25, 109]. The k-ε low-Reynolds-number model employed in the present work was the model by Launder and Sharma [82].

3.2 Closure of the Reynolds-stress equations

Most of the models for the Reynolds-stress equations (Eq. 2.28) have been developed for constant-density flows. Therefore, this modeling practice, by using Reynolds averaging, is discussed here. There are a lot of additional uncertainties regarding second-moment closures developed for variable density. Thus, investigating models developed for constant density first, seems to be a wise choice. The models discussed here, can be cast into Favre-averaged quantities, and then be applied as models for the Favre-averaged Reynolds-stress equations (see Eq. 2.29 in Sec. 2.6). This process is discussed in Sec. 3.3.

The Reynolds-stress equations (Eq. 2.28) may be written in symbolic form as

$$C_{ij} = P_{ij} + D_{ij,\mathrm{v}} + D_{ij,\mathrm{t}} + \Phi_{ij} - \varepsilon_{ij}, \tag{3.8}$$

where the terms C_{ij}, P_{ij} and, $D_{ij,\mathrm{v}}$ consist of known quantities, whereas the terms $D_{ij,\mathrm{t}}$, Φ_{ij}, and ε_{ij} are unknown and require modeling to close the equations.

3.2.1 Turbulence diffusion, $D_{ij,\mathrm{t}}$

The turbulence diffusion term consists of a velocity part and a pressure part. Pressure diffusion is difficult to measure [42]. For this reason, most diffusion models for this term have only been developed for the triple correlation. This does not mean that the pressure diffusion part is negligible. Craft and Launder [34] reported the importance of modeling the pressure diffusion term when treating near-wall flows, whereas the term is negligible for shear-free flows (see Chapter 7). Numerous approaches have been reported for the triple correlation. Daly and Harlow [35] employed a gradient model as

$$-\overline{u_i' u_j' u_k'} = C_s \frac{k}{\varepsilon} \overline{u_k' u_l'} \frac{\partial \overline{u_i' u_j'}}{\partial x_l}, \tag{3.9}$$

where C_s is a model constant. Shir [126] introduced the simpler model

$$-\overline{u_i' u_j' u_k'} = C_s \frac{k}{\varepsilon} k \frac{\partial \overline{u_i' u_j'}}{\partial x_k}. \tag{3.10}$$

According to Younis et al. [142], this model does not exhibit correct symmetry. However, it is simple and practical in use. Hanjalić and Launder (HL) [56] presented an invariant form where

$$-\overline{u_i' u_j' u_k'} = C_s \frac{k}{\varepsilon}\left[\overline{u_i' u_l'}\frac{\overline{u_j' u_k'}}{\partial x_l} + \overline{u_j' u_l'}\frac{\overline{u_k' u_i'}}{\partial x_l} + \overline{u_k' u_l'}\frac{\overline{u_i' u_j'}}{\partial x_l}\right]. \tag{3.11}$$

Cormack et al. [29] investigated four different models for the diffusion term and compared them to solving balance equations for the triple moments. Three of these models were the models in Eqs. 3.9–3.11. They found that solving the balance equations was superior to the four "one-parameter" models. Among the four, they found the HL model to approximate experimental data better than the others and recommended it for computational use. However, the HL may be less numerically stable than the simpler models [40, 41]. In many cases, the differences between these models are believed to be of minor importance [128].

3.2.2 Redistribution, Φ_{ij}

By taking the divergence of the Navier-Stokes equations, and subtracting its mean part, a Poisson equation can be produced with the fluctuating pressure as its subject [79]. Chou [28] showed that, by using this Poisson equation, the correlation between fluctuating velocities and fluctuating pressure gradients can be expressed as volume integrals of correlations between velocity fluctuations from two different points in the flow. In this Poisson equation, processes involving nonlinear interactions between fluctuating velocities, mean velocity gradients, and one arising from fluctuating body forces can be identified. Therefore, a successful model for Φ_{ij} is expected to contain terms corresponding to these three processes [79]. The two first terms are often called the "rapid" and the "slow" term, since the first contains quantities representing rapid movements (turbulent fluctuations), whereas the second contains slow (mean velocity gradients). The most widely used model for the first part, also called the turbulence-turbulence part, is Rotta's model from 1951 [123],

$$\Phi_{ij,1} = -C_1 \frac{\varepsilon}{k}\left(\overline{u_i' u_j'} - \frac{1}{3}\delta_{ij}\overline{u_k' u_k'}\right). \tag{3.12}$$

The most frequently adopted model for the second part is the isotropization of production (IP) model by Naot et al. [106],

$$\Phi_{ij,2} = -C_2\left(P_{ij} - \frac{1}{3}\delta_{ij}P_{kk}\right), \tag{3.13}$$

A general shortcoming of these models is that they are not able to mimic the pressure fluctuations arising in wall flows and free-surface flows. Pressure fluctuations normal to a solid

surface serves to damp the velocity fluctuations normal to the wall, and there is a need for a term who can mimic these processes. A so-called wall-damping term has to be included. Gibson and Launder [46] developed wall-damping terms based on a proposal by Shir [126] to account for pressure fluctuations normal to a solid surface. These terms included wall-normal distances and were expressed as

$$\Phi_{ij,\mathrm{w}} = \Phi_{ij,\mathrm{w1}} + \Phi_{ij,\mathrm{w2}}, \tag{3.14}$$

where

$$\Phi_{ij,\mathrm{w1}} = C_1' \frac{\varepsilon}{k} \left(\overline{u_k' u_m'} n_k n_m \delta_{ij} - \frac{3}{2} \overline{u_k' u_i'} n_k n_j - \frac{3}{2} \overline{u_k' u_j'} n_k n_i \right) f_n, \tag{3.15}$$

$$\Phi_{ij,\mathrm{w2}} = C_2' \left(\Phi_{km,2} n_k n_m \delta_{ij} - \frac{3}{2} \Phi_{ik,2} n_k n_j - \frac{3}{2} \Phi_{jk,2} n_k n_i \right) f_n, \tag{3.16}$$

$$f_n = \frac{k^{3/2}}{\varepsilon C_l \delta n}. \tag{3.17}$$

Here, $n_{i,j,k,m}$ represents directional cosines and δn is the minimum distance normal to a wall. Craft and Launder [32, 33] later developed these terms further and especially for impinging jet flow. While making improvements for impinging flows, they never actually made much improvement on a general basis. There has been much discussion on how the best expression for these wall-damping terms should be, e.g. that the terms were not applicable for complex geometries due to difficulties in computing the wall normals [84]. More complex models for $\Phi_{ij,2}$ are based on the quasi-isotropic (QI) model [79]

$$\Phi_{ij,2} = \frac{\partial \overline{u}_k}{\partial x_l} (a_{lkij} + a_{lkji}), \tag{3.18}$$

where a_{lkij} is a fourth-order tensor comprising Reynolds-stress elements. Several groups have developed complex models for the redistribution term based on the QI model following the work by Lumley [88]. The major improvement between these realizable models and the previous models, was the adoption of alternative expressions for the pressure-fluctuation term and the introduction of Lumley's flatness parameter [88] (see Eq. 3.23) making the models follow the two-component limit towards the wall. (Realizability means that the variables resulting from solutions of these model equations are consistent with a physical realization of a turbulent flow [88].) Craft and Launder [34] developed a model for the damping of normal stresses towards the wall without terms containing wall normals. They developed terms containing normalized length-scale gradients (see Chapter 7), following the work of Launder and Tselepidakis [85], and Launder and Li [80], making the model attractive for use in flows with complex geometries .

Hanjalić [54] presented a general way of expressing the pressure-fluctuation tensor. He expressed $\Phi_{ij,1}$ and $\Phi_{ij,2}$ as

$$\Phi_{ij,1} = -\varepsilon\left[C_1 a_{ij} + C_1'\left(a_{ik}a_{jk} - \frac{1}{3}A_2\delta_{ij}\right)\right], \tag{3.19}$$

$$\begin{aligned}\Phi_{ij,2} = {} & C_2 P a_{ij} \\ & + C_3 k s_{ij} \\ & + C_4 k\left(a_{ik}s_{jk} + a_{jk}s_{ik} - \frac{2}{3}a_{kl}s_{kl}\delta_{ij}\right) \\ & + C_5 k(a_{ik}\omega_{jk} + a_{jk}\omega_{ik}) \\ & + C_6 k(a_{ik}a_{kl}s_{jl} + a_{jk}a_{kl}s_{il} - 2a_{kj}a_{li}s_{kl} - 3a_{ij}a_{kl}s_{kl}) \\ & + C_7 k(a_{ik}a_{kl}\omega_{jl} + a_{jk}a_{kl}\omega_{il}) \\ & + C_8 k\left[a_{mn}^2(a_{ik}\omega_{jk} + a_{jk}\omega_{ik}) + \frac{3}{2}a_{mi}a_{nj}(a_{mk}\omega_{nk} + a_{nk}\omega_{mk})\right],\end{aligned} \tag{3.20}$$

where

$$P = \overline{u_i' u_j'}\frac{\partial \overline{u}_i}{\partial x_j} \quad , \quad s_{ij} = \frac{1}{2}\left(\frac{\partial \overline{u}_i}{\partial x_j} + \frac{\partial \overline{u}_j}{\partial x_i}\right) \quad , \quad \omega_{ij} = \frac{1}{2}\left(\frac{\partial \overline{u}_i}{\partial x_j} - \frac{\partial \overline{u}_j}{\partial x_i}\right), \tag{3.21}$$

represent production, deformation and rotation respectively, and

$$a_{ij} = \frac{\overline{u_i' u_j'}}{k} - \frac{2}{3}\delta_{ij} \tag{3.22}$$

is the dimensionless stress anisotropy tensor. Lumley's flatness parameter is defined as

$$A = 1 - \frac{9}{8}(A_2 - A_3), \tag{3.23}$$

where the second and third invariants of stress anisotropy are given by

$$A_2 = a_{ij}a_{ji}, \quad A_3 = a_{ij}a_{jk}a_{ki}. \tag{3.24}$$

In this way, several of the models developed over the last decades could be expressed using Eq. 3.19 and Eq. 3.20. The model constants are shown in Tables 3.2 and 3.3, where $r = \min(0.6, A)$. The abbreviations identify the modelers: LRR is Launder, Reece and Rodi [81], SSG is Speziale, Sarkar and Gatski [132], ChL is Choi and Lumley, SH is Shih and Lumley [125], CL is Craft and Launder [32], and LT is Launder and Tselepidakis [84]. β and γ are functions of invariants and the turbulence Reynolds number [125]

(see Eqs. 3.50–3.51). Different approaches can then be modeled only by adjusting the constants. This way of expressing Φ_{ij} may be attractive for model building and for testing different models. The LRR (IP) model was employed in the work presented in Chapter 6.

If buoyancy and gravitational forces are neglected, the pressure-fluctuation term can then be modeled as

$$\Phi_{ij} = \Phi_{ij,1} + \Phi_{ij,2} + \Phi_{ij,\mathrm{w}}, \tag{3.25}$$

where $\Phi_{ij,1}$, $\Phi_{ij,2}$ and, $\Phi_{ij,\mathrm{w}}$ may be given by Eqs. 3.12–3.13 (or Eqs. 3.19–3.20) and Eqs. 3.14–3.17 respectively.

3.2.3 Dissipation, ε_{ij}

Dissipation of turbulence energy is inhomogeneous distributed in turbulent flow. It will be concentrated in certain regions and its appearance will have an intermittent behavior [42]. In turbulence modeling, the dissipative correlations are usually modeled according to Kolmogorov's universal equilibrium theory of the small-scale structure. This theory suggests that the smallest scales are statistically independent of the largest scales and the mean flow, and that all directions are of equal probability (assuming local isotropy) [42, 58, 133]. Based on this theory, the dissipation tensor may be modeled as [42, 79]

$$\varepsilon_{ij} = \frac{2}{3}\varepsilon\delta_{ij}, \tag{3.26}$$

This model is not valid for low-Reynolds-number flow, since local isotropy exists only for high Reynolds numbers [133]. This isotropic model for ε_{ij} (Eq. 3.26) is therefore not

Table 3.2: Coefficients in $\Phi_{ij,1}$ (Eq. 3.19) [54].

	$\Phi_{ij,1}$	
	Linear	Quadratic
Developers	C_1	C_1'
LRR (IP)	1.8	–
LRR (QI)	1.8	–
SSG	1.7	-1.05
ChL, SL	0.5β	0.25γ
CL	$3.1(A_2 A)^{1/2}$	1.2
LT	$6.3AF^{1/2}(1-f)$	$0.7C_1$
$F = \min(0.6, A_2)$, $f = \max(1 - Re_\mathrm{T}/140,\ 0)$		

Table 3.3: Coefficients in $\Phi_{ij,2}$ (Eq. 3.20) [54].

	$\Phi_{ij,2}$						
	Linear				Quadratic		Cubic
Developers	C_2	C_3	C_4	C_5	C_6	C_7	C_8
LRR (IP)	–	0.8	0.6	0.6	–	–	–
LRR (QI)	–	0.8	0.873	0.6555	–	–	–
SSG	0.9	$0.8\text{-}0.625A_2^{1/2}$	0.625	0.2	–	–	–
ChL, SL	–	0.8	$0.6(1+0.8A^{1/2})$	–	0.2	0.2	–
CL	–	0.8	0.6	0.866	0.2	0.2	1.2
LT	–	0.8	0.6	0.866	0.2	0.2	$2r$

sufficient for modeling near-wall flow where large anisotropies arise (see Chapter 7).

The dissipation rate ε can be found by solving a transport equation for the dissipation rate similar to Eq. 3.5 [28, 36, 79]. The models in Eq. 3.9, Eqs. 3.12–3.17 and Eq. 3.26, together with an equation for ε (similar to Eq. 3.5), are often referred to as "the Basic Model" [78].

3.2.4 Low-Reynolds-number modeling

The common way of modeling low-Reynolds-number effects has mostly been to extend high-Reynolds-number versions to low Reynolds numbers by applying low-Reynolds-number functions similar to those used in k-ε models or by using Lumley's invariant parameters. Hanjalić and Launder [57] carried out pioneering work in developing low-Reynolds-number closures. Craft and Launder [30, 34] later developed a low-Reynolds number second-moment closure for use in complex geometries. This model is described in detail in Chapter 7. Hanjalić and Jakirlić [55, 62] developed a low-Reynolds-number second-moment closure, similar to the methods mentioned above, and compared it to high-Reynolds-number closures for several flows. They showed improved behavior by the low-Reynolds-number closure for most mean and turbulent flow properties. A somewhat different approach was invented by Durbin [39], where the redistributive terms in the Reynolds-stress equations were modeled by an elliptic relaxation equation. Durbin derived an elliptic balance equation for a length-scale variable starting from the pressure Possion equation and related it to the redistribution tensor in the exact equations for the Reynolds stresses. Hence, in contrast to previous mentioned approaches, Durbin did not express the redistribution term as an algebraic expression of mean quantities of the flow. This model approach has showed encouraging results for the pressure-strain tensor close to walls, it is tensorial invariant,

and does not include wall-damping terms with wall normals. Durbin's approach has later been further developed by Manceau and Hanjalić [96], since they argued that the pressure-fluctuations normal to the wall were not modeled in the original formulation by Durbin. They proposed a new form of the elliptic relaxation equation based on introducing length-scale gradients to account for inhomogeneity effects. The new model showed improved behavior of the elliptic relaxation equation in the logarithmic layer.

3.3 Variable-density turbulence models

Jones and Whitelaw [68, 69] discussed the use of turbulence closures for variable-density flows, and emphasized the importance of using Favre averaging in combusting flows where large density-variations appear. They also showed a k-ε model for variable-density flows with additional terms compared to the model shown in Sec. 3.1. However, a k-ε model will have difficulties to account for certain important effects in combusting flows, that serve to modulate individual components of the Reynolds stresses. Such effects cannot be incorporated into eddy-viscosity formulations in a generally applicable manner [64], like for example, variable-density effects such as the counter-gradient diffusion observed in flames. According to Jones, second-moment closures appear to represent about the simplest level at which sufficient detail can be included. Based on the Reynolds-stress equations for variable density (Eq. 2.29), Jones and Musonge [64, 67] presented the following model for the pressure-fluctuating term

$$\begin{aligned}\Phi_{ij} =& -C_1\tilde{\varepsilon}\left(\frac{\widetilde{u_i''u_j''}}{\tilde{k}}-\frac{2}{3}\delta_{ij}\right)+C_2\delta_{ij}\widetilde{u_k''u_m''}\frac{\partial\tilde{u}_k}{\partial x_m}+C_3\left(\widetilde{u_k''u_i''}\frac{\partial\tilde{u}_j}{\partial x_k}+\widetilde{u_k''u_j''}\frac{\partial\tilde{u}_i}{\partial x_k}\right)\\ &+C_4\tilde{k}\left(\frac{\partial\tilde{u}_i}{\partial x_j}+\frac{\partial\tilde{u}_j}{\partial x_i}\right)+C_5\widetilde{u_i''u_j''}\frac{\partial\tilde{u}_k}{\partial x_k}+C_6\left(\overline{\rho}\widetilde{u_k''u_i''}\frac{\partial\tilde{u}_k}{\partial x_j}+\overline{\rho}\widetilde{u_k''u_j''}\frac{\partial\tilde{u}_k}{\partial x_i}\right)\\ &+C_7\overline{\rho}\tilde{k}\delta_{ij}\frac{\partial\tilde{u}_k}{\partial x_k}.\end{aligned} \tag{3.27}$$

The coefficients are shown in Table 3.4. Representative values for C_5 have so far not been found. It has to be determined through trial and error [63]. Hence, $C_5 = 0$ seems like the best choice for now. It is a paradox that these effects may be those including the most important differences compared to closures developed for constant density and reformulated into Favre-averaged equations. For constant-density flows, the present model is similar to models developed for constant density since, by continuity, the term $\frac{\partial\tilde{u}_k}{\partial x_k}$ will be zero. Jones [64] indicated that density variations in turbulent flames will provide an important

Table 3.4: The constants in Jones and Musonge's model [64].

C_1	C_2	C_3	C_4	C_5	C_6	C_7	$C_{\varepsilon 1}$	$C_{\varepsilon 2}$
3.0	-0.44	0.46	-0.23	0	$-(\frac{3}{2}C_2 + C_3)$	$-\frac{2}{3}(C_4 + C_5)$	1.40	1.90

additional contribution to the fluctuating pressure-terms appearing in the second-moment equations. He further argued that rewriting the second-moment closures, originally developed for constant-density flows, into Favre-averaged equations can often be sufficient for a reasonably accurate representation of turbulent transport in many variable-density and combusting flow configurations. The remaining unknowns in the equations (Eq. 2.29), $D_{ij,\mathrm{t}}$ and ε_{ij} were modeled through the same methods as described in Sec. 3.2. Jones and Musonge used the diffusion model by Daly and Harlow (Eq. 3.9) and the isotropic version of the dissipation tensor (Eq. 3.26). They employed a dissipation-rate equation similar to Eq. 3.5, with some slight differences in the constants $C_{\varepsilon 1}$ and $C_{\varepsilon 2}$ (see Table 3.4). The model by Jones and Musonge was employed in the calculations of the lifted jet flame presented in Chapter 6.

3.4 Modeling the mean chemical reaction term

There are a wide variety of models for turbulent combustion. For example probability-density-function (PDF) methods [22, 117, 118], flamelet approaches [111] or conditional-moment-closure (CMC) methods [8]. Large-eddy simulation (LES) [137] and direct numerical simulation (DNS) [21, 113] are also used in describing turbulent combustion. The method employed in the present work was Magnussen's Eddy Dissipation Concept which is given an extended description in the next section.

3.5 The Eddy Dissipation Concept

3.5.1 Model description

The Eddy Dissipation Concept (EDC) for turbulent combustion by Magnussen [90, 91, 94] is based on an energy-cascade model which is a stepwise model for energy transfer from larger to smaller scales [43]. The energy-cascade model gives a connection between the smallest scales, the fine structures, where the main part of the molecular mixing takes place,

and the characteristics of the larger eddies. The fine structures are of a size proportional to the Kolmogorov scales, and it is assumed that the chemical reactions take place in these structures. The characteristics of the larger scales can be modeled by standard turbulence models, like the k-ε model or the Reynolds-stress-equation model described in previous sections (Sec. 3.1–3.3). If the fine structures are treated as a well-mixed reactor, the mean chemical reaction term for a chemical species i can be expressed as [49, 51]

$$-\overline{R}_i = \bar{\rho}\frac{\gamma_\lambda^2 \chi}{\tau^*}(Y_i^\circ - Y_i^*), \tag{3.28}$$

where

$$\gamma_\lambda = 2.1\left(\frac{\nu\varepsilon}{k^2}\right)^{1/4} \tag{3.29}$$

is the mass fraction of fine-structure regions and

$$\tau^* = 0.4\left(\frac{\nu}{\varepsilon}\right)^{1/2} \tag{3.30}$$

is the reactor residence time. χ is the fraction of burning fine structures. Y_i° and Y_i^* are the surroundings mass fraction and the fine-structure mass fraction of species i respectively. The connection between the mass-averaged state and the surrounding state can be expressed as [42]

$$\widetilde{Y}_i = \gamma^* \chi Y_i^* + (1 - \gamma^* \chi) Y_i^\circ, \tag{3.31}$$

where γ^* is the mass exchange rate between the fine structure and the surroundings and is modeled as

$$\gamma^* = \gamma_\lambda^3 = 9.8\left(\frac{\nu\varepsilon}{k^2}\right)^{3/4}. \tag{3.32}$$

γ^* and γ_λ act like some kind of intermittency parameters. They express the probability of finding fine structures or fine-structure regions in a point [42].

The term $(Y_i^\circ - Y_i^*)$ can be found in several ways, for example by assuming fast, reduced or finite-rate chemistry. The present work employed finite-rate chemistry calculations only. A fast chemistry assumption was employed for producing initial conditions for these calculations. However, assuming infinitely fast chemistry leads to a very attractive, and simple, expression, which is perhaps the most widely used expression in conjunction with EDC (see Sec. 3.5.3). While employing a fast-chemistry assumption may be more practical, employing finite-rate chemistry can be attractive for more detailed analysis. Determining the fraction of burning fine structures may also be difficult in finite-rate chemistry calculations when employing detailed mechanisms. There are methods referring to the global reaction [91]. Gran [49] suggested using $\chi = 1$ and let the chemistry decide the amount of reaction. The latter approach was adopted in the present work. However, better methods may be derived. For more detailed analysis, see Gran and Magnussen [49, 51, 92].

3.5.2 Finite-rate chemistry

Effects of finite-rate chemical kinetics were taken into account by treating the reacting turbulence fine structures as constant-pressure homogeneous reactors. The set of governing equations for such a reactor, when radiative heat transfer is neglected, can be written [49]

$$\begin{aligned} \frac{dh}{dt} &= 0, \\ \frac{dp}{dt} &= 0, \\ \frac{dY_i^*}{dt} &= \omega_i^* + \nu_r(Y_i^\circ - Y_i^*) \qquad i = 1, ..., N_\mathrm{S}, \end{aligned} \tag{3.33}$$

for each species i, where $\omega_i^* = R_i^*/\rho^*$ is the specific reaction rate. Superscript $^\circ$ refers to the fluid entering the reactor and ν_r is the rate of mixing. This equation (Eq. 3.33) is integrated from $t = t_0$ to $t = t_0 + \Delta t$. (An external equation solver was employed in the present work (LIMEX [37])). In the present work, the reactors were assumed to be stationary with mixing rate $\nu_r = 1/\tau^*$ and $\Delta t \to \infty$. This corresponds to a perfectly stirred reactor with residence time τ^* [49]. Integration of Eq. 3.33 to steady state leads to the following set of equations for the mass fractions

$$\frac{Y_i^* - Y_i^\circ}{\tau^*} = \omega_i^* \qquad i = 1, ..., N_\mathrm{S}. \tag{3.34}$$

The reactor's specific reaction rate can be found in many ways, for example single-step, reduced or detailed chemical mechanisms.

Single-step mechanisms

The easiest way is to assume a single-step mechanism. This can be convenient to use for example when computer resources are limited or during model building. A single-step global chemical reaction for premixed gases can be expressed as

$$\mathrm{F(Fuel)} \xrightarrow{k_F} \mathrm{P(Product)}, \tag{3.35}$$

where k_F is the rate coefficient. For this case, the reaction rate given by Eq. 2.8 is

$$\omega_F^* = -k_F Y_F^*, \tag{3.36}$$

since $c_i = Y_i \rho / M_i$ [42]. By using Eq. 2.9 for the rate coefficient, the reaction rate can then be written as

$$\omega_F^* = -A_F (T^*)^{\beta_F} Y_F^* \exp\left(-\frac{E_{a_F}}{R_\mathrm{u} T^*}\right). \tag{3.37}$$

Reduced mechanisms

Reduced mechanisms are not treated here. Such mechanisms are described in detailed by for example Warnatz et al. [139].

Detailed mechanisms

Detailed mechanisms can be used for calculating ω_i^*. The present work employed a detailed mechanism from GRI-Mech 2.11 by Bowman et al. [11].

3.5.3 Infinitely fast chemistry assumption

If the chemical reactions are assumed to occur "infinitely fast", the global reaction can be described by a single-step stoichiometric reaction (equation) as

$$1 \text{ kg fuel (F)} + r_F \text{ kg oxidant (O)} \rightarrow (1+r) \text{ kg product (P)}, \tag{3.38}$$

where r_F is the stoichiometric amount of the oxidizer. Then the mean chemical reaction term can be written as [49]

$$-\overline{R}_F = \bar{\rho}\frac{\gamma_\lambda^2 \chi_1}{\tau^*(1-\gamma^*\chi)}\min\left(\widetilde{Y}_{\min}, \frac{\widetilde{Y}_P}{1+r_F}, \left(\tilde{Y}_{\min}+\frac{\widetilde{Y}_P}{1+r_F}\right)\gamma_\lambda\right), \tag{3.39}$$

where $\widetilde{Y}_{\min}$ is expressed as

$$\widetilde{Y}_{\min} = \min\left(\widetilde{Y}_{\mathrm{F}}, \frac{\widetilde{Y}_{\mathrm{O}}}{r_F}\right). \tag{3.40}$$

This expression is applicable to both premixed and non-premixed flames. Expressions for χ_1 and χ are described in the next section.

3.5.4 The fraction of burning fine structures

Not all of the fine structures react. If the chemical reactions are assumed to take part as a global single-step reaction, then the fraction of burning fine structure can be described as [42]

$$\chi = \chi_1 \cdot \chi_2 \cdot \chi_3, \tag{3.41}$$

where χ_1 is the probability of coexistence of the reactants,

$$\chi_1 = \frac{\left(\widetilde{Y}_{\min}+\widetilde{Y}_{\mathrm{P}}/(1+r_F)\right)^2}{\left(\widetilde{Y}_{\mathrm{F}}+\widetilde{Y}_{\mathrm{P}}/(1+r_F)\right)\left(\widetilde{Y}_{\mathrm{O}}/r_F+\widetilde{Y}_{\mathrm{P}}/(1+r_F)\right)}, \tag{3.42}$$

χ_2 expresses the degree of heating,

$$\chi_2 = \min\left[\frac{\widetilde{Y}_{\mathrm{P}}/(1+r_F)}{\gamma_\lambda\left(\widetilde{Y}_{\mathrm{P}}/(1+r_F)+\widetilde{Y}_{\mathrm{min}}\right)}, 1\right], \tag{3.43}$$

and χ_3 limits the reaction due to lack of reactants,

$$\chi_3 = \min\left[\frac{\gamma_\lambda\left(\widetilde{Y}_{\mathrm{P}}/(1+r_F)+\widetilde{Y}_{\mathrm{min}}\right)}{\widetilde{Y}_{\mathrm{min}}}, 1\right]. \tag{3.44}$$

The expressions for χ are discussed in detail by Magnussen and Gran [49, 51, 92].

3.6 Some characteristics of turbulent reacting flows

Some scales and dimensionless numbers are commonly used to describe and characterize turbulent flames.

The large eddies in a turbulent flow can be described by characteristic scales for velocity u', length l' and time $\theta = l'/u'$. These are the scales resolved in turbulent models and represent the second level in the energy cascade (the first level represents the mean flow). In terms of the turbulence variables, these length or time scales can be written as [42]

$$l_{\mathrm{t}} = \frac{k^{3/2}}{\varepsilon}, \tag{3.45}$$

$$\tau_{\mathrm{t}} = \frac{k}{\varepsilon}. \tag{3.46}$$

The smallest eddies are in turbulent flow characterized by viscous forces and dissipation of turbulence energy, ε. Small-scale motion in turbulence are often characterized by the Kolmogorov scales. These scales are expressed in terms of viscosity and dissipation as [42, 133]

$$v = (\nu\varepsilon)^{1/4}, \tag{3.47}$$

$$\eta = \left(\frac{\nu^3}{\varepsilon}\right)^{1/4}, \tag{3.48}$$

$$\tau = \frac{\eta}{v} = \left(\frac{\nu}{\varepsilon}\right)^{1/2} = \frac{\eta^2}{\nu}. \tag{3.49}$$

By using Eq. 3.49, the two first scales can be written in terms of the time scale as $v = (\nu/\tau)^{1/2}$ and $\eta = (\nu\tau)^{1/2}$. The Reynolds number based on these scales is $Re_\eta = \eta v/\nu = 1$.

A turbulence Reynolds number based on the turbulence models variables can be defined as

$$Re_{\mathrm{T}} = \frac{k^2}{\nu\varepsilon}. \tag{3.50}$$

A turbulence Reynolds number can also be defined as

$$Re_{\lambda} = \frac{u'\lambda}{\nu}, \tag{3.51}$$

where λ is the Taylor microscale defined as $\lambda^2 = 10\nu k^2/\varepsilon$ for anisotropic turbulence [42, 133].

Quantities often used to characterize premixed flames are the laminar flame speed and laminar flame thickness. For a premixed flame with high activation energy, Borghi expressed these quantities as [10]

$$u_{\mathrm{L}} = K\left(\frac{D}{\tau_{\mathrm{c}}}\right)^{1/2}, \tag{3.52}$$

$$e_{\mathrm{L}} = K'(D\tau_{\mathrm{c}})^{1/2}, \tag{3.53}$$

where D is a diffusivity and K and K' are constants. A turbulence Dahmköhler number can be defined as the ratio between the turbulence time scale from Eq. 3.46, and a characteristic time scale representing the chemical processes as

$$Da_{\mathrm{t}} = \frac{\tau_{\mathrm{t}}}{\tau_{\mathrm{c}}}. \tag{3.54}$$

This number can be a relevant parameter describing turbulence-chemistry interactions [10].

The scales and parameters described here are often used to characterize flames in certain flame regimes for both non-premixed and premixed flames (see for example Borghi [10] or Ertesvåg [42]).

Chapter 4

A review of turbulent reacting near-wall flows

4.1 Introduction

There has been carried out some research on turbulent reacting near-wall flows, but compared to other areas, like for instance non-reacting turbulent flow, it is still a small field. In general, few have reported on such flows in detail lately. The present chapter gives a brief review of some of the research conducted on the subject. Furthermore, a characterization of chemically reacting boundary-layer flows, given by Kuo [77] is briefly presented. Finally, some typical cases of turbulent reacting boundary-layer flows are described.

The understanding of turbulent combustion near walls is dependent on collaborative contributions from experimental-, analytical-, and numerical research. Experimental work has to create the basis for this. However, there have so far been few experiments performed, and it is not an active subject in many groups, which may be so since such work is both difficult and expensive. Combustion close to walls is believed by some to be of less importance for the combustion itself in many devices [111]. As commented by Bruneaux et al. [18]: "In turbulent flows, modeling of flame-wall interaction has not yet been recognized as an important issue." This may be a result of the difficulties associated with the subject, and that little is known about it. The main interest in combustion near walls, so far, seems to be investigating heat fluxes through the walls. Even if control of heat through the wall were the only subject of interest, it would still require the understanding of the underlying processes, such as turbulence and chemical reactions. Laminar flame calculations have shown that a detailed description of chemical kinetics and transport properties improves the predictions

of phenomena such as heat fluxes through a wall and flame wall quenching [114, 119].

Kuo [77] addressed the practical relevance of chemically reacting boundary-layer flows, and several areas that require knowledge and the solution of boundary-layer flows. Some examples are; catalytic reactors in chemical industries, erosive burning of solid propellants in high-performance rocket motors, flame stabilization by plates and rods in premixed flowing gases, metal-surface erosion by high-temperature shear flows, and fires on vertical walls. One of the areas where Kuo performed research of interest for the present work, was the modeling of erosive burning of solid propellants in rocket motors. Other applications that may seem naturally interesting for the present work are internal combustion engines and gas turbine combustion chambers.

Poinsot [113] reviewed flame-wall interactions and DNS and referred to work conducted on this matter, mainly DNS work by himself and coworkers. Poinsot concluded that "DNS is a useful tool studying turbulent combustion only if it is used in combination with theory, experiments, and physical modeling". Maly [95] addressed combustion close to walls in SI-engine combustion. He emphasized that little is known on the subject, and that models can not predict wall-flame interaction, with some exceptions. Maly also addressed common aspects occurring close to a wall, such as turbulence-flame interaction, turbulence change of scales, wall quenching, and unburned hydrocarbons. Spalding [131] reviewed mathematical modeling of turbulent flames. He included some facts on confined flames, and presented some early thoughts on low-Reynolds-number effects on chemical reaction rates close to walls.

The brief review given here attempts to give a broad view, but may, of natural reasons, be somewhat concentrated on the modeling part. This may also be a consequence of that the increasing availability of computer resources has led to increasing possibilities for using DNS to study near-wall phenomena in turbulent reacting flows. There has also been carried out theoretical work, and of interest may be the review given by Kuo [77]. He reviewed several investigations of pioneering theoretical approaches on chemically reacting boundary-layer flows. Turbulence modeling, which plays a major part in turbulent reacting boundary-layer flow, was briefly reviewed in Chapter 3. Also, a second-moment closure for near-wall flows was investigated in Chapter 7.

4.2 Experimental work

Cheng et al. [24] studied experimentally the general features of H_2-air combustion in a heated boundary layer. Measured mean and root-mean-square (RMS) profiles of velocity and density in the boundary layer were reported with and without combustion. Ng

et al. [107] performed experimental studies of turbulence-combustion interaction of an ethylene-air mixture in a turbulent boundary layer over a heated plate. The boundary layer over the flat surface was allowed to develop to a fully turbulent stage before ignition was induced by heating a section of the surface. They reported measured time-averaged statistical quantities of density, Reynolds stresses (both normal and shear stresses) and the triple correlation $\overline{u'k_1}$, where $k_1 = (u')^2 + (v')^2$. Their results demonstrated effects of turbulence-combustion interaction. Large-scale turbulence structures seemed to dominate the combustion process, whereas combustion, on the other hand, caused expansion of the turbulence boundary layer and large deflections of the streamlines away from the surface. The local wall-friction coefficient was increased due to the increased fluid viscosity. Li et al. [86] reported the results of measurements in two premixed impinging jet flames where the jet exit Reynolds number varied from 8100 to 10100. The data reported were mean axial velocity, the mean progress variable, Reynolds stresses and the mean axial flux of the progress variable. They found that turbulence production was associated with heat release, and, as expected, that the flame thickness was proportional to the turbulence integral length scale. These data from Li et al. were later used for model building by Bray et al. [15, 16] (see modeling review in Sec. 4.4). Zhang and Bray [143] reported and discussed five different combustion modes in the characterization of jet flames impinging on a flat plate. Escudié and Haddar [44] commented on experimental studies of a premixed turbulent stagnating methane-air flame. They reported that, in general, there were two effects of importance for quenching the flame towards the wall. The strain rate (defined as the mean axial velocity gradient in the vicinity of the wall), which was believed to be the most important effect, and the heat loss to the plate. They showed evolution profiles of mean axial velocity and compared isothermal and reacting cases. An increase in the strain rate was associated with a decrease in the mean flame thickness and the flame was pushed towards the wall.

4.3 Direct numerical simulations

Poinsot et al. [115] studied the interaction between turbulent premixed flames and walls using two-dimensional DNS on a head-on configuration. They found that quenching distances (the distance from the wall where the flame quenches locally) and maximum heat fluxes remained of the same order as for laminar flames. They claimed that the quenching zone was located in the viscous sub-layer and used this result as a basis to develop a "law-of-the-wall" model for premixed turbulent combustion (used in piston engines). Later, Bruneaux et al. [17] studied turbulent premixed flames interacting with a constant-density channel flow using 3D DNS (in this way turbulence and combustion are decoupled). They found that the quenching distances decreased and that the maximum heat fluxes increased relative to laminar flame values, scaling with the turbulent strain rate. Those effects were due

to large coherent structures (horseshoe vortices) which pushed the flame towards the wall. They also found that, unlike previous results [115], the laminar quenching distances could be outside the viscous sub-layer which for two different turbulent cases were $\delta_Q^+ \approx 18$ and $\delta_Q^+ \approx 28$, where δ_Q^+ is the normalized quenching distance from the wall. Alshaalan and Rutland [2, 3, 4] investigated turbulent premixed flames in a turbulent side-wall Couette-flow configuration with variable density. They reported on how the flame changed the turbulent wall-boundary layer quantities as well as the turbulent scalar flux and the flame-surface density near the wall. The mean velocity profile was accelerated, whereas the scaled velocity was reduced outside the viscous sub-layer. This was due to the flame being responsible for additional transport mechanisms (especially velocity-pressure correlations). Furthermore, they reported that the flame reduced the turbulence length scale ($k^{3/2}/\varepsilon$), which they believed was due to an increase in the turbulence energy dissipation rate. Near the wall, the reduction was smaller due to heat loss to the wall causing weaker reaction rates. The reported results from Alshaalan and Rutland were statistically stationary, unlike the transient predictions performed by Poinsot et al. [115] and by Bruneaux et al. [17], discussed above.

4.4 Modeling work

Bruneaux et al. [18] developed a modeled flame-surface density equation based on flamelet ideas that accounted for wall effects. The models were validated against previous performed DNS results [115]. Kojima and Nishiwaki [76] developed a model for turbulence premixed flame-wall interaction to avoid unrealistic acceleration of the flame against a wall in a SI-engine CFD code. The model was based on the Eddy Dissipation Concept by Magnussen and Westbrooks empirical reaction rate for octane (one physical part based on the turbulence time scale and one chemical part describing the exothermic reaction). They reported that their model was able to deal with near-wall phenomena such as turbulence-reaction controlled combustion in the near-wall region, and that it avoided unrealistic flame shapes due to near-wall acceleration of the turbulent flame. Abu-Orf and Cant [1] developed a new model for the mean chemical reaction rate for premixed flames in SI engines. The reaction rate was developed to give realistic flame behavior, both away from and close to the wall, and was based on a laminar flamelet approach. They validated their predictions against experimental engine cylinder pressure histories.

Spalding [129, 130, 131] discussed confined jet flames, where a flame holder was placed in a duct downstream of the mixing device. The flame holder may be a bluff-body, causing recirculation, or it may be a pilot jet flame providing hot gases from a separate combustion chamber. Spalding discussed the influence of low-Reynoldsnumber effects on the chemical reaction rates and the increasing importance of chemical kinetics for such conditions. He

presented the introduction of Reynolds-number functions to make the reaction rate satisfy the low-Reynolds-number regime. The reaction-rate proposals were of the form [131]

$$\frac{1}{R_c} = \frac{Re_\mathrm{T}/R_\mathrm{EBU} + (Re_\mathrm{T} + A)/R_\mathrm{lam}}{Re_\mathrm{T} + A}, \tag{4.1}$$

where R_c is the time-average production of species c, R_EBU is the value of R_c given by Spalding's Eddy Breakup model (EBU), R_lam is the reaction rate of a laminar fluid, Re_T is the turbulence Reynolds number, and A is a constant. Spalding also proposed simpler models for the EBU approach in conjunction with the mixing-length hypothesis of turbulence for confined flames, where the reaction rate was predicted as proportional to the mean transversal velocity gradient.

Razdan and Kuo [120] investigated a steady two-dimensional, chemically reacting turbulent boundary layer over a propellant surface. They developed a boundarylayer model based on the EBU model of Spalding [129], following arguments of Lockwood [87]. Razdan and Kuo started from the EBU model [120]

$$R_\mathrm{EBU} \sim -\overline{\rho}\frac{\varepsilon}{k}\sqrt{\overline{Y_F'^{\,2}}}, \tag{4.2}$$

where Y_F' is the fuel concentration fluctuation. Instead of solving the conservation equation for $\overline{Y_F'^{\,2}}$, they used a simplification for the reacting boundary layer. They assumed that the production and dissipation term in the conservation equation dominate in the near-wall region. Based on this assumption, they proposed the expression

$$\overline{Y_F'^{\,2}} \sim \frac{\mu_\mathrm{t}}{\overline{\rho}}\frac{\varepsilon}{k}\left(\frac{\partial \widetilde{Y}_F}{\partial y}\right)^2, \tag{4.3}$$

and consequently, the expression for the mean chemical reaction term was

$$\overline{R}_F = -C_R\overline{\rho}\sqrt{k}\left|\frac{\partial \widetilde{Y}_F}{\partial y}\right|, \tag{4.4}$$

where C_R is a constant. This expression is limited to fast chemical kinetics and boundary--layer flows and was assumed particularly valid for reactions taking place under high pressure. Razdan and Kuo compared their predictions with experimental data and concluded that the (erosive) burning rate was augmented by the heat feedback introduced by the increase in transport coefficients and the turbulence-enhanced mixing and reaction of the oxidizer and fuel gases. Bray et al. [15, 16] calculated Reynolds stresses and fluxes in a turbulent premixed reactant stream impinging on a wall and compared their predictions to the data of Li et al. [86]. Bray et al. examined models for pressure fluctuations and reported a new set of second-moment equations. Later, they evaluated models for the mean chemical reaction

term. The algebraic models discussed by Bray et al. seemed to be similar to, or in some sense related to, the EBU model discussed above.

There has also been conducted research on wall fires. Kennedy et al. [72] studied buoyancy-controlled turbulent wall-diffusion flames by the use of a k-ε-g low-Reynolds-number turbulence model (where g is the mean square fluctuation of the mixture fraction, and represents a transport equation in order to account for buoyancy), and a chemical source term for combustion. Their results were only compared to a non-reacting flow due to the lack of experimental data. Wang and Joulain [138] used 3D modeling to predict wall fires with buoyancy-induced flow along a vertical rectangular channel. They tested four different combustion models, where one of them was an EBU-like model based on the Eddy Dissipation Model by Magnussen and Hjertager [93]. The models were tested against experimental data to study the influence of a turbulent diffusion flame between parallel walls on the solid fuel burning rate. They found relatively good agreement between the limited available experimental data and all four models, but they concluded that success in understanding a significant portion of present combustion problems depends on a detailed and correct understanding of the coupling between turbulence and reaction kinetics.

4.5 Characterization of reacting boundary-layer flows

Reacting boundary-layer flows can be classified in several ways. Kuo [77] classified chemically reacting boundary-layer flow according to Table 4.1. The $(*)$ indicates the approaches investigated in the present work. An interesting part for the present work is the equilibrium cases versus the non-equilibrium. According to Kuo, the most interesting part when concerning chemically reacting boundary-layer flows lies in the non-equilibrium case. In the equilibrium case, chemical reactions are considered to take place infinitely fast, so that chemical-rate kinetics is no longer a factor. In the non-equilibrium case, chemical reactions take place at a finite rate. The most interesting features of the chemically reacting boundary layers are due to the coupling of the boundary-layer characteristics with the finite-rate chemical reactions.

4.6 Turbulent reacting boundary-layer flows

4.6.1 Wall flames

There are some configurations commonly used to study flames interacting with a wall. For example a reacting flame over a plate [24, 107] (side-wall configuration) or towards it (head-

Table 4.1: Types of chemically reacting boundary-layer flow (from Kuo [77]).

Parameters	Types
Magnitude of reaction rate	Equilibrium or non-equilibrium$^{(*)}$
Site of chemical reaction	Gas-phase$^{(*)}$, heterogenous, or both
Turbulence level	Laminar or turbulent$^{(*)}$
Geometric contour	Planar (2D)$^{(*)}$, axisymmetric$^{(*)}$ or 3D
Steadiness of boundary-layer flow	Steady$^{(*)}$ or unsteady
Presence of particles	Single-phase$^{(*)}$ or multiphase
Free-stream Mach number	Subsonic$^{(*)}$, transonic, supersonic, or hypersonic
Exothermicity of reaction	Exothermic$^{(*)}$ or endothermic
Mixing conditions of reactants	Premixed$^{(*)}$ or diffusion$^{(*)}$
Solution methods	Integral methods, numerical PDE's $^{(*)}$ or experimental methods

on configuration) [15, 16, 86]. These cases are often called side-wall quenching or head-on quenching, since quenching is mostly the phenomenon studied (or of interest). The latter configuration is similar to that of impinging jet studies. Confined flames are flames between parallel plates or in a pipe or channel [131] and may be classified as side-wall configurations. Turbulent reacting Poiseuille flow [17, 115] and Couette flow [2, 3, 4] are examples of such flames.

4.6.2 Jet flames

Turbulent non-premixed flames, such as jet flames, are of special interest in many applications, for example jet engines in contrast to premixed flames appearing in many spark-ignited engines [139]. Jet flames present an opportunity to study related phenomena appearing near walls such as for example localized extinction, and the large shear layer that arise between the jet issuing into stagnant air or a coflow. Jet flames have been studied extensively, in contrast to wall flames, and well established experimental data exist [111].

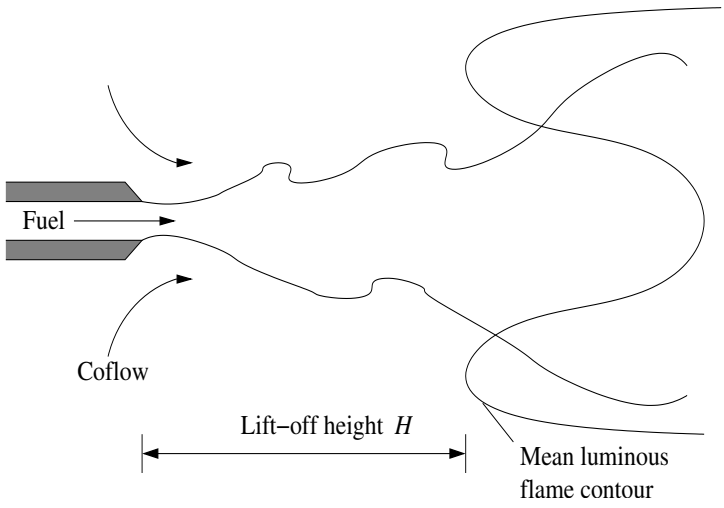

Figure 4.1: Schematic view of a lifted jet diffusion flame.

Attached jet flames

There are many different types of jet flames. For more detailed description, see for example Peters [111]. An attached jet consists of a high-velocity fuel jet issuing from a nozzle most often into stagnant air or coflowing air (or another gaseous mixture). The large velocity difference between the jet and the air leads to a growing boundary layer where fuel and air mix and chemical reactions occur. Attached jets are attractive in lab experiments as well as model building and validation, since their nature has been characterized for several years.

Lifted jet flames

Lifted jet flames are not wall-interacting flames (except for the wall at the nozzle exit), but they may serve as excellent cases to study certain phenomena occurring in flame-wall interacting flows. Some of the phenomena present are localized extinction and re-ignition which have been investigated in detail for several years [111]. Unlike for wall flames, there are detailed experimental data of the chemistry for lifted jet flames. The calculation of effects such as local extinction in lifted turbulent jet flames will provide important information for the study of turbulent reacting near-wall flow. Hence, studying a lifted jet flame is beneficial for the research on wall flames.

Lifted turbulent jet diffusion flames are not attached to the burner rim, but are stabilized a distance downstream of the nozzle exit. A highly unsteady region from the rim to the base of the flame (see Fig. 4.1) is present in such flames, and the distance from the burner rim to the base of the lifted flame is called the lift-off height, H [111]. In this region, no chemical reactions are present, but mixing of reactants and oxidizers occurs. This type of combustion is therefore also called partially premixed combustion (in addition to non--premixed combustion). If the jet velocity is low enough, the flame will be attached to the nozzle. By increasing the jet velocity, the flame will lift off from the rim.

Due to the presence of the highly unsteady region between the nozzle and the base of the flame, predicting a lifted turbulent jet flame may be a challenge to present CFD codes. Both since it involves unsteady turbulent flow (which requires using complex turbulence models), but also since both non-premixed and premixed combustion occur. Hence, the generality of the combustion model will be an important issue.

URN:NBN:no-7265

Chapter 5

Numerical method

The general-purpose CFD code SPIDER, developed by Melaaen [98], was employed in the present work. Gran later implemented Magnussen's Eddy Dissipation Concept (EDC) for turbulent combustion [48, 49]. SPIDER is an elliptic solver for turbulent non-reacting and combusting flows and employs curvilinear non-orthogonal coordinates. The present chapter gives only a short description of the code. Details on discretization, coordinate transformations, implementation of the EDC etc., are given by Melaaen [98, 99, 100] and Gran [48, 49, 50, 51], respectively. The present version of SPIDER employed a Graphical User Interface (GUI), called LIZARD, developed by Vembe [136]. LIZARD introduces a very convenient way of pre-proceccing the calculations, including grid generation, setting up boundary conditions, and graphical investigation of the calculations in the course of the computations.

5.1 Discretization

The discretization of the equations is based on the finite-volume concept where the computational domain is divided into small control volumes (see Fig. 5.1). The mean scalar transport equation (Eq. 2.27) is written on the invariant form

$$\frac{\partial}{\partial t}(\rho\varphi) + \nabla \cdot \boldsymbol{J} = S, \tag{5.1}$$

where

$$\boldsymbol{J} = \rho \boldsymbol{U}\varphi - \Gamma \nabla \varphi. \tag{5.2}$$

This equation is integrated over a general control volume. By applying Gauss' divergence theorem on the volume integral of the flux in Eq. 5.2, this term is integrated over the control

volume faces rather than the control volume itself. Introducing implicit time discretization (backward Euler) and integrating the fluxes over the control-volume faces, the following equations appear:

$$a_P \varphi_P = \sum_{\text{nb}} a_{\text{nb}} \varphi_{\text{nb}} + b, \tag{5.3}$$

where

$$a_P = \sum_{\text{nb}} a_{\text{nb}} + a_P^\circ + a_{\text{f}} - \overline{S}_{2P}, \tag{5.4}$$

$$b = b_{\text{NO}} + a_P^\circ \varphi_P^\circ + \overline{S}_{1P}, \tag{5.5}$$

$$a_P^\circ = \frac{\rho_P^\circ \delta V_P}{\delta t}, \tag{5.6}$$

$$a_{\text{f}} = \frac{\rho_P - \rho_P^\circ}{\delta t} \delta V_P + F_e - F_w + F_n - F_s + F_t - F_b, \tag{5.7}$$

$$F_{nn} = (\rho \hat{U}^i)_{nn}. \tag{5.8}$$

The non-orthogonal terms included in b_{NO} are not described here. The subscript nb indicates the neighbor nodes surrounding the center node P, whereas the subscript nn indicates the values on the control-volume faces (see Fig. 5.1) . $(\hat{U}^i)_{nn}$ and F_{nn} is the volumetric flow rate in i direction and the mass flow rate respectively at face nn. The source term has been linearized on the form

$$\overline{S}_P = \int_{\delta V} S dV = \overline{S}_{1P} + \overline{S}_{2P} \varphi_P \ . \tag{5.9}$$

Here, $\overline{S}_{2P}$ has to be chosen negative to assure only positive coefficients in the solution algorithm. This assures working towards a numerically stable solution. The diffusive terms were approximated using central differences, whereas the convective terms were approximated by either a power-law scheme (POW) or a second-order upwind scheme (SOU). The POW scheme was in the present work only used for its stable behavior to produce initial conditions for calculations employing the SOU scheme. More details on these schemes can be found in Melaaen [98].

By using the discretization method presented above, all equations are expressed in the same general applicable manner, but different effects for each equation are introduced through for instance the source terms or the boundary conditions.

5.2 Pressure-velocity coupling

In SPIDER, the pressure field can be corrected by using the SIMPLE algorithm described in the next section (other algorithms, like e.g. SIMPLEC [98] may also be employed). The

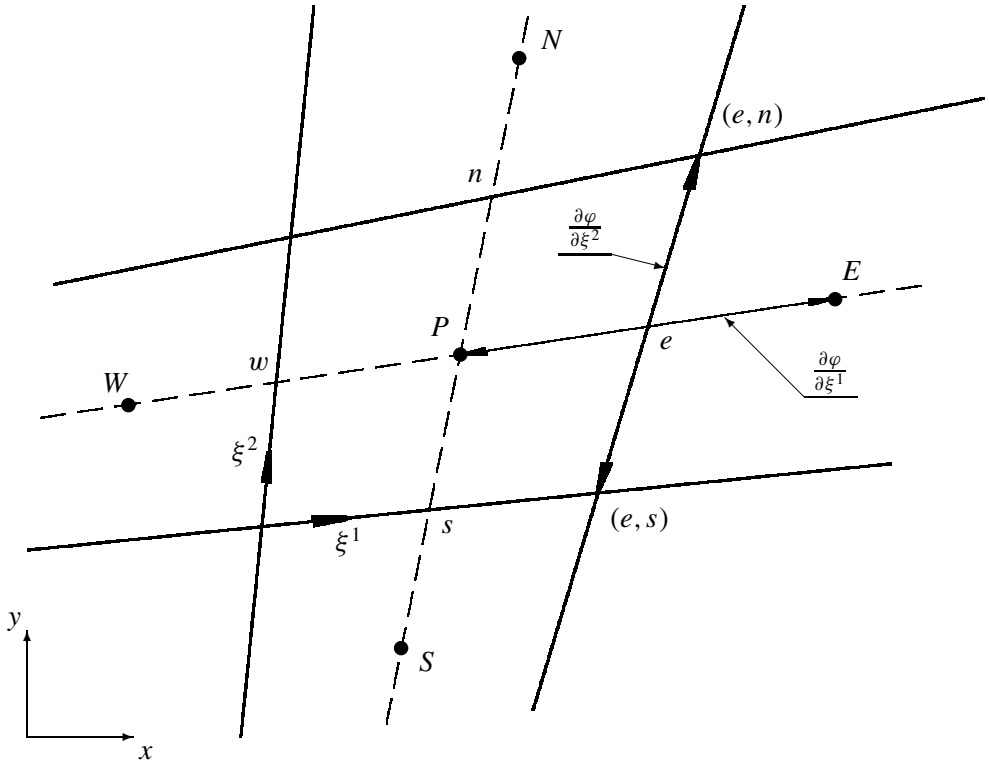

Figure 5.1: Example of a two-dimensional control volume in SPIDER.

SIMPLE algorithm tries to find updated velocity and pressure fields obeying the discrete momentum and continuity equations. First, tentative velocity and pressure field are guessed. These tentative fields are corrected by solving a pressure-correction equation derived from the overall mass conservation equation (Eq. 2.1). Rhie & Chow interpolation [122] is used to avoid checkerboard oscillations (about pressure-velocity coupling, see Melaaen [98] for details). An equation of state couples density, pressure and temperature. A non-staggered grid was employed in the present work.

5.3 Solution algorithm (SIMPLE)

The SIMPLE algorithm by Patankar [108] was used to find updated velocity and pressure fields obeying the discrete momentum and continuity equations for the converged solution. For stationary flow, SIMPLE can be summarized as [98]:

1. Guess initial conditions for all variables.
2. Update boundary conditions.
3. Obtain the density values from the current temperature and pressure fields.
4. Calculate the coefficients and sources of the momentum equations by using the last available values of the various variables. Solve the momentum equations to obtain velocities from the pressure field.
5. Find the velocity fluxes from Rhie & Chow interpolation formulae.
6. Solve the pressure-correction equation.
7. Correct the pressure and density fields, mass flow rate and Cartesian velocity components.
8. Solve the turbulence equations.
9. Solve the enthalpy equation and the mean mass fraction equations.
10. Calculate the temperature, density and viscosity.
11. Use the new values in a new global iteration step and repeat steps 2 to 10 until convergence is reached.

When convergence is reached by using the SIMPLE algorithm, the equations are exactly solved within the convergence and truncation-error criteria. This means that numerical errors appearing are due to discretization errors only.

5.4 Equation solver and convergence criterion

The equation solver used in the present work was a line-by-line Tri-Diagonal-Matrix Algorithm (TDMA) (for details, see Patankar [108]). The equations were solved iteratively in succession. To terminate the whole iteration procedure when the solution has converged, residuals were used. The l_1-norm of the residuals was made non-dimensional by a characteristic flux of the flow field. The solution has converged when the scaled residual are less than or equal to a convergence criterion (typical 10^{-4} or less) for all variables.

Chapter 6

A Numerical Investigation of a Lifted H_2/N_2 Turbulent Jet Flame in a Vitiated Coflow

For submission to Combustion Science and Technology (2003).

URN:NBN:no-7265

URN:NBN:no-7265

A Numerical Investigation of a Lifted H_2/N_2 Turbulent Jet Flame in a Vitiated Coflow

T. Myhrvold, I. S. Ertesvåg, I. R. Gran

Department of Energy and Process Engineering
Norwegian University of Science and Technology
Trondheim, Norway

R. Cabra, J.-Y. Chen

Department of Mechanical Engineering
University of California at Berkeley
California, USA

For submission to:

Combustion Science and Technology
2003

Corresponding Author:

Tore Myhrvold
Department of Energy and Process Engineering
Norwegian University of Science and Technology
Kolbjørn Hejesv. 1b, No-7491 Trondheim, Norway
Tel: +47 73590979, Fax: +47 73593580
E-mail: Tore.Myhrvold@sintef.no

Abstract

The present work presents a numerical investigation of a lifted H_2/N_2 turbulent jet flame in a vitiated coflow of hot gases. Most results presented were calculated using Magnussens's Eddy Dissipation Concept (EDC) for turbulent combustion, and the main discussion is concerned the EDC. However, the EDC predictions were compared to numerical results from a PDF calculation using a parabolic solver, and experimental results. The EDC was used in conjunction with a detailed chemical mechanism from GRI-Mech 2.11 and the calculations were performed with the general purpose CFD code SPIDER, which is a finite-volume code

URN:NBN:no-7265

solving Favre-averaged Navier-Stokes equations. In the present work SPIDER employed an axisymmetric two-dimensional geometry. In addition to previously presented results of the same flame [20], the present work presents a more detailed discussion of the results predicted by the EDC. A discussion on the mechanisms in the EDC responsible for predicting the lifted jet flame in the vitiated coflow burner is reported. Results from employing two additional turbulence models and effects of grid dependencies are also presented and discussed. Four different turbulence models were applied; the standard k-ε model, the Reynolds-stress-equation model of Launder, Reece and Rodi (LRR), a modified k-ε model and the Reynolds-stress-equation-model by Jones and Musonge (JM). The experimentally predicted lift-off height was approximately 10 nozzle diameters. With the standard k-ε model, a lift-off height of about 8.5 nozzle diameters was predicted, while with the LRR model, and with the modified k-ε model, the lift-off height was predicted to approximately 5 nozzle diameters. The JM model predicted a lift-off height of 3.5. The different predicted lift-off height seems to be due to different predicted residence times in the reactor model. The predictions indicate that the flame stabilizes at a point where turbulence micro mixing (represented through the reactor residence time) and chemistry are in balance. The present predictions show that the EDC in conjunction with detailed chemistry is capable of predicting a lifted turbulent jet flame. The EDC predictions indicate that transport of hot combustion products to the base of the flame may be one of the processes stabilizing the flame, whereas the PDF results leads us not to exclude autoignition as the stabilizing mechanism.

Introduction

For lifted flames great efforts have been set forth to investigate the mechanisms that stabilizes such flames, i.e. how to maintain the flame in a certain position. Chomiak [26] discussed methods on how to stabilize flames. Such methods can be the use of vortices formed behind bluff bodies and recirculation caused by the swirling of the flow. Other methods can be to involve formation of regions where the mean flow velocity is lower than the flame propagation velocity or simply to use a pilot jet as a constant ignition source.

Peters [111] gave an extended review of a substantial number of research efforts and proposed theories concerning lifted, turbulent jet flames. He presented the view that stabilization of a lifted flame involves the propagation of a turbulent partially premixed flame at a speed that balances the local stream-wise convective velocity. This description consolidates ideas involving turbulent premixed flame propagation and triple flame (or edge flame) propagation. A substantial number of numerical methods have been proposed for predicting lifted turbulent jet flames. For example, Conditional Moment Closures (CMC) [8, 75],

Probability Density Functions Methods (PDF) [20], and Flamelet Models [12, 23, 104, 111] have been used to predict lifted turbulent reacting jets. Direct numerical simulation (DNS) has also been a useful tool in predicting lifted flames [137]. Recently Mizobuchi et al. [101] presented DNS predictions of a lifted H_2 flame.

Byggstøyl and Magnussen [19] developed a model for flame extinction in chemically reacting turbulent flow based on the Eddy Dissipation Concept. Both lift-off and out conditions were calculated and compared with experimental data by considering infinitely fast chemical reactions. According to this extinction model and the result for the turbulent flame speed, a lifted diffusion flame will be stabilized near the position of the stoichiometric contour where the fine-structure time scale equals the chemical time scale. Gran et al. [52] investigated turbulent reacting flows inside a gas turbine combustion chamber using the same extinction model. Byggstøyl and Magnussen also wrote that the stabilization point will be located at a position where the mean flow velocity is nearly equal to the maximum flame propagation velocity just before the flame is blown off. They also estimated that the burning velocity was of order two times the axial turbulent fluctuations at the base of the flame.

In the present work, Magnussen's Eddy Dissipation Concept (EDC) for turbulent combustion [42, 43, 51, 91] is employed in conjunction with a detailed chemical mechanism to calculate the lifted turbulent H_2/N_2 jet flame in a coflow of products from a lean hydrogen/air combustion. The results from the calculations are compared with experimental data and PDF modeling predictions. Cabra et al. [20] presented both experimental and numerical (EDC and PDF modeling) results of this lifted jet flame. They indicated that the flame was stabilized by turbulent premixed flame propagation by small scale recirculation and mixing of hot products into reactants and subsequent rapid ignition of the mixture. The present work discusses what mechanisms in the EDC model are responsible for predicting lift off in the vitiated coflow burner. In addition, results from employing two other turbulence models are shown. Also, some numerical aspects are discussed. In general, the results indicate that effects (such as turbulence modeling, grid dependencies etc.) influences the prediction of the reactor residence time and hence, the predicted lift-off height. First, the EDC combustion model is discussed. Then the effects of turbulence modeling, grid dependencies and a parametric study are shown. Finally, based upon the present results and discussion, possible flame stabilizing mechanism are discussed.

Experimental Method

The simplified flow of the vitiated coflow burner provides experimental and numerical access to fundamental combustion features of recirculation burners. The combustor (Fig. 6.1.)

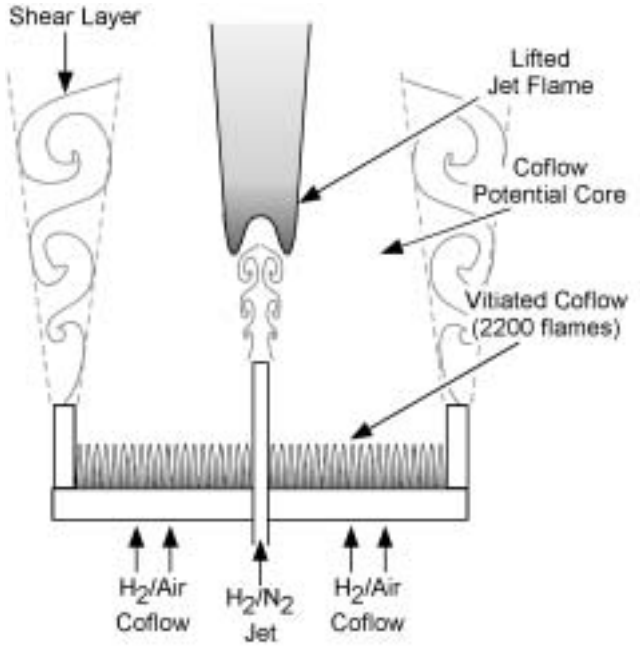

Figure 6.1: Schematic view of the experimental setup [20].

consists of a jet flame in a coaxial flow of hot combustion products from a lean premixed H_2/Air flame (vitiated coflow). The reacting flow associated with the central jet exhibits similar chemical kinetics, heat transfer, and molecular transport as recirculation burners without the recirculating fluid mechanics.

Experiments were conducted on a lifted H_2/N_2 jet flame in a vitiated coflow. (See main data in Table 6.1. For more detailed information, see Cabra et al. [20].) The lift-off height was $H = 10d$ and the height of the flame was $H_F = 30d$, where d is the inner diameter of the fuel-jet nozzle. The coflow flame is stabilized on a perforated disk with 87% blockage. Highly turbulent jet flames with low Damköhler numbers are readily stabilized in this high temperature coflow.

Laser-based multi-scalar experiments were conducted in the Turbulent Diffusion Flame (TDF) Laboratory at the Combustion Research Facility of Sandia National Laboratories, California (USA). Measurements from this advanced laser diagnostic facility are used to produce joint statistics of the temperature and the major and minor species. Experimental uncertainties were estimated by the standard deviations (RMS) of the flat (Hencken) flame measurements; Temperature 1.2%, N_2 3.2%, H_2O 5.4%, OH, 12% and NO 10%. Details

and references of the experimental setup, the calibration techniques, and estimation of uncertainties are presented elsewhere [20].

Modeling

Governing Equations and Turbulence Modeling

The general-purpose CFD code SPIDER with Magnussen's Eddy Dissipation Concept [42, 43, 51, 91] was used in the present calculations of the turbulent jet flame. SPIDER, developed at the Norwegian University of Science and Technology (NTNU), Division of Thermodynamics, in Trondheim (Norway) [98, 99, 100], is a finite-volume (elliptic) code that uses curvilinear non-orthogonal coordinates. In these calculations, a two-dimensional axisymmetric grid was employed. In SPIDER, the turbulent reacting flow is modeled by the Favre-averaged (i.e. mass-weighted Reynolds-averaged) conservation equations for momentum components, energy, and mass of all involved species. Turbulence was modeled by the standard k-ε model [65, 83], a modified k-ε model, the Reynolds-stress-equation model (RSM) by Launder, Reece and Rodi (LRR) [81] and the Reynolds-stress-equation model by Jones and Musonge (JM) [64, 67]. In the modified k-ε model, the constant $c_{\varepsilon 2}$ was 1.83 in the $\widetilde{\varepsilon}$ equation and the turbulence Prandtl-Schmidt numbers σ_{Y_i} and σ_h in the species mass-fraction equations and the enthalpy equation was set to 0.5 instead of 0.7.

The Eddy Dissipation Concept

Magnussen's Eddy Dissipation Concept for turbulent combustion was used to model the mean chemical reaction rate. When detailed chemistry is assumed, the mean chemical reaction rate for a chemical species can be expressed as [51]

$$\overline{R}_i = -\frac{\bar{\rho}\gamma^* \dot{m}^* \chi}{(\gamma^*)^{1/3}}(Y_i^\circ - Y_i^*). \tag{6.1}$$

The model assumes that the reactions occur in the fine structures which are considered as a well-mixed reactor. The superscripts * and $^\circ$ denote the fine structure state and the surrounding fluid state, respectively. The quantities γ^* and $\dot{m}^*$ are the mass fraction of turbulence fine structures and its mass exchange with the surrounding fluid, respectively. They are related to the turbulence-cascade model of the EDC [42, 43] and are expressed as

$$\gamma^* = 9.8 Re_{\mathrm{T}}^{-3/4}, \tag{6.2}$$

$$\dot{m}^* = 2.5\left(\frac{\widetilde{\varepsilon}}{\nu}\right)^{1/2}, \tag{6.3}$$

where $Re_T = \widetilde{k}^2/\nu\widetilde{\varepsilon}$ is the turbulence Reynolds number. The mass exchange is the reciprocal of the fine-structure residence time, $\tau^* = 1/\dot{m}^*$, which is proportional to the Kolmogorov time scale. χ is the fraction of burning fine structures. Gran [49] proposed $\chi = 1$ (for detailed chemistry) which gives an attractive expression for the mean chemical reaction rate in finite-rate chemistry calculations. Y_i° and Y_i^* are the mass fractions into and out of the reactor. The reacting turbulence fine structure is regarded a reactor with the mass balance

$$\frac{dY_i^*}{dt} = \omega_i^* + \nu_r(Y_i^\circ - Y_i^*) \tag{6.4}$$

for each species i. In the present work, the reactor is assumed to have constant pressure and to be adiabatic (i.e. radiative heat transfer is neglected). The reactor mixing rate was taken $\nu_r = (\tau^*)^{-1}$ which corresponds to a perfectly stirred reactor (PSR). $\omega_i^* = R_i^*/\rho^*$ is the specific reaction rate where R_i^* is found from chemical-kinetics data from GRI-Mech 2.11 [11]. These species mass balances were solved for the reactor by integrating to steady state (see [51]).

PDF Method

The model utilizes the joint scalar PDF for composition only and the k-ε turbulence model for a parabolic flow [127]. The turbulent flux and scalar dissipative terms appearing in the PDF transport equation are modeled by a gradient diffusion model and the Curl mixing model [117], respectively. Monte Carlo simulation was used to compute the transport equation for the PDF [22]. Four hundred stochastic particles per grid were used. A 7-step reduced chemistry (6 steps for combustion and 1 for NO formation) was integrated directly in time for each particle.

Present Predictions

Description of the Flow

Lifted turbulent jet diffusion flames are characterized by that the base of the flame is not attached to the burner rim, but is stabilized a distance downstream of the nozzle exit. The highly unsteady region from the rim to the base of the flame (see Fig. 6.1) is called the lift-off height H [111]. In this region no chemical reactions are present, but mixing of reactants and oxidizers occurs. If the jet velocity is low enough, the flame will be attached to the nozzle. By increasing the jet velocity, the flame will lift off from the rim.

Table 6.1: Flame and flow conditions of the jet flame and the coflow.

	Central Jet	Coflow
Volumetric flow of H_2 (standard liter/min)	25	225
Volumetric flow of N_2 (standard liter/min)	75	
Volumetric flow of Air (standard liter/min)		2100
Temperature (K)	305	1047
Mean velocity (m/s)	107	3.5
Reynolds number	23600	18600
Diameter (m)	0.00457	0.21
Equivalence ratio		0.25
Mean Mole Fraction, H_2	0.2537	0.0005
Mean Mole Fraction, N_2	0.7427	0.7532
Mean Mole Fraction, O_2	0.0021	0.1474
Mean Mole Fraction, H_2O	0.0015	0.0989

Computational Mesh and Boundary Conditions

The grid employed in the present calculations (except the parametric study presented in Sec. 6) was a 150×55 mesh (150 points in axial direction and 55 in radial direction). The grid was nonuniform and rectilinear with the grid lines chosen so that the grid lines coincide with the fixed geometric points defined by the fuel tube radius. The grid lines were concentrated in the high shear region between the jet stream and the coflow radially and in the lift-off area axially. The fuel jet was resolved with 10 control volumes and the jet inlet profile was fully developed turbulent pipe flow for the jet and a uniform flow field for the coflow. The inlet coflow turbulence variables $\widetilde{k}$ and $\widetilde{\varepsilon}$ were determined using rough estimates of the integral length scale and turbulence intensity ($l_o = 1$mm and $u' = 0.05\widetilde{u}_{\text{coflow}}$). The computational domain extended radially $r = 12d$ and axially $z = 40d$ from the jet nozzle center. The inlet boundary conditions are shown in Table 6.1. Symmetry conditions were

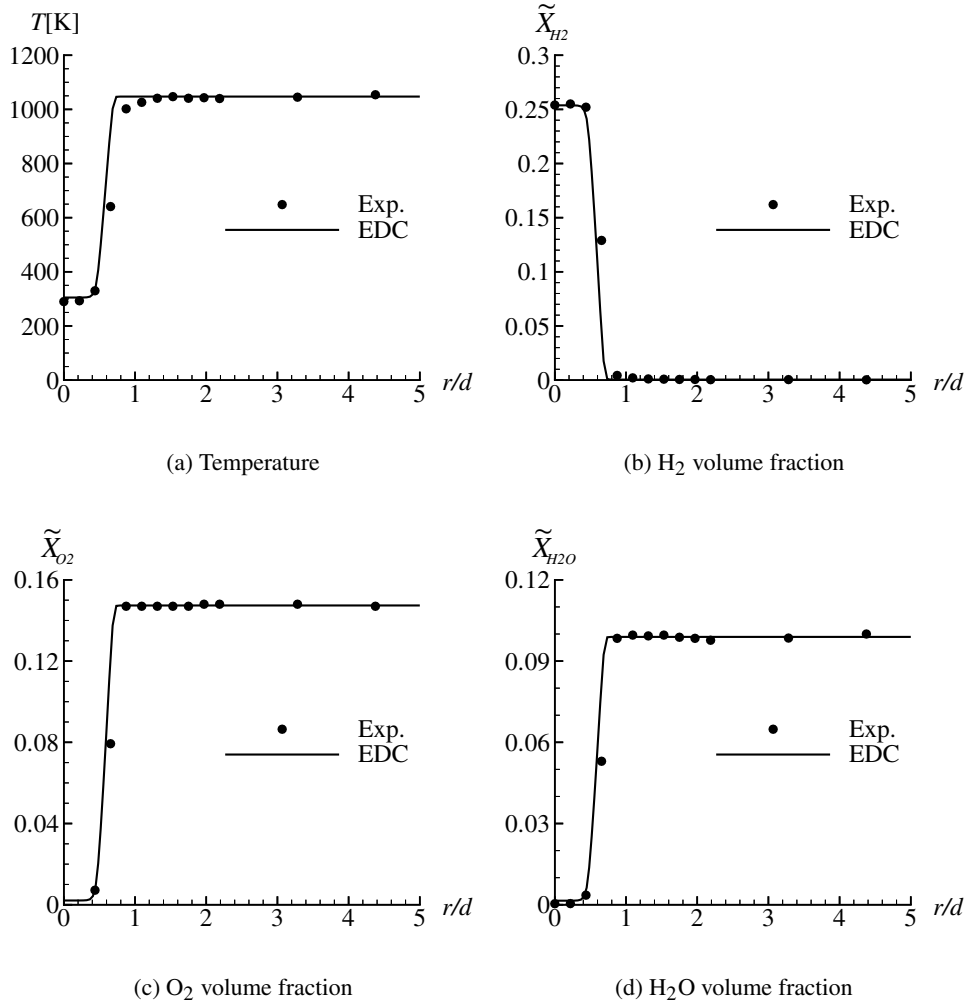

(a) Temperature

(b) H_2 volume fraction

(c) O_2 volume fraction

(d) H_2O volume fraction

Figure 6.2: Radial profiles at axial location $z/d = 1$, 150x55 grid. Experimental values versus EDC predictions with the standard k-ε turbulence model.

applied for the central axis ($r = 0d$), while zero transverse diffusion was applied on the outer boundary ($r = 12d$). Zero diffusion was also assumed at the outlet boundary ($z = 40d$). The calculations were started from an "initial flame" which was the converged steady-state solution of a flame calculated by assuming infinitely fast chemistry. This initial flame was attached to the burner rim. When the finite-rate chemistry calculations start, local exctinction mechanisms in the model are responsible for initially "lifting" the flame off

the rim. The numerically predicted (EDC) boundary conditions versus those measured one nozzle diameter upstream are shown in Fig. 6.2. It can be seen that the boundary conditions for temperature and main species are well captured.

Previous work [105] found the importance of having the mesh clustered outside the nozzle. In the present work it was found that a fine mesh was needed throughout the lift-off area from the nozzle to the base of the flame. A fine grid with 210×70 computational cells was employed to investigate possible grid dependencies. Here, the jet flow was resolved with 15 control volumes and the computational domain was shrinked to $r = 12d$ and $z = 27d$. The calculation with this grid produced insignificant changes in the results compared to the 150×55 case. Therefore, the 150×55 grid was assumed to produce grid-independent results.

Numerical Accuracy

All calculations were performed with a second-order upwind discretization scheme (SOU). However, the results from a first-order power-law scheme (POW) calculation were used as initial field for higher order schemes calculations. This method was used since the POW scheme is less sensitive to poor initial conditions than the SOU.

The different schemes could predict different results. An illustrative example is a calculation made with the JM Reynolds-stress-equation model with SOU and POW. The calculations with the SOU scheme predicted a lifted flame, whereas with the POW scheme the flame was predicted attached to the rim with the exact same boundary conditions and grid resolution. In general, POW will give less error on coarser grids, whilst the SOU will predict results closer to the actual solution on finer grids.

Results and Discussion

The present predictions were compared with the measured temperature and species concentrations contours and the centerline profiles as well as with numerical predictions performed with the PDF model. Centerline measurements were taken from $z/d = 1$ to 34 upstream of the nozzle exit. Radial profiles were obtained at several axial locations ($z/d = 1$, 8, 9, 10, 11, 14, and 26).

Flame Structure and Lift-Off Height

The OH mass fraction, $\widetilde{Y}_{\mathrm{OH}}$, was used as a marker of the average flame lift-off height in both measured and modeled results. Several points were taken in the flame stabilization region to provide adequate resolution for determination of the lift-off height, $H \approx 10d$, which was taken to be the location where the Favre average $\widetilde{Y}_{\mathrm{OH}}$ reaches 600 ppm ($\widetilde{Y}_{\mathrm{OH}} = 6 \cdot 10^{-4}$).

Contour Profiles

Figure 6.3 and 6.5 show the OH and temperature contours from the different models compared to the experimental results. The PDF model with the standard k-ε model yields a lift-off height of $H_{\mathrm{PDF}} \approx 7d$. Using the same k-ε model, EDC predicts $H_{\mathrm{EDC}} \approx 8.5d$, while EDC with the LRR RSM and the modified k-ε model, predicted a shorter lift-off height of $H_{\mathrm{LRR}} \approx 5d$. The JM RSM predicted the lift-off height to be $H_{\mathrm{JM}} \approx 3.5d$. The overall flame shape predicted by the Reynolds-stress-equation models and the modified k-ε model is narrower than that predicted by the standard k-ε model and in better agreement with the measured flame width, even though the lift-off height is more underpredicted.

Axial Profiles

Figure 6.4 and 6.6 compare centerline profiles of mixture fraction, temperature, and the mass fractions of O_2 and OH. Temperature was predicted reasonably well with all models, while the oxygen mass fraction is overpredicted by EDC with the standard k-ε model. The OH centerline mass fraction was generally overpredicted by EDC compared to the measured values (see Figs. 6.4(d) and 6.6(d)). The peak in oxygen seen near $z \approx 14d$ (Fig. 6.4(c)) illustrates the upstream penetration (increased with lift-off height) and subsequent consumption of oxygen by the flame. By presenting an entrainment-rate profile similar to the $\widetilde{Y}_{\mathrm{O2}}$ centerline profile, Han and Mungal [53] observed a similar correlation between mixing and lift-off height. Since the standard k-ε model is known to overpredict turbulence diffusion for round jets [118], the predicted oxygen penetration is much higher than the measured data, as evident by the early (PDF) or high (EDC) centerline $\widetilde{Y}_{\mathrm{O2}}$ peaks and the rapid decay in mixture fraction.

Boundary Conditions

In general, the lift-off height seems to be very sensitive to changes in the jet inlet conditions, while changes in the coflow conditions only predict moderate changes. A bulk profile predicted shorter lift off than a fully developed pipe-flow profile, but this also depends on the estimated turbulence energy dissipations rate $\widetilde{\varepsilon}$ in the plug profile. A fully developed pipe-flow profile was used in all calculations. The pipe flow in the experiments was a fully

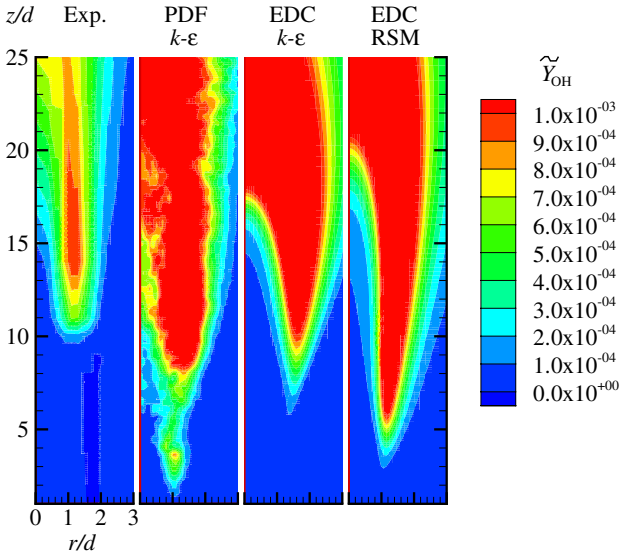

(a) OH mass fraction

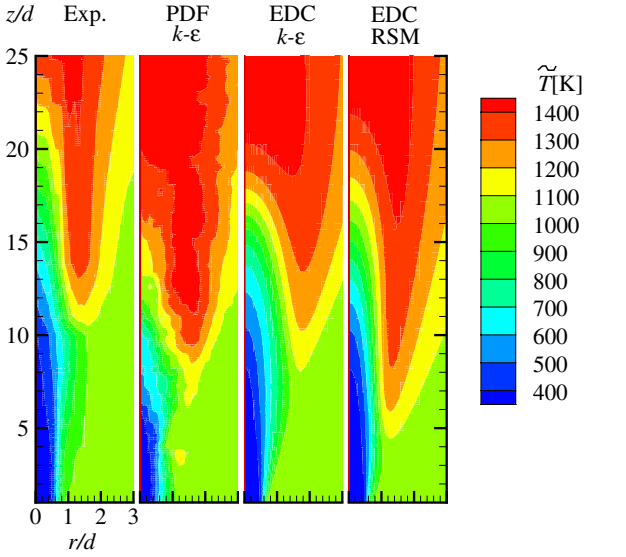

(b) Temperature

Figure 6.3: OH mass fraction and temperature predictions shown from left to right (150×55 grid): Experiments, PDF with standard k-ε model, EDC with standard k-ε model and EDC with LRR Reynolds-stress-equation model.

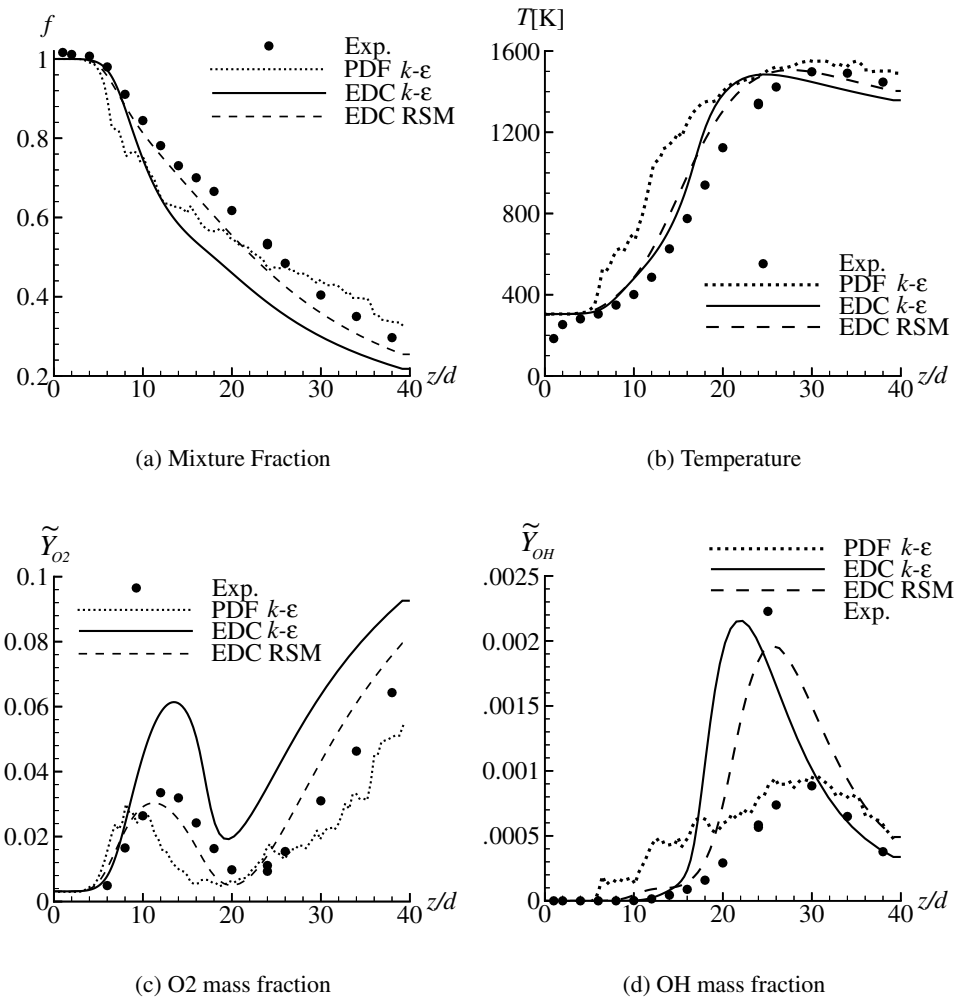

(a) Mixture Fraction

(b) Temperature

(c) O2 mass fraction

(d) OH mass fraction

Figure 6.4: Axial profiles along centerline, 150×55 grid: Experiments, PDF with standard k-ε model, EDC with standard k-ε model and EDC with LRR Reynolds-stress-equation model.

developed turbulent pipe flow with a Reynolds number of 23600. The inlet profile for the computations was calculated through an independent turbulent pipe flow calculation, since experimental values for the mean flow were not measured.

Combustion Modeling

The present study investigates whether EDC, in conjunction with a detailed chemical mechanism (GRI-Mech. 2.11 without reactions involving C), predicts lift off in a partially premixed turbulent jet flame. In previous work, when a fast chemistry assumption was employed, an extinction model was applied [19, 52]. The mean chemical reaction term ($\overline{R}_i$ in Eq. 6.1) was then set to zero if the computed residence time scale was below an estimated chemical time scale. According to this extinction model, a lifted diffusion flame will stabilize at the position where the turbulence fine structure time scale equals the chemical time scale. The Eddy Dissipation Concept assumes that the extinction (and autoignition) processes occur in the small-scale turbulent structure (the fine structure). In the present calculations, the detailed chemical mechanism will decide whether extinction or autoignition occurs or not. This can be interpreted as a competition between chemistry and turbulence micro-scalar mixing in the reactor (which are represented through the first and second term on the right-hand side of Eq. 6.4). When τ^* takes a value below a certain limit (a certain chemical time scale), GRI-Mech. reactions in the PSR ceases. The steady-state solution of Eq. 6.4 is then $Y_i^* = Y_i^\circ$ and hence $\overline{R}_i = 0$ in Eq. 6.1.

The predicted lift-off heights with the EDC method and the PDF method (see Fig. 6.3) are not very different ($H \approx 8.5d$ with the EDC versus $H \approx 7d$ with the PDF). The simulations with the EDC were performed with a 2D elliptic flow solver in an axisymmetric geometry, while the PDF predictions were computed with a 1D Parabolic solver. Both approaches seem to predict the flame reasonably well.

Effects of Turbulence Modeling

Some effects of employing different turbulence models are shown in Figs. 6.5 and 6.6. These figures show predictions with the modified k-ε model, the RSM LRR model and the RSM JM model compared to the standard k-ε model. The predictions of the lift-off height by the modified k-ε model and the RSM turbulence models were consistently lower than those by the standard k-ε model (see Fig. 6.5). The modified k-ε model predicted a lift-off height close to that predicted with the RSM LRR model ($H \approx 5d$). The reason for this was probably that the different turbulence models predicted different residence times τ^*. The models predicted different mixing and hence different values of $\widetilde{k}$ and $\widetilde{\varepsilon}$. This resulted in

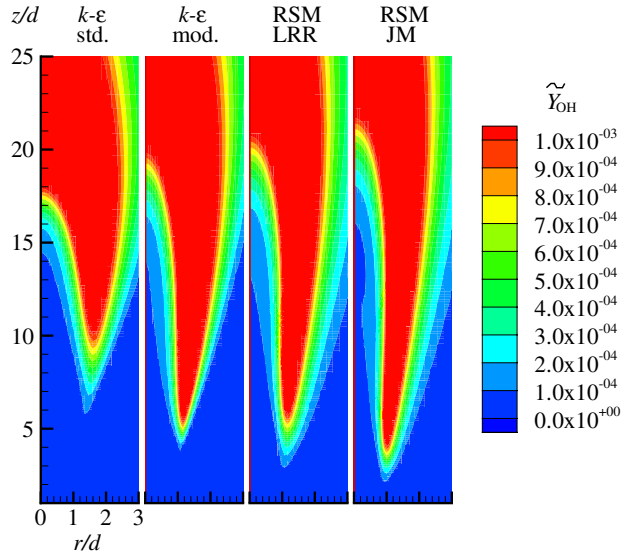

(a) OH Mass fraction

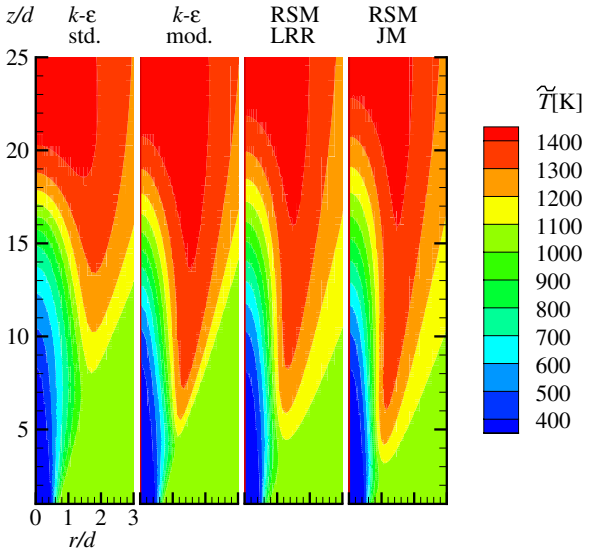

(b) Temperature

Figure 6.5: OH mass fraction and temperature predictions (150×55 grid): EDC calculations with different turbulence models.

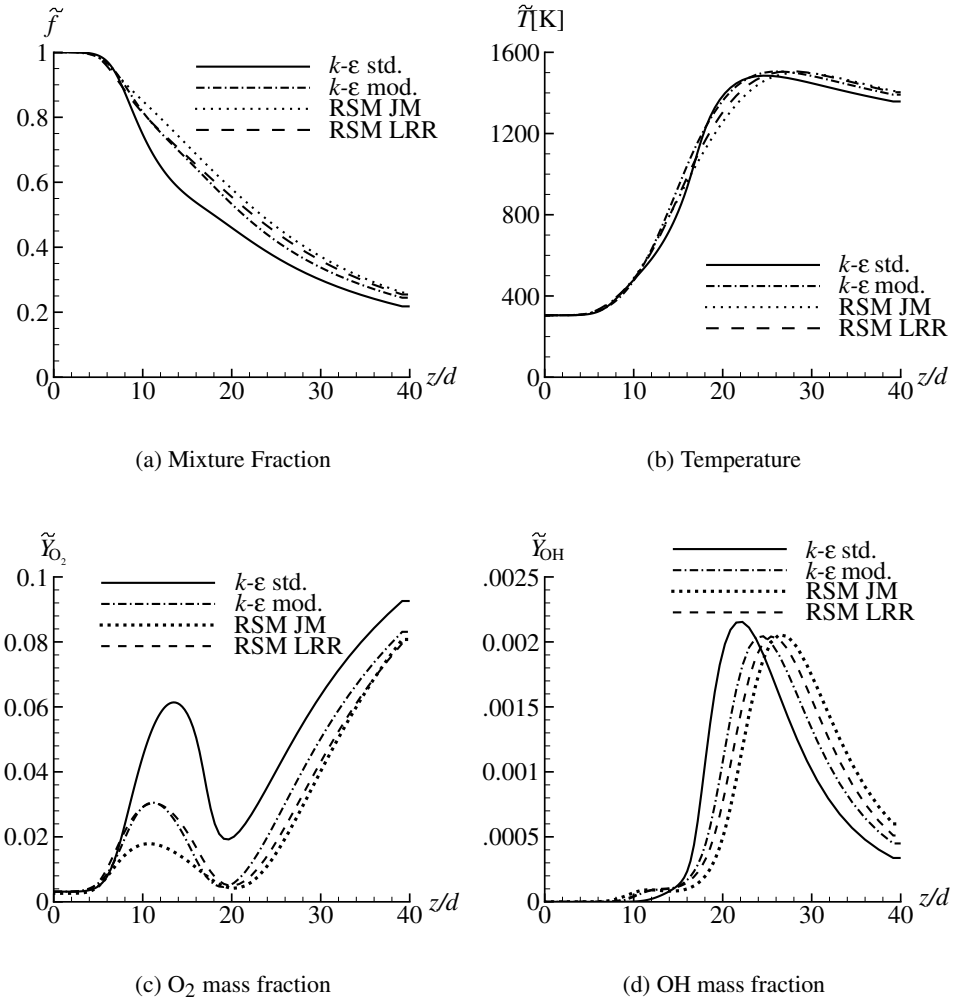

(a) Mixture Fraction

(b) Temperature

(c) O_2 mass fraction

(d) OH mass fraction

Figure 6.6: Axial profiles along centerline (150×55 grid): EDC calculations with different turbulence models.

a different computed residence time, which can be seen in Fig. 6.7. Calculations with the standard k-ε model, which predicted the largest lift-off height, predicted the lowest residence time. The same tendency was also found in previous work performed by Myhrvold et al. [105]. There, it was found that the standard k-ε model, predicted extinction (blow off), while the RSM did not. This was indicated by that the RSM predicted a higher residence time than the k-ε model. In that case, the flame was not supposed to blow off.

The centerline profiles for the different turbulence models show the results of the different predicted turbulence diffusion between the models (see Fig. 6.6). The standard k-ε model predicted more turbulence diffusion than the other models, which previously mentioned, led to the different predicted lif-off heights. The lifted flame predicted by the standard k-ε diffused more O_2 to the centerline which can be seen from both the mixture fraction variable (Fig. 6.6(a)) and the O_2 mass fraction variable (Fig. 6.6(c)). A higher concentration of O_2 consequently leads to a higher concentration of OH at the centerline (Fig. 6.6(d)).

A Parametric Study

A parametric study was conducted to explore the sensitivity of the predicted lift-off height to boundary conditions, turbulence modeling, and grid resolution (see Table 6.2). The base case employed the standard k-ε model with a mesh of 60×55 (axial $\times$ radial) with grids clustered near the jet exit, due to the long computational time with the 150×55 grid. An increase in coflow turbulence parameters led to no change in the predicted lift-off height, whereas an increase in coflow velocity from 3.5 m/s to 10 m/s led to an increased lift-off height (H/d) from 4 to 6. An increase in the jet velocity from 107 m/s to 120 m/s, increased the lift-off height from 4 to 5. A 50 % increase in the jet values of $\widetilde{k}$ and $\widetilde{\varepsilon}$ had smaller effect (increased the lift-off height from 4 to 4.5). The parametric study showed that errors in the inlet conditions could lead to large errors in the predicted lift-off height. The nozzle wall was also modeled, which seemed to have no effect on the predicted lift-off height. Applying the base case with LRR or JM turbulence models decreased the lift-off height from 4 to 2 and 1.5 respectively. The same tendencies were seen on the finer 150×55 grid where the standard k-ε model predicted the lift-off height to be 8.5, while applying the LRR or JM turbulence models decreased the lift-off height from 5 and 3.5 respectively. The calculations with the 150×55 grid was found to produce grid-independent results (see Sec. 6).

Grid Dependencies

Calculations with the coarser 60×55 grid predicted a shorter lift-off height than with 150×55 grid. This seemed to be a direct consequence of the different predicted turbu-

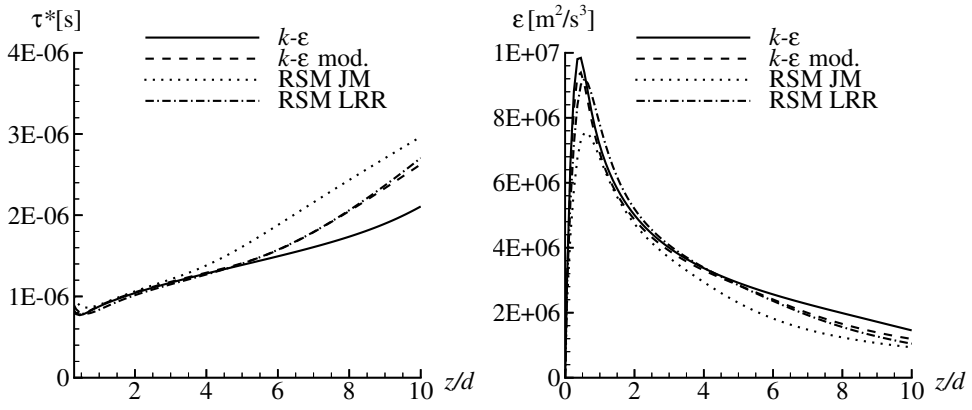

(a) Residence time $r/d = 0.5$

(b) Turbulence energy dissipation rate $r/d = 0.5$

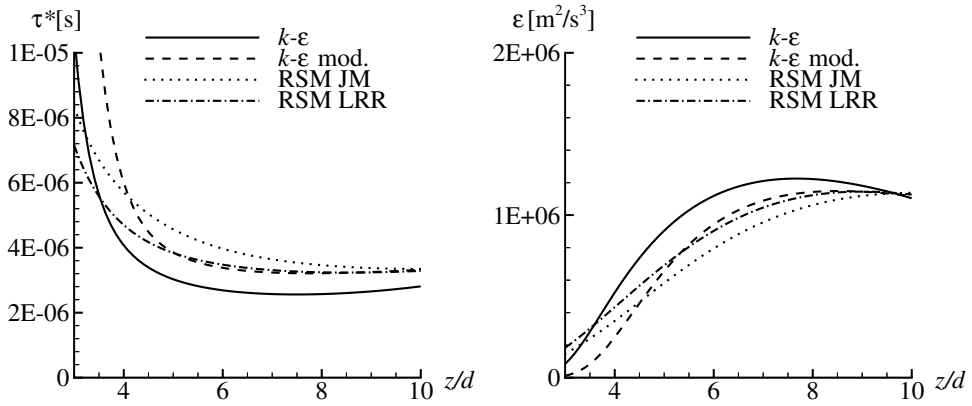

(c) Residence time $r/d = 1.0$

(d) Turbulence energy dissipation rate $r/d = 1.0$

Figure 6.7: Residence time τ^* and turbulence energy dissipation rate at radial location $r/d = 0.5$ and $r/d = 1.0$ with the different turbulence models (150×55 grid).

URN:NBN:no-7265

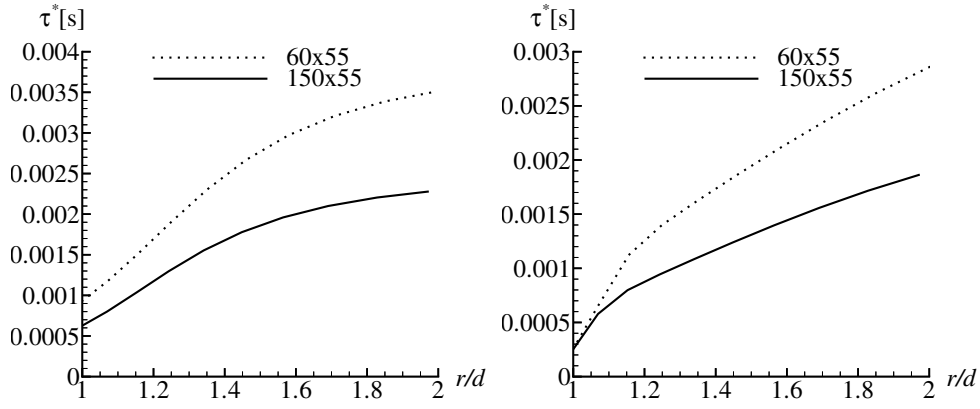

(a) τ^* at $z/d = 0.4$

(b) τ^* at $z/d = 2$

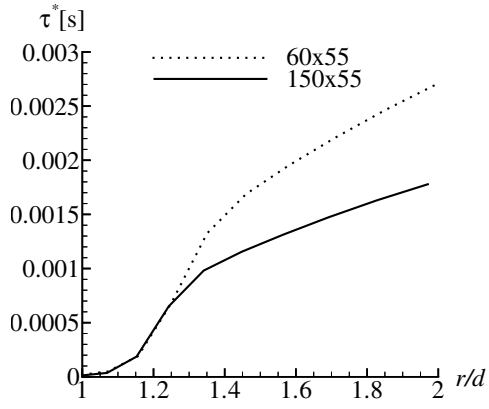

(c) τ^* at $z/d = 3$.

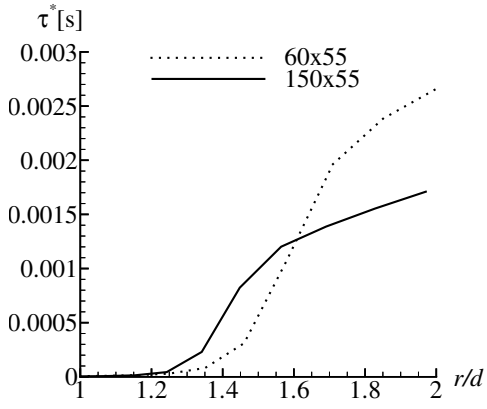

(d) τ^* at $z/d = 4$.

Figure 6.8: Radial profiles of the residence time with different grid resolutions at different axial locations.

Table 6.2: Parametric study of the effect of different conditions on the lift-off height.

Case	Case Description	H
Benchmark	k-ε turbulence model, fully developed jet pipe flow	4
1	Increased coflow turbulence ($l = 3$ mm,$u'/\widetilde{u}_{\text{Coflow}} = 10\%$)	4
2	Increased coflow velocity ($\widetilde{u}_{\text{Coflow}} = 10$ m/s)	6
3	Increased jet velocity ($\widetilde{u}_{\text{Jet}} = 120$ m/s)	5
4	Increased jet turbulence (50% in $\widetilde{k}$ and $\widetilde{\varepsilon}$)	4.5
5	Nozzle Wall modeled	4
6	Reynolds-stress-equation model (LRR)	2
7	Reynolds-stress-equation model (JM)	1.5
8	Standard k-ε model, 150×55 grid	8.5
9	Modified k-ε model, 150×55 grid	5
10	Reynolds-stress-equation model (LRR), 150×55 grid	5
11	Reynolds-stress-equation model (JM), 150×55 grid	3.5

lence fields and residence time, which can be seen in Fig. 6.8. The figures show radial profiles of the residence time in the non-reacting lift-off area at different axial locations for EDC calculations with the standard k-ε model. The calculations with the coarser grid resolution predicted a higher residence time than with the finer grid resolution. Differences in the predicted turbulence energy dissipation rate led to differences in the predicted residence time and hence differences in the predicted lift-off height.

Flame Stabilization

Being able to control lift off and stabilizing a flame is desirable and different methods are applied in practical combustion devices. The use of a pilot jet flame or controlled recirculation of hot products to the flame base are examples of such methods [26]. Premixed flame propagation and recirculation of hot products are stabilizing mechanisms discussed

Table 6.3: 2 $\times$ stream-wise velocity fluctuation and mean velocity at the stabilization point in EDC calculations.

Turbulence Model	$2u''$ (m/s)	$\widetilde{u}$ (m/s)
Standard k-ε model	16.2	12.5
Modified k-ε model	8	6
LRR Reynolds-stress-equation model	15.6	10
JM Reynolds-stress-equation model	13.8	8.3

in literature [26, 111]. Peters [111] also discussed triple flames as a key element in partially premixed flames. Montgomery et al. [102] reported on transient behavior of lifted turbulent jet flames. From transient numerical calculations of lifted methane-air jet flames (2D axisymmetrical DNS calculations), both the axial and radial location of the stabilization point varied in time with 1-2 cm. The flame structure is highly dependent on the conditions of the jet and the coflow, such as temperature, composition, and Reynolds number. Pitts [112] reported that the composition mixture at the base of a lifted jet flame had a highly intermittent behavor. In SPIDER, with EDC in conjunction with detailed chemistry, the flame will stabilize at a point where the turbulence micro-scalar mixing and chemistry are in balance (see the Combustion Modeling section). Upstream of the stabilization point, a low residence time will prevent reactions from taking place. Initially, the calculations start from a flame calculated from a fast-chemistry assumption. This flame is attached to the burner. During computational time, local extinction effects are responsible for "lifting" the flame from the rim. However, the lifted steady-state solution (calculated with detailed chemistry) is the only state from where indications or conclusions about the actual flame can be drawn, but, the initial conditions and the iterative procedure can be useful to discuss possible mechanisms in the EDC model. Local extinction in the PSR during the iterative procedure serves to quench the already existing reactions from the nozzle up to the stabilization point. At the base of the flame, no local extinction occur due to the increasing residence time (see the Combustion Modeling section). Thus, the present flame will stabilize at the upstream location above the nozzle where local extinction of the initial flame no longer takes place. The flame at the stabilization point will be maintained by the already existing combustion processes.

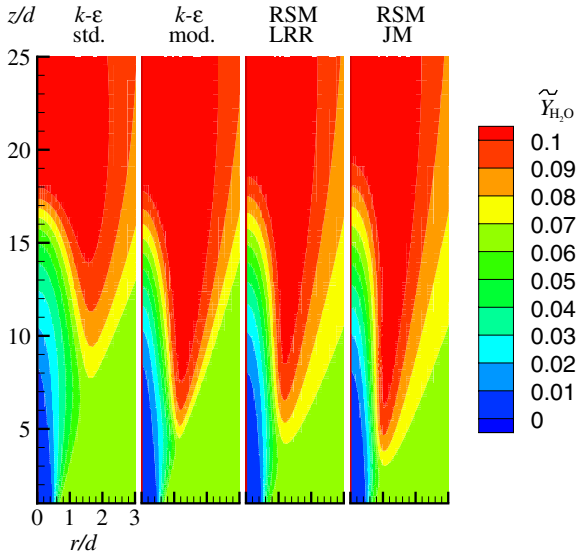

Figure 6.9: H_2O contour with the different turbulence models.

Flame stabilization for the present flame have previously been discussed by Cabra et al. [20]. It was reported that the flame could be stabilized by turbulent premixed flame propagation due to small-scale recirculation and mixing of hot products into reactants and subsequent rapid ignition of the mixture. Some of the investigations made of the presents predictions further supports this theory. Based on the results from the EDC calculations, one possible reason for stabilizing the flame may be explained from the transport of hot combustion products to the base of the flame. If transport of hot products is responsible for maintaining combustion at the base of the flame, then there should be a considerable amount of products upstream of the stabilization point. This transport is carried out by the difference between convective and diffusive terms determined by the turbulence stresses (products of velocity fluctuations). Figure 6.9 shows contours of water around the base of the flame showing some amounts at a location up to 1 nozzle diameter upstream of the stabilization point. This amount of water may be present due to turbulence diffusion. The question is whether this is sufficient for maintaining combustion of the mixture at the base of the flame. In the combustion model, transport of hot products to the base of the flame leads to an increasing amount of energy and mixing of hot products with reactants in the reactor. If this transport is large enough, this will probably lead to flame propagation. If the flame is stabilized by turbulent transport of products to the flame base with subsequent premixed flame propagation, then,

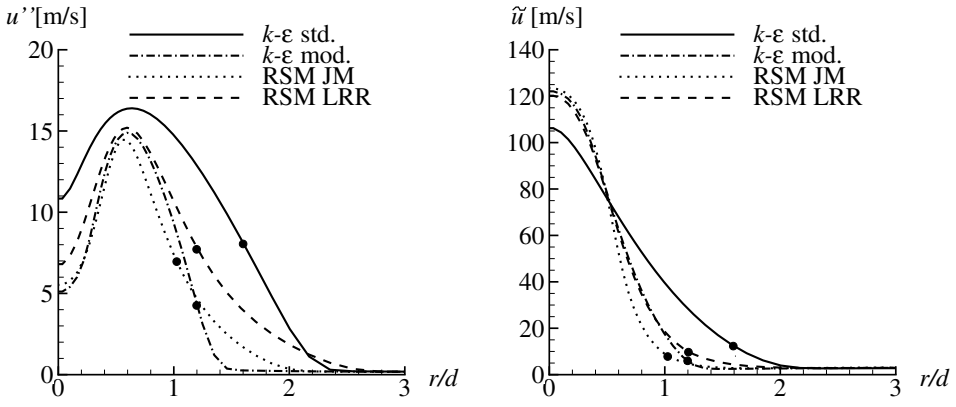

(a) Stream-wise velocity fluctuations u''

(b) Mean stream-wise velocity $\widetilde{u}$

Figure 6.10: Stream-wise velocity fluctuation and mean stream-wise velocity at the stabilization point. The dot indicates the radial location of the stabilization point. Note that there are differences in the axial locations.

according to Byggstøyl and Magnussen [19], the flame base should be located at a point where the mean axial velocity equals the turbulent burning velocity. They estimated that the burning velocity was two times the axial turbulent fluctuations at the base of the flame ($S_T \sim 2u''$). Profiles of the axial turbulent fluctuations and the mean stream-wise velocity for the present calculations with the different turbulence models are shown in Fig. 6.10. The numerical values are shown in Table 6.3. The predictions from all calculations seem to be in reasonable accordance with the model of Byggstøyl and Magnussen.

Autoignition has also been discussed as a possible stabilization mechanism. The parabolic PDF simulation did not include flame propagation as the stabilization mechanism as the downstream information was not allowed to propagate back upstream. Yet, the PDF seems to yield reasonable results leading us not to exclude autoignition as the flame stabilization mechanism.

Conclusions

The present work investigated the numerical effort set forth to model a lifted turbulent hydrogen/nitrogen jet flame in a coflow of hot gases. Most results presented were calculated using Magnussens's Eddy Dissipation Concept (EDC) for turbulent combustion, and the main discussion is concerned around the EDC. However, the EDC predictions were compared to numerical results from a PDF calculation using a parabolic solver, and experimental results. The Eddy Dissipation Concept (EDC) was used in conjunction with detailed chemistry in the CFD code SPIDER which is an elliptic fluid flow solver. In all calculations, an axisymmetric two-dimensional geometry was employed. The results show that the Eddy Dissipation Concept is capable of reproducing the complicated nature of a lifted turbulent jet flame. Four different turbulence models was used in conjunction with EDC. The standard k-ε model, a modified k-ε model, the Reynolds-stress-equation model (RSM) of Launder, Reece & Rodi (LRR) and, the RSM of Jones & Musonge (JM). With the k-ε model, the predicted lift-off height (H/d) was about 8.5, while the modified k-ε model and the LRR RSM predicted the lift-off height to be about 5 . The JM RSM predicted the lift-off height to be about 3.5.

For the EDC predictions, the flame stabilizes at a point where there is balance between chemistry and turbulent micro mixing in the reactor model. The flame is, during computational time, initially "lifted " due to local extinction effects since the detailed chemistry calculations start from an attached flame. The lifted flame (at steady state) is maintained at the stabilization point by the already existing combustion processes since local extinction is prevented due to the increasing residence time.

In summary, the main findings from the present work with the EDC are:

- The Eddy Dissipation Concept in conjunction with detailed chemistry is capable of predicting a lifted turbulent jet flame.
- A high grid resolution from the nozzle throughout the base of the flame seems to be important for best numerical representation of this flame.
- The standard k-ε model predicted a lift-off height closer to the experimentally predicted value than the Reynolds-stress-equation model. On the other hand, the Reynolds-stress-equation model predicted a flame shape (axial profiles and flame length) which was in better agreement with the measured flame.
- The flame predicted by the EDC stabilizes at an upstream location where turbulent micro mixing and chemistry are in balance.

URN:NBN:no-7265

- The presents predictions with the EDC model indicate that transport of hot products to the flame base, may be a possible stabilizing mechanism for the present flame. Some rough estimations suggest that flame propagation associated with this transport of hot products could be possible. The PDF calculations indicate that autoignition can also be a possible mechanism stabilizing the flame.

Acknowledgements

This work was supported by the Research Council of Norway.

The research by R. Cabra and J.-Y. Chen was part of a project supported by NASA Glenn Research Center Contract NAG3-2103 (USA).

URN:NBN:no-7265

URN:NBN:no-7265

Chapter 7

A second-moment closure for near-wall flows

7.1 Introduction

Detailed description of the anisotropic behavior of the Reynolds stresses allows better understanding of turbulent reacting boundary-layer flows. The best compromise between computer capabilities and model performance for description of the Reynolds stresses today, seems to be found in the Reynolds-stress-equation (RSE) models (second-moment closures). The modeling of the Reynolds-stress equations (Eq. 2.28) was described in detail in Chapter 3. The present chapter presents and discusses the implementation and test of a low-Reynolds-number second-moment closure by comparing predictions against DNS data from Kim et al. [74]. The model was first introduced by Craft and Launder [34] and later by Craft [30] with some modifications. A special feature is that it does not include so called "wall normals" (see Sec. 3.2.2). Hence, it will be more convenient for use in cases with complex geometries. Instead of computing the distance normal to a wall, the model employs normalized length-scale gradients which indicate the direction where strong inhomogeneity exists. This model may be attractive for use in conjunction with SPIDER (see Chapter 5) in which flows with complex geometries may be calculated. The present work was intended to be a first step in a process of computing a reacting wall flow with a full low-Reynolds-number second-moment closure. Some of the modifications in the Craft model were aimed at improving backward-facing-step flow, free surface flow, and impinging jet flow. These modifications were not implemented at the present stage.

The groups of Hanjalić and Launder have been developing second-moment closures for

more than three decades. Hanjalić and Launder [56, 57] and Launder, Reece and Rodi [81] presented early proposals of closing the Reynolds-stress equations. Gibson and Launder [46] later developed wall-damping terms based on the proposal by Shir [126] to account for pressure fluctuations normal to a solid surface and included them into the pressure-strain model. The Gibson and Launder approach is often referred to as the "Basic Model" [78]. One of the shortcomings of the closures at that time was that they failed to predict that turbulent flow approaches two-dimensional flow close to a wall. Fu (Ph.D. thesis, according to Craft [30]) developed a *realizable* model, which the later models from the Launder group are based upon. The major improvement between the realizable model and the previous models, was the adoption of an alternative expression for the pressure-fluctuation term, and the introduction of Lumley's flatness parameter [88], making the models follow the two-component limit towards the wall (see Sec. 3.2.2). The present model by Craft [30] was first developed by Craft and Launder [34] and was based on the work of Launder and Tselepidakis [85] and Launder and Li [80].

7.2 The closure

The exact Reynolds-stress transport equations (Eq. 2.28) was described in Chapter 2 and the modeling part was described in Chapter 3. These equations can be rewritten in symbolic form as

$$C_{ij} = P_{ij} + D_{ij,\mathrm{v}} + D_{ij,\mathrm{t}} + \Pi_{ij} - \varepsilon_{ij}, \tag{7.1}$$

where C_{ij}, P_{ij}, $D_{ij,\mathrm{v}}$ and ε_{ij} are given by Eq. 2.28. The pressure-strain correlation term Π_{ij} was in Eq. 2.28 split into a redistributive and a pressure diffusion part as

$$\Pi_{ij} = -\frac{1}{\overline{\rho}}\left(\overline{u_i'\frac{\partial p'}{\partial x_j}} + \overline{u_j'\frac{\partial p'}{\partial x_i}}\right) = \underbrace{\frac{1}{\overline{\rho}}\overline{p'\left(\frac{\partial u_i'}{\partial x_j} + \frac{\partial u_j'}{\partial x_i}\right)}}_{\Phi_{ij}} \underbrace{-\frac{1}{\overline{\rho}}\left(\frac{\partial \overline{p'u_i'}}{\partial x_j} + \frac{\partial \overline{p'u_j'}}{\partial x_i}\right)}_{D_{ij}^{\mathrm{p}}}, \tag{7.2}$$

where the pressure diffusion part D_{ij}^{p} was put into the turbulence diffusion term D_{ij}^{t}. Craft and Launder [34] employed a non-conventional way of splitting the pressure correlation term. They split Π_{ij} as

$$\Pi_{ij} = \Phi_{ij}^{*} + d_k^{\mathrm{p}}\frac{\overline{u_i'u_j'}}{k}, \tag{7.3}$$

where

$$d_k^{\mathrm{p}} = -\frac{1}{\overline{\rho}}\frac{\partial(\overline{p'u_k'})}{\partial x_k} \tag{7.4}$$

is pressure diffusion of turbulence kinetic energy. The motivation for this split was that Φ^*_{ij}, unlike Φ_{ij}, shows the same qualitative behavior for near-wall flows and free-surface flows. Also, it enables detailed modeling of the pressure diffusion part which is present near a wall (whereas it is zero for homogeneous flows). When the splitting in Eq. 7.3 is adopted, the turbulence diffusion term is given by

$$D_{ij,\mathrm{t}} = \frac{\partial}{\partial x_k}\left(-\overline{u'_i u'_j u'_k}\right). \tag{7.5}$$

As in Eq. 2.28, the terms $D_{ij,\mathrm{t}}$, Π_{ij}, and ε_{ij} in Eq. 7.1 require modeling to close the equations. The modeling practice of these terms is described below. These models are identical to those presented by Craft [30] unless otherwise noted. For a more detailed description, see Craft and Launder [30, 34].

7.2.1 The turbulence diffusion term, $D_{ij,\mathrm{t}}$

To model the turbulence diffusion term, Craft [30] solved a balance equation for the triple correlation. The diffusion model adopted in the present work was a modification of the isotropic model in Eq. 3.10 proposed by Shir [126]

$$-\overline{u'_i u'_j u'_k} = C_\mu f_\mu \frac{k}{\varepsilon} k \frac{\partial \overline{u'_i u'_j}}{\partial x_k}, \tag{7.6}$$

where f_μ is the Reynolds-number function proposed by Launder and Sharma [82] given by Eq. 8.6. The modified Shir model was adopted for its simple form. The different model practice is discussed later (see Sec. 7.4.3).

7.2.2 The pressure correlations, Π_{ij}

The redistributive part Φ^*_{ij} was modeled as

$$\Phi^*_{ij} = \Phi^*_{ij1} + \Phi^*_{ij2} + \Phi^{\mathrm{inh}}_{ij1} + \Phi^{\mathrm{inh}}_{ij2}, \tag{7.7}$$

where

$$\Phi^*_{ij1} = -C_1 \widehat{\varepsilon}\left[a_{ij} + C'_1\left(a_{ik}a_{kj} - \frac{1}{3}A_2\delta_{ij}\right)\right] - \widehat{\varepsilon} f'_A a_{ij}, \tag{7.8}$$

$$
\begin{aligned}
\Phi^{*}_{ij2} = & -0.6(P_{ij} - \frac{1}{3}\delta_{ij}P_{kk}) + 0.3a_{ij}P_{kk} \\
& - 0.2\left[\frac{\overline{u'_k u'_j}\;\overline{u'_l u'_i}}{k}\left[\frac{\partial \overline{u}_k}{\partial x_l} + \frac{\partial \overline{u}_l}{\partial x_k}\right] - \frac{\overline{u'_l u'_k}}{k}\left[\overline{u'_i u'_k}\frac{\partial \overline{u}_j}{\partial x_l} + \overline{u'_j u'_k}\frac{\partial \overline{u}_i}{\partial x_l}\right]\right] \\
& - C_2[A_2(P_{ij} - D_{ij}) + 3a_{mi}a_{nj}(P_{mn} - D_{mn})] \\
& + C'_2\left\{\left(\frac{7}{15} - \frac{A_2}{4}\right)(P_{ij} - \frac{1}{3}\delta_{ij}P_{kk})\right. \\
& + 0.1[a_{ij} - \frac{1}{2}(a_{ik}a_{kj} - \frac{1}{3}\delta_{ij}A_2)]P_{kk} - 0.05a_{ij}a_{lk}P_{kl} \\
& + 0.1\left[\left(\frac{\overline{u'_i u'_m}}{k}P_{mj} + \frac{\overline{u'_j u'_m}}{k}P_{mi}\right) - \frac{2}{3}\delta_{ij}\frac{\overline{u'_l u'_m}}{k}P_{ml}\right] \\
& + 0.1\left[\frac{\overline{u'_l u'_i}\;\overline{u'_k u'_j}}{k^2} - \frac{1}{3}\delta_{ij}\frac{\overline{u'_l u'_m}\;\overline{u'_k u'_m}}{k^2}\right] \times \left[6D_{lk} + 13k\left[\frac{\partial \overline{u}_l}{\partial x_k} + \frac{\partial \overline{u}_k}{\partial x_l}\right]\right] \\
& \left. + 0.2\frac{\overline{u'_l u'_i}\;\overline{u'_k u'_j}}{k^2}(D_{lk} - P_{lk})\right\}, \qquad (7.9)
\end{aligned}
$$

$$
\begin{aligned}
\Phi^{\mathrm{inh}}_{ij1} = & f_{\mathrm{w}1}\frac{\varepsilon}{k}\left(\overline{u'_l u'_k}d^A_l\delta_{ij} - \frac{3}{2}\overline{u'_i u'_k}d^A_j - \frac{3}{2}\overline{u'_j u'_k}d^A_i\right)d^A_k \\
& + f_{\mathrm{w}2}\frac{\varepsilon}{k^2}\overline{u'_l u'_n}\left(\overline{u'_n u'_k}d^A_k\delta_{ij} - \frac{3}{2}\overline{u'_i u'_n}d^A_j - \frac{3}{2}\overline{u'_j u'_n}d^A_i\right)d^A_l \\
& + f_{\mathrm{w}3}\nu\left(a_{il}\frac{\partial\sqrt{k}}{\partial x_l}\frac{\partial\sqrt{k}}{\partial x_j} + a_{jl}\frac{\partial\sqrt{k}}{\partial x_l}\frac{\partial\sqrt{k}}{\partial x_i} - \frac{2}{3}a_{nl}\frac{\partial\sqrt{k}}{\partial x_l}\frac{\partial\sqrt{k}}{\partial x_n}\delta_{ij} - \frac{4}{3}a_{ij}\frac{\partial\sqrt{k}}{\partial x_l}\frac{\partial\sqrt{k}}{\partial x_l}\right) \\
& + f'_{\mathrm{w}1}\frac{k^2}{\varepsilon}\left(\overline{u'_k u'_l}\frac{\partial\sqrt{A}}{\partial x_k}\frac{\partial\sqrt{A}}{\partial x_l}\delta_{ij} - \frac{3}{2}\overline{u'_i u'_k}\frac{\partial\sqrt{A}}{\partial x_k}\frac{\partial\sqrt{A}}{\partial x_j} - \frac{3}{2}\overline{u'_j u'_k}\frac{\partial\sqrt{A}}{\partial x_k}\frac{\partial\sqrt{A}}{\partial x_i}\right), \qquad (7.10)
\end{aligned}
$$

$$
\Phi^{\mathrm{inh}}_{ij2} = f_I k\frac{\partial \overline{u}_l}{\partial x_n}d_l d_n\left(d_i d_j - \frac{1}{3}d_k d_k\delta_{ij}\right), \qquad (7.11)
$$

$$
D_{ij} = \left(\overline{u'_i u'_k}\frac{\partial \overline{u}_k}{\partial x_j} + \overline{u'_j u'_k}\frac{\partial \overline{u}_k}{\partial x_i}\right), \qquad (7.12)
$$

$$
\widehat{\varepsilon} = \varepsilon - 2\nu\left(\frac{\partial\sqrt{k}}{\partial x_j}\right)^2. \qquad (7.13)
$$

Table 7.1: Coefficients in the redistribution term of Π_{ij}.

C_1	C_1'	C_2
$3.1 f_A f_{R_\mathrm{T}} A_2^{0.5}$	1.1	$\min\left(0.55, A^{1.5}\right)$
f_A	f_A'	C_2'
$\left(\frac{A}{14}\right)^{0.5}$ if $A < 0.05$ $\frac{A}{7^{0.5}}$ if $0.05 < A < 0.7$ $A^{0.5}$ if $A > 0.7$	$A^{0.5} f_{R_\mathrm{T}} + A(1 - f_{R_\mathrm{T}})$	$\min\left(0.6, A^{1.5}\right)$
$f_{\mathrm{w}1}$	$f_{\mathrm{w}2}$	$f_{\mathrm{w}3}$
$0.4 + 1.6 f'_{R_\mathrm{T}}$	$0.1 + 0.8 A_2 f''_{R_\mathrm{T}}$	$2.5 A^{0.5}$
$f'_{\mathrm{R_T}}$	$f''_{\mathrm{R_T}}$	f_{R_T}
$\min\left(1, \max\left(0, 1 - \frac{(R_\mathrm{T}-55)}{20}\right)\right)$	$\min\left(1, \max\left(0, 1 - \frac{(R_\mathrm{T}-50)}{85}\right)\right)$	$\min\left(\frac{R_\mathrm{T}}{160}, 1\right)$

The "normalized length-scale gradients" introduced by Craft and Launder [34] are defined as

$$d_i = \frac{N_i}{0.5 + (N_k N_k)^{0.5}}, \quad \text{where} \quad N_i = \frac{\partial\left(k^{1.5}/\varepsilon\right)}{\partial x_i}, \tag{7.14}$$

$$d_i^A = \frac{N_i^A}{0.5 + (N_k^A N_k^A)^{0.5}}, \quad \text{where} \quad N_i^A = \frac{\partial\left(k^{1.5} A^{0.5}/\varepsilon\right)}{\partial x_i}. \tag{7.15}$$

a_{ij} is defined by Eq. 3.22, and A, A_2, and A_3 are defined by Eqs. 3.23–3.24. The model coefficients are given in Table 7.1. In addition, $f'_{\mathrm{w}1} = 0.22$ and $f_I = 2.5 f_A$. The coefficients C_2 and C_2' were taken from the Craft and Launder model [34], since the expressions from Craft [30] for C_2 and C_2' were specially tuned for backward-facing-step flow. The final term in $\Phi_{ij1}^{\mathrm{inh}}$ was designed for free-surface flow, whereas the $\Phi_{ij2}^{\mathrm{inh}}$ term was designed for impinging jet flows. These terms were in the present work not included in Φ_{ij}^*. Finally, the correlation between fluctuating pressure and velocity in the pressure-diffusion term was modeled as

$$\overline{p' u_k'} = -\overline{\rho}(0.5 d_k + 1.1 d_k^A)(\nu \varepsilon k A A_2)^{1/2} \times \left[C_{p\mathrm{d}1} A_2 + C_{p\mathrm{d}2} R_\mathrm{T}^{-1/4} \exp(-R_\mathrm{T}/40)\right], \tag{7.16}$$

where $C_{p\mathrm{d}1} = 1.0 + 2.0\exp(-R_\mathrm{T}/40)$, and $C_{p\mathrm{d}2} = 0.4$.

7.2.3 The dissipation tensor, ε_{ij}

The dissipation tensor was modeled as

$$\varepsilon_{ij} = (1-f_\varepsilon)\left(\varepsilon'_{ij}+\varepsilon''_{ij}+\varepsilon'''_{ij}\right)/D + \frac{2}{3}f_\varepsilon\varepsilon\delta_{ij}, \tag{7.17}$$

where

$$\varepsilon'_{ij} = \varepsilon\frac{\overline{u'_iu'_j}}{k} + 2\nu\frac{\overline{u'_lu'_n}}{k}\frac{\partial\sqrt{k}}{\partial x_l}\frac{\partial\sqrt{k}}{x_n}\delta_{ij} + 2\nu\frac{\overline{u'_lu'_i}}{k}\frac{\partial\sqrt{k}}{\partial x_j}\frac{\partial\sqrt{k}}{x_l} + 2\nu\frac{\overline{u'_lu'_j}}{k}\frac{\partial\sqrt{k}}{\partial x_i}\frac{\partial\sqrt{k}}{x_l}, \tag{7.18}$$

$$\varepsilon''_{ij} = \varepsilon\left(2\frac{\overline{u'_lu'_k}}{k}d_l^Ad_k^A\delta_{ij} - \frac{\overline{u'_lu'_i}}{k}d_l^Ad_j^A - \frac{\overline{u'_lu'_j}}{k}d_l^Ad_i^A\right), \tag{7.19}$$

$$\varepsilon'''_{ij} = C_{\varepsilon s}\nu k\left(\frac{\partial\sqrt{A}}{\partial x_k}\frac{\partial\sqrt{A}}{\partial x_k}\delta_{ij} + 2\frac{\partial\sqrt{A}}{\partial x_i}\frac{\partial\sqrt{A}}{\partial x_j}\right), \tag{7.20}$$

$$D = (\varepsilon'_{kk}+\varepsilon''_{kk}+\varepsilon'''_{kk})/(2\varepsilon), \tag{7.21}$$

$$f_\varepsilon = A^{1.5}, \tag{7.22}$$

and $C_{\varepsilon s} = 0.2$. In the present work, the ε'''_{kk} term, which is only significant in free-surface flow was set to zero. Away from the wall, the present model of ε_{ij} returns close to isotropic dissipation (see Eq. 3.26), since $f_\varepsilon \to 1$ here.

7.2.4 The dissipation-rate equation

The transport equation for $\widehat{\varepsilon}$ was modeled as

$$\begin{aligned}\frac{\partial}{\partial t}(\overline{\rho}\widehat{\varepsilon}) + \frac{\partial}{\partial x_j}(\overline{\rho}\widehat{\varepsilon}\widehat{u}_j) = {} & \frac{\partial}{\partial x_j}\left[\left(\mu+\frac{\mu_t}{\sigma_\varepsilon}\right)\frac{\partial\widehat{\varepsilon}}{\partial x_j}\right] + C_{\varepsilon1}\frac{\widehat{\varepsilon}}{2k}\overline{\rho}P_{kk} - C_{\varepsilon2}\frac{\widehat{\varepsilon}^2}{k}\overline{\rho} \\ & - C'_{\varepsilon2}\frac{(\varepsilon-\widehat{\varepsilon})\widehat{\varepsilon}}{k}\overline{\rho} + C_{\varepsilon3}\mu\overline{u'_iu'_j}\frac{k}{\varepsilon}\left(\frac{\partial^2\overline{u}_k}{\partial x_i\partial x_l}\right)\left(\frac{\partial^2\overline{u}_k}{\partial x_j\partial x_l}\right),\end{aligned} \tag{7.23}$$

where μ_t was modeled as $\mu_t = C_\mu f_\mu k^2/\varepsilon$ (compare to Eq. 3.7). The difference between this equation and the high-Reynolds-number version (Eq. 3.5), is that viscous effects in the exact $\widehat{\varepsilon}$ equation have been included by using the Reynolds-number function f_μ in the diffusion model and the inclusion of the $C_{\varepsilon3}$ term [57]. The $C'_{\varepsilon2}$ term was included to return the correct behavior of $\widehat{\varepsilon}$ very close to the wall. Also, $C_{\varepsilon2}$ was modified for near-wall flow by using A and A_2 (see Eq. 3.23 and Eq. 3.24). The coefficients in the $\widehat{\varepsilon}$ equation are shown

Table 7.2: Coefficients in the $\widehat{\varepsilon}$ equation [30].

σ_ε	$C_{\varepsilon 1}$	$C_{\varepsilon 2}$	$C'_{\varepsilon 2}$	$C_{\varepsilon 3}$	A_d	C_μ
1.3	1.0	$\frac{1.92}{1+0.7A_d A_2^{0.5}}$	1.0	0.875	$\max(0.25, A)$	0.09

in Table 7.2. The present $\widehat{\varepsilon}$ equation was identical to the one used by Craft except for the diffusion term. Craft employed the form

$$D_\varepsilon = \frac{\partial}{\partial x_l}\left[\left(\mu\delta_{lk} + C_\varepsilon \overline{u'_l u'_k}\frac{k}{\varepsilon}\right)\frac{\partial \widehat{\varepsilon}}{\partial x_k}\right]. \tag{7.24}$$

This form is probably more precise than the form in Eq. 7.23, which was employed for simplicity, since it involves the exact information from the Reynolds stresses instead of using the eddy viscosity. However, the diffusion term was not believed to be the most crucial part, and therefore the simpler model was adopted at the present stage. Different diffusion models are discussed in Sec. 7.4.3.

7.3 Numerical implementation

The model was implemented into the CFD code SPIDER described in Chapter 5. The diffusion term was included in the diffusive flux term, whereas the other terms were put into a common source term as

$$S_{ij} = P_{ij} + \Pi_{ij} - \varepsilon_{ij}. \tag{7.25}$$

The source term was linearized as described in Eq. 5.9. All the terms were lumped into S_{1P} for simplicity. This may be a dangerous practice since a negative S_{1P} may produce a diverging solution [98]. In the computations, the Reynolds-stress equations needed considerable relaxation. This might be a result of the above mentioned practice. It may also be a result of the stiff nature of such equations. A system of differential equations is said to be stiff if its numerical solution, by some method, requires a significant depression of the step-size to avoid instability [61]. Second-moment closures are known to be stiff, and especially if they are integrated up to the wall.

7.4 Pressure-driven turbulent Poiseuille flow

7.4.1 Description of the flow

Pressure-driven turbulent Poiseuille flow is a plane turbulent flow between two parallel plates with a pressure difference as the driving force of the flow. In the present calculations, the classical data set from Kim et al. [74] was used for comparison. This data set was the results from a DNS of a turbulent channel flow with Reynolds number 3300 based on the channel half height and the centerline velocity. The flow is fully turbulent, but still not very far from the area of transition from laminar to turbulent flow ($Re_{\mathrm{tr}} \approx 2300$). The Reynolds number based on the wall shear velocity was $Re_\tau = 180$.

7.4.2 Computational mesh and boundary conditions

The calculations were performed on a two-dimensional 100×10 grid (100 points in transversal direction). The grid was uniform in the longitudinal direction and clustered near the walls in the transversal direction, and assumed to be sufficient to resolve the boundary layer. Close to the wall Craft [30] used around $10-15$ nodes (for $Re_{\mathrm{T}} < 150$). Approximately the same number of control volumes was used near the wall in the present work. The grid and computational domain were constructed to make the grid expansion ratio and grid aspect ratio optimal throughout the domain. A higher grid density was tried out, but led to increasing stiffness of the equation system.

A calculation with the low-Reynolds-number k-ε model by Launder and Sharma [82] was used to produce initial conditions for the present model. Cyclic boundary conditions were applied at the inlet-outlet, which is similar to solving an infinitely long channel. Dirichlet conditions [45] were applied at the walls for all equations. Velocities and stresses were all zero at the wall. The dissipation rate has a finite value at the wall, and the expression in Eq. 7.13 assures $\widehat{\varepsilon} = 0$ at the wall (see also Sec. 2.9.2).

7.4.3 Results and discussion

The equations solved were $\overline{u}_1, \overline{u}_2$, pressure correction, $\widehat{\varepsilon}$, and the four Reynolds stresses $\overline{u_1'u_1'}, \overline{u_2'u_2'}, \overline{u_3'u_3'}, \overline{u_1'u_2'}$. The predictions shown here were all performed without the pressure-diffusion term and with the constant $C_2' = 0$, since the inclusion of these terms led to instabilities or unsatisfying results. More investigation is needed to include these terms. Transverse profiles of the mean velocity distribution are shown in Fig. 7.1. The model predicted a reasonable profile with some discrepancy towards the center of the channel (Fig. 7.1(a)).

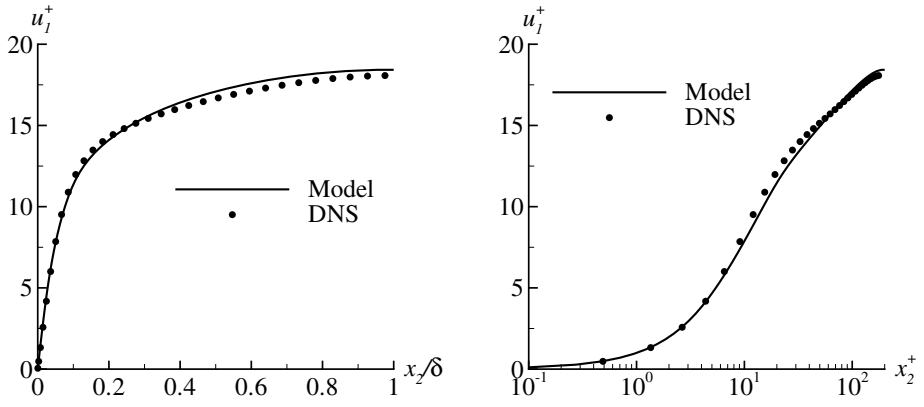

(a) u_1^+ versus x_2/δ (b) u_1^+ versus x_2^+

Figure 7.1: Velocity profiles. δ is half the channel width. DNS data from Kim et al. [74].

The model seems to perform well in the boundary layer (Fig. 7.1(b)) compared to the DNS, even though there is a small discrepancy in the buffer region.

Profiles of RMS of the Reynolds normal stresses and of the Reynolds shear stress are shown in Fig. 7.2. The profile of $u_1'^+$ (see Fig. 7.2(a)), shows a too low peak close to the wall. This was also experienced by Craft and Launder [34], but their results were closer to the DNS than the present calculations. Craft [30] improved the prediction of the low peak in $u_1'^+$ by introducing an inhomogeneity correction in the velocity gradient in the model for the pressure correlation Φ_{ij}^* following the same method as Launder and Tselepidakis [85]. This term was supposed to improve the predictions in the separation region in backward-facing-step flows, and to improve the prediction of the peak in the $\overline{u_1'u_1'}$ normal stress profile. This correction was not included in the present predictions since it led to instabilities. A second reason for the discrepancies may be the exclusion of the C_2' term and the pressure-diffusion term. These terms are supposed to be almost negligible in shear-free flows but are not supposed to be neglected inside the boundary layer.

The $u_2'^+$ and $u_3'^+$ (Fig. 7.2(b) and Fig. 7.2(c)) profiles were in reasonable accordance with the DNS data. The predicted $\overline{u_1'u_2'}^+$ (Fig. 7.2(d)) are too low according to the DNS data. Some of the discrepancies may be due to the terms not included in the present predictions. The different models are further discussed below.

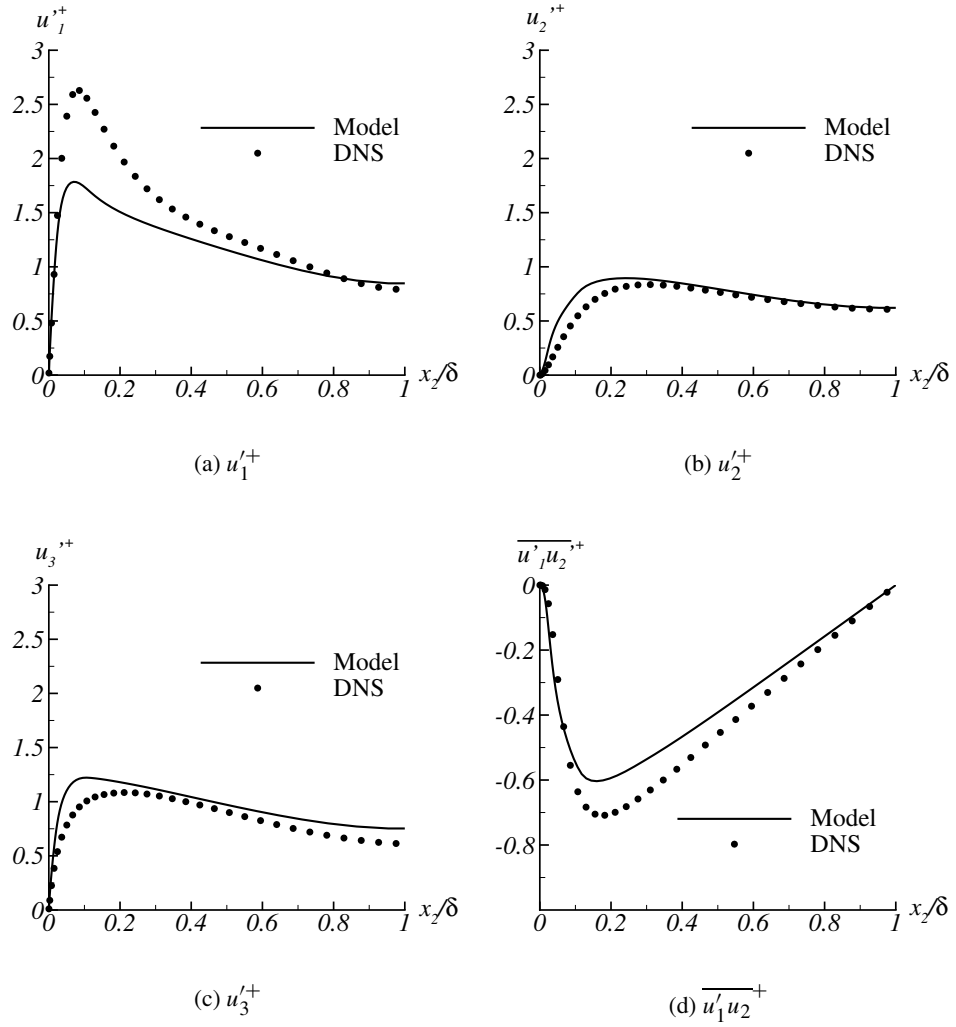

(a) $u_1'^+$ (b) $u_2'^+$

(c) $u_3'^+$ (d) $\overline{u_1' u_2}^+$

Figure 7.2: RMS of the normal stresses and normalized shear stress versus DNS data from Kim et al. [74].

The turbulence diffusion term, $D_{ij,\mathrm{t}}$

The diffusion term was calculated according to the isotropic model of Shir, whereas Craft solved a balance equation for the triple moments. The behavior of the variables in the Shir model is shown in Fig. 7.3. The ratio between the eddy viscosity and the molecular

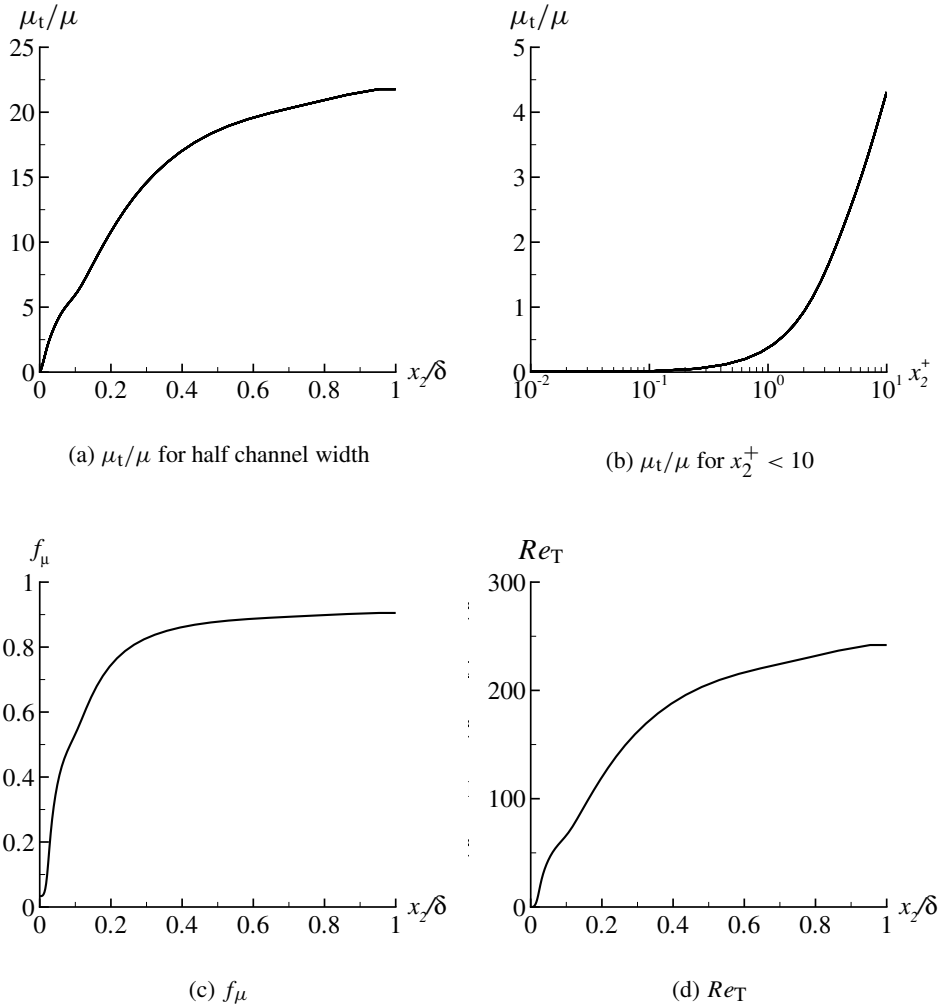

(a) μ_t/μ for half channel width

(b) μ_t/μ for $x_2^+ < 10$

(c) f_μ

(d) Re_T

Figure 7.3: Investigation of variables in the diffusion term

viscosity (Figs. 7.3(a)–7.3(b)) shows that the molecular forces become dominant only very close to the wall. The Reynolds number function f_μ (Fig. 7.3(c)) also shows an expected beavior varying from close to zero at the wall and approaching unity in the middle of the channel. The turbulence Reynolds number (Re_T) is shown in Fig. 7.3(d). The different modeling practice of the diffusion term obviously will lead to some discrepancies in the predictions, the question is how much. The different methods were not analyzed here.

However, this has been done by others. So et al. [128] investigated four different diffusion models, where the Shir model was one of them. They reported that the invariant model by Hanjalić and Launder (HL) [56] (Eq. 3.11) predicted the most reasonable results of the four models, whereas the best results were obtained by solving a balance equation for the triple moments. Craft and Launder used the model in Eq. 3.11 while Craft solved a balance equation like mentioned above. The differences introduced through the different diffusion modeling are believed to be slight [128]. Launder et al. [81] reported a comparison between the model in Eq. 3.11 and the simpler model by Daly and Harlow [35]. They found only slight differences. The practical effects of employing the Shir model are that it is simpler and more stable [40, 41] than the HL model. In later work, Craft et al. [31] also employed the Shir model.

The pressure correlations, Π_{ij}

The behavior of Φ^*_{ij} was shown by Craft and Launder [34] for shear-free flows and free surface flows. This behavior is not shown here. However, the behavior of the coefficients and the Reynolds-number functions in the pressure-correction model are shown in Fig. 7.4. No irregular behavior was discovered, they seem to behave as expected. Perhaps more interesting is the behavior of the normalized length-scale gradients shown in Fig. 7.5. Compared to the profiles obtained by Craft and Launder [34], there are large discrepancies, especially towards the center of the channel. Especially the d_2 function shows large discrepancies, whereas d_2^A show a somewhat better behavior. There also seem to be some near-wall problems in the present model. Both d_2 and d_2^A exhibit a "dip" in the buffer region, not unlike in d_2 from Craft and Launder, and both have much too high values in the center of the channel. These problems may come from other difficulties than the length-scale gradients themselves, and further investigation is needed in this.

The dissipation tensor, ε_{ij}

The dissipation tensor is supposed to vary from the term $(\varepsilon'_{ij} + \varepsilon''_{ij} + \varepsilon'''_{ij})/D$ to close to the isotropic expression $\frac{2}{3}\varepsilon\delta_{ij}$ in the middle of the channel, where the turbulence Reynolds number is above 200 and viscous effects are assumed to be negligible. The function f_ε is supposed to achieve this. The profile of f_ε in Fig. 7.6(a) shows that this is fulfilled in the present predictions, since f_ε is zero at the wall and are above 0.8 in the middle of the channel. Craft et al. [31] used $f_\varepsilon = A$, which would give higher values of f_ε towards the center of the channel (see Fig. 7.4(c)).

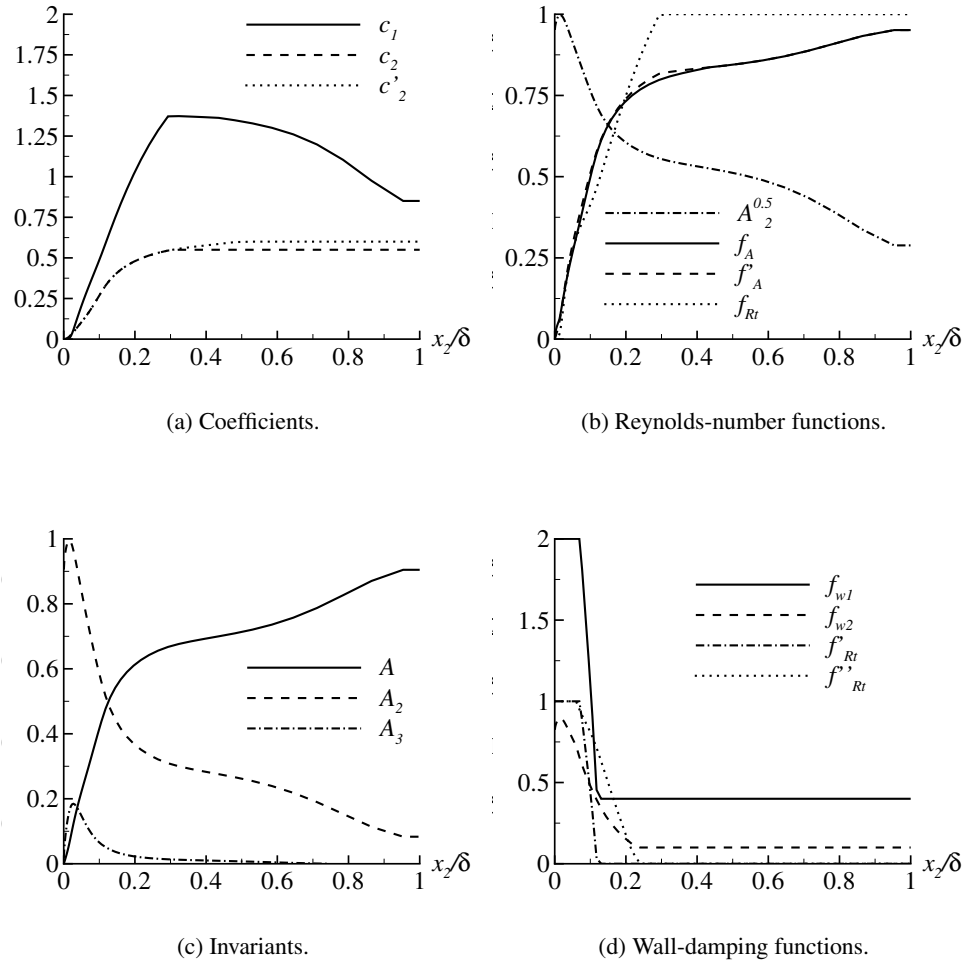

(a) Coefficients.

(b) Reynolds-number functions.

(c) Invariants.

(d) Wall-damping functions.

Figure 7.4: Investigation of pressure-diffusion term, Φ^*_{ij}.

The dissipation-rate equation

The dissipation-rate equation employed in the present model introduced two differences compared to the model by Craft. Both were assumed to be negligible. First, the differences introduced in the diffusion term discussed above (on $D_{ij,\mathrm{t}}$) are assumed to apply also for the $\widehat{\varepsilon}$ equation. Second, Craft employed a correction term designed to improve the behavior

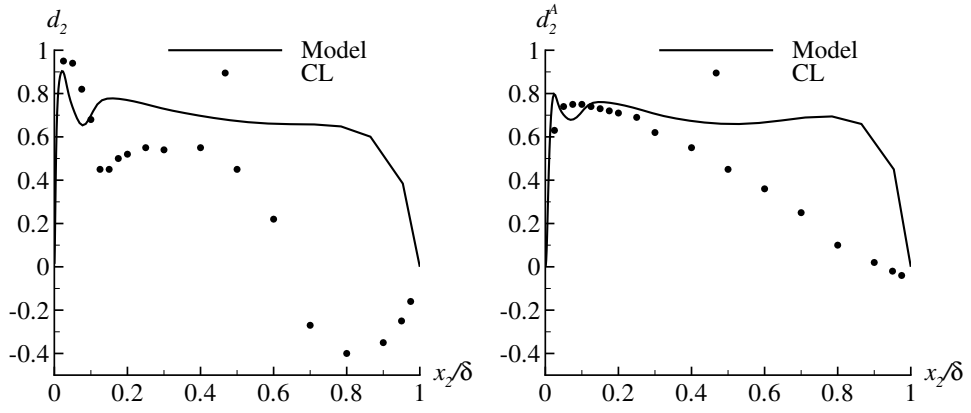

(a) d_2 (b) d_2^A

Figure 7.5: Normalized length-scale gradients, d_2 and d_2^A versus modeling results by Craft and Launder (CL) [34].

around the separation region in backward-facing-step flows. This term was not included here. The limiting behavior of ε and $\widehat{\varepsilon}$ close to the wall can be seen in Fig. 7.6(b), showing that the boundary condition $\widehat{\varepsilon} = 0$ is well captured, whereas ε has a finite value at the wall.

7.5 Conclusions and recommendations

The present chapter has shown the implementation and testing of the low Reynolds-number second-moment closure by Craft and Launder [30, 34], and compared the predictions against DNS data from Kim et al. [74]. The following assumptions and simplifications were made in the present work

- The simpler diffusion model by Shir was adopted rather than solving a balance equation for the triple moments.
- The diffusion model by Shir was also adopted in the $\widehat{\varepsilon}$ equation.
- The terms specifically designed to account for backward-facing-step flows, impinging jet flows and free-surface flows were not included.

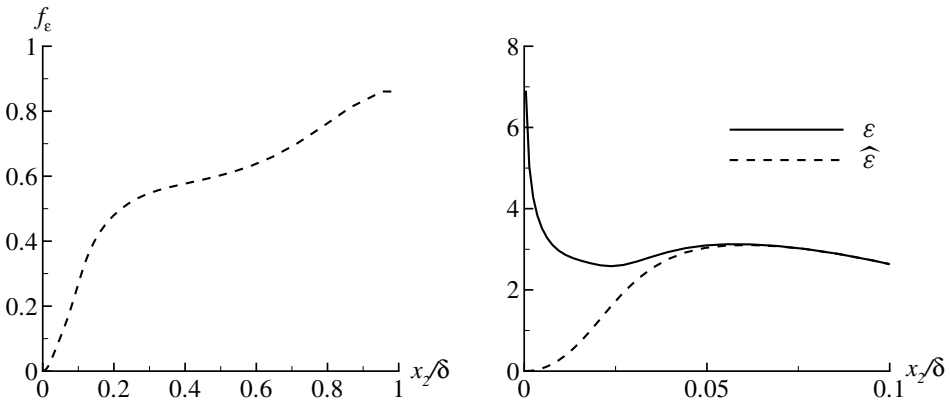

(a) f_ε (b) ε versus $\widehat{\varepsilon}$

Figure 7.6: Behavior of f_ε and ε versus $\widehat{\varepsilon}$.

- The pressure-diffusion term and the coefficient C_2' were set equal to zero due to numerical instabilities.

Despite these simplifications, most of the predictions were in reasonable accordance with the DNS data. However, the peak in $u_1'^+$ and the absolute value of $\overline{u_1' u_2'}^+$ close to the wall were far too much underpredicted compared to the DNS data and previous results reported by Craft and Launder. The exclusion of the pressure-diffusion term and the C_2' term may be one of the reasons for the discrepancies.

Some recommendations for future work are

- The pressure-diffusion term and the near-wall C_2' term need more investigation.
- The different components of Φ_{ij}^* and ε_{ij} should be compared against DNS data similar to what was done in the work by Craft and Launder [34].
- The assumptions on the terms specifically designed for backward-facing-step flows and free-surface flows should be checked to see if they are, in fact, negligible for the present case.
- The inhomogeneity correction of the velocity gradient in the pressure-fluctuation term needs more investigation.

- The present diffusion model should be compared to the more exact models for both the stress equations and the dissipation equation.

Chapter 8

Towards a model for turbulent reacting near-wall flows

A model for prediction of flame-wall interacting flows must be able to account for effects associated with low Reynolds numbers. It is well known that the standard version of Magnussen's Eddy Dissipation Concept (EDC) (see Chapter 3) was developed for high-Reynolds-number flows. The present chapter presents an investigation of the standard model and proposes a modification attempt for near-wall flows. Other model approaches for prediction of turbulent reacting boundary-layer flows were briefly discussed in Chapter 4.

8.1 Model expectations

What can be expected from the "standard" EDC for computations of a turbulent reacting boundary layer where the turbulence Reynolds number are low? The Eddy Dissipation Concept was developed for high-Reynolds-number flows. This means that the model is developed for flows where turbulence diffusion is much larger than molecular diffusion. Even though these facts are "known", and easily deduced from the definitions of the EDC variables, it appears that the behavior of EDC close to a wall with comparison to experimental data or DNS has so far not been reported. Close to a wall, turbulence diffusion decreases, molecular effects become more dominant, and the turbulence Reynolds number approaches zero. For such conditions, for example if $Re_{\mathrm{T}} = 0.5$, the EDC variables (see Sec. 3.5) are $\gamma_\lambda = 2.533$ and $\gamma^* = 16.252$ respectively. It is more than obvious that the reactor model have no meaning for such values. In high-Reynolds-number flows, where regions includ-

ing low Reynolds numbers are not considered having importance for the desired results, or if one simply want to avoid numerical problems, a certain upper limit can be introduced on γ_λ. A realistic limit may be $\gamma_\lambda < 0.5$ [48]. In numerical calculations, when using a finite-volume technique, the low-Reynolds-number regions can be avoided by putting the innermost control volume at a "safe" distance from the wall. (For example for turbulence Reynolds numbers greater than 300, which corresponds to $\gamma_\lambda < 0.5$.) For calculations where detailed information of the flow in the boundary layer is desirable, introducing a lower limit would most likely lead to unacceptable model performance.

8.2 Behavior of EDC close to a wall

In the present study, the investigation was concerned about finite-chemistry calculations, which means that the method of analysis will be similar for single-step-, reduced- or detailed mechanisms. Methods for infinitely fast chemistry calculations were not treated here. The mean chemical reaction term can, for finite-rate chemistry, be written as [49]

$$-\overline{R}_i = \bar{\rho}\frac{\gamma_\lambda^2}{\tau^*}(Y_i^\circ - Y_i^*). \tag{8.1}$$

The present investigation focused on the behavior of γ_λ and τ^* in the turbulent reacting boundary layer since these variables consist of turbulence large-scale quantities. If $Re_\mathrm{T} = k^2/(\nu\varepsilon)$ is the turbulence Reynolds number and x_2 is the distance from the wall, then

$\gamma_\lambda = 2.1 Re_\mathrm{T}^{-1/4} \to \infty$ when Re_T (or x_2) $\to 0$, and

$\tau^* = 0.4\,(\nu/\varepsilon)^{0.5} \to$ finite value when Re_T (or x_2) $\to 0$, since ε has a finite value at the wall.

It is obvious that a new model expression for γ_λ is needed. It is not so clear if the residence time has to be modified. The expression $(Y_i^\circ - Y_i^*)$ may be calculated in the same way as previously described (see Sec. 3.5.2), as long as γ_λ has reasonable limits according to the reactor model. The mass fraction of fine-structure regions, γ_λ, expresses the ratio between these regions and the total mass, and is mathematically expressed by Eq. 3.29. Since γ_λ is an expression for a mass fraction, its value must be between 0 and 1. For $\gamma_\lambda = 1$, then $Re_\mathrm{T} = 2.1^4 \approx 19.4$ which corresponds to a certain distance away from the wall. The turbulence Reynolds number, Re_T, can be much lower than unity close to the wall and approaches zero at the wall itself. Hence, if care is not taken, γ_λ can take values greater than unity close to a wall.

From series expansions, it can be shown [41, 62, 65, 79] (see Sec. 2.9.2) that the turbulence energy dissipation rate $\varepsilon \to \varepsilon_w$, where ε_w is finite, at the wall. The turbulence energy $k \to 0$ (no slip) at the wall. Since $k \to 0$, then $\gamma_\lambda \to \infty$ at the wall. The question is then what the desired value of γ_λ at the wall, or in the region close to it is.

It is assumed that turbulence can be represented by a cascade model [14, 43, 73, 133]. This means that the turbulence motions associated with the largest scales most likely are transferred onto smaller and smaller scales until they are transformed into heat by viscous forces, predominantly on the smallest scales. These scales are of the order of the Kolmogorov scales (see Sec. 3.6). In EDC, the fine-structure regions are the regions where these scales appear. Molecular mixing, and hence the combusting processes are in EDC assumed to take place on these scales. When approaching a wall, the turbulence energy spectrum becomes narrower as $Re_T \to 0$, which means that the Kolmogorov length scales approaches the integral length scales [40]. Very close to the wall, the flow is probably occupied by the smallest scales only, which in EDC means that the flow is occupied by fine-structure regions only. If so, then $\gamma_\lambda \to 1$ when $x_2 \to 0$.

The boundary values for the mean and surrounding variables, when $\gamma_\lambda \to 1$, are the fine-structure values, since all of the flow approaches the fine-structure state. This means that, for a general scalar variable

$$\widetilde{\varphi} \to \varphi^* \text{ and } \varphi^\circ \to \varphi^*, \tag{8.2}$$

when $\gamma_\lambda \to 1$. For the mean variables, this can also be shown by using the relation between the mass averaged state and the surrounding state, given by [42]

$$\widetilde{\varphi} = \gamma^* \chi \varphi^* + (1 - \gamma^* \chi)\varphi^\circ. \tag{8.3}$$

If $\chi = 1$ is chosen, $\gamma_\lambda \to 1$ gives $\gamma^* \chi \to 1$ (by Eq. 3.32) and consequently $\widetilde{\varphi} \to \varphi^*$. This shows that, when assuming $\gamma_\lambda \to 1$ at the wall, the mean chemical reaction term

$$\overline{R}_i \to R_i^* \tag{8.4}$$

at the wall. As described in Sec. 3.5.2, R_i^* can be expressed by e.g. an Arrhenius model. Accordingly, the limiting expression for the mean chemical reaction rate at zero turbulence Reynolds number is the laminar reaction rate.

8.3 Proposal for a low-Reynolds-number version of EDC

8.3.1 The fraction of the flow occupied by fine-structure regions

Based on the indications in the previous chapter, the proposed modification of γ_λ may be a function based on the turbulence Reynolds number approaching the standard version of

γ_λ for high Reynolds numbers (for example when $Re_T > 300$) and approaching unity at the wall. This behavior can be achieved by employing Reynolds-number functions similar to those widely used in turbulence modeling of non-reacting flows [30, 54, 79]. In turbulence modeling, such functions have been applied to high-Reynolds-number models to make them valid for low Reynolds numbers [30, 65, 66, 82] (see Chapters 3 and 7). The functions applied here are based upon the Reynolds-number functions introduced by Jones and Launder (JL) [65] where

$$f_{\mu\mathrm{JL}} = \exp\left(\frac{-2.5}{(1+Re_T/50)}\right), \tag{8.5}$$

and by Launder and Sharma (LS) [82] where

$$f_{\mu\mathrm{LS}} = \exp\left(\frac{-3.4}{(1+Re_T/50)^2}\right). \tag{8.6}$$

These functions were originally introduced to adjust the model for the eddy viscosity due to low Reynolds numbers in k-ε turbulence models. Furthermore, to adjust γ_λ very close to the wall, a simple Reynolds-number function based upon the thoughts of Spalding [129]

$$f = \frac{Re_T}{Re_T + \mathrm{Constant}} \tag{8.7}$$

was employed. By applying these functions, together with the standard version of γ_λ, the desirable distribution for γ_λ was chosen as

$$\gamma_\lambda = \underbrace{\left(1 - f_1^{1/2} f'_\mu\right)}_{(f_i)} + \underbrace{f_2 f_\mu \gamma'_\lambda}_{(f_{ii})}, \tag{8.8}$$

where

$$f_1 = \frac{Re_T}{Re_T + 0.5}, \tag{8.9}$$

$$f_2 = \frac{Re_T}{Re_T + 1.0}, \tag{8.10}$$

$$f'_\mu = \exp\left(\frac{-1.4}{(1+Re_T/50)^2}\right) = \left(f_{\mu\mathrm{LS}}\right)^{1.4/3.4}. \tag{8.11}$$

Here, f_μ can be either the JL (Eq. 8.5) or the LS (Eq. 8.6) expression. γ'_λ is the standard EDC expression from Eq. 3.29. The behavior of the proposed γ_λ and its different functions are shown in Figs. 8.1 and 8.2. The LS function seems to give a better approximation for larger Reynolds numbers (it makes the new model approach the standard version faster than the JL function, at $Re_T \approx 300$ which may be desirable). $f_1^{1/2} f'_\mu \to 1$ when Re_T increases, which means that $f_i \to 0$ when molecular forces are negligible. $f_2 f_\mu \to 0$ close to the wall

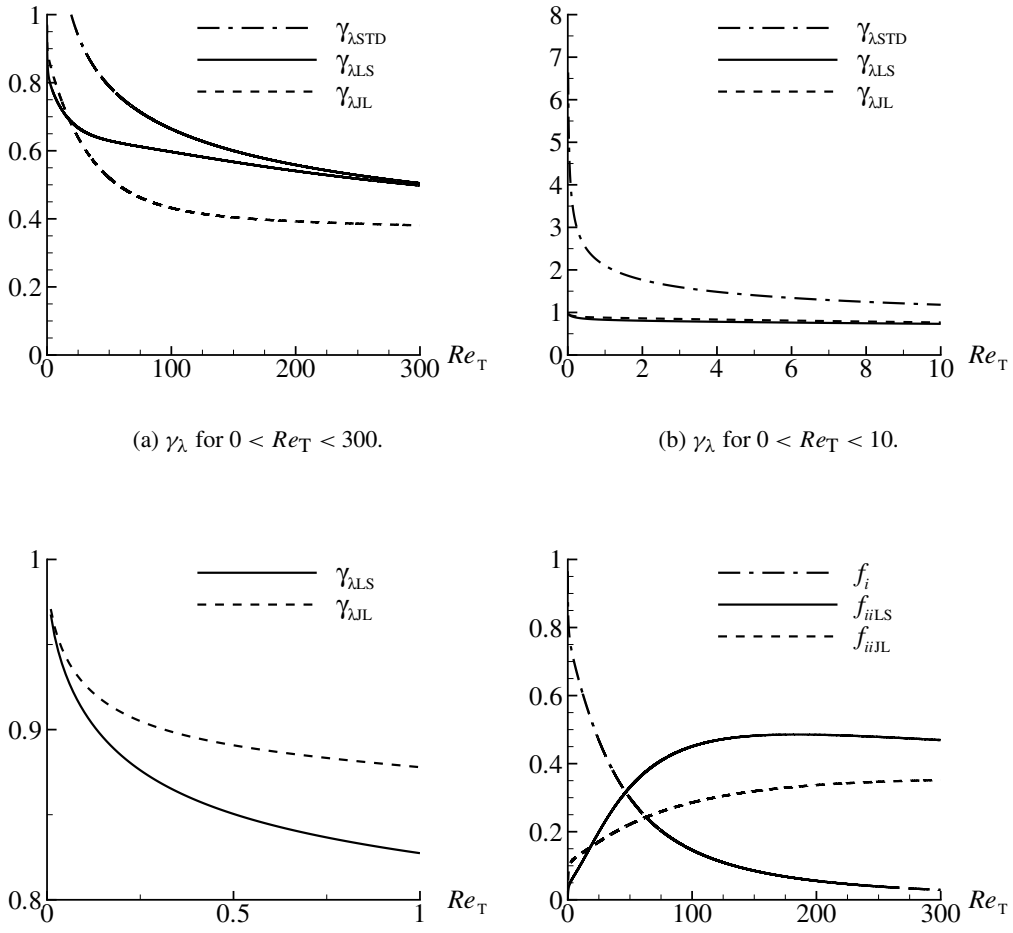

(a) γ_λ for $0 < Re_T < 300$.

(b) γ_λ for $0 < Re_T < 10$.

(c) γ_λ for $0 < Re_T < 1$.

(d) f_i and f_{ii} for $0 < Re_T < 300$.

Figure 8.1: Behavior of the functions in the proposed expression for γ_λ.

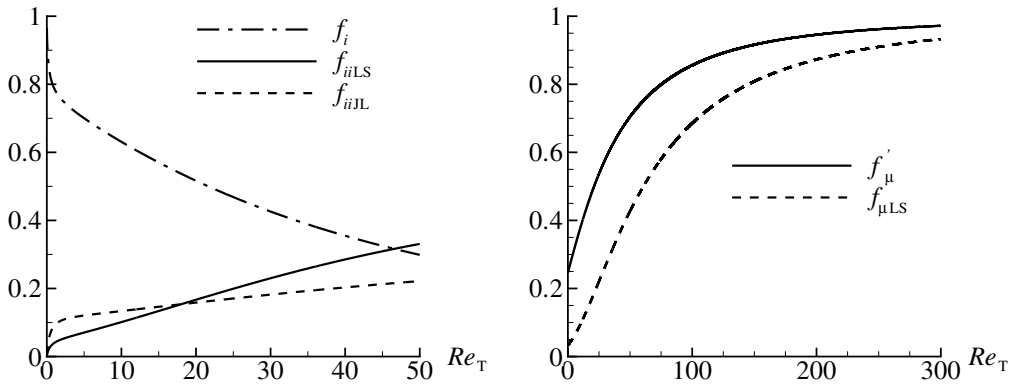

(a) f_i and f_{ii} for $0 < Re_T < 50$.

(b) f'_μ versus $f_{\mu\mathrm{LS}}$ for $0 < Re_T < 300$.

(c) f_μ for $0 < Re_T < 300$.

(d) f_1 and f_2 for $0 < Re_T < 300$.

Figure 8.2: Behavior of Reynolds-number functions in the proposed γ_λ.

when molecular forces dominate. Hence, for high Reynolds number, the new expression will be equal to the standard γ_λ, and for low Reynolds numbers the function f_i will be more dominant and the new expression will go towards unity at the wall.

When $\gamma_\lambda \rightarrow 1$, numerical problems may arise since all of the flow is approaching the fine-structure state. For this reason, care must be taken to assure a numerically stable solution procedure.

8.3.2 The residence time, τ^*

In the standard EDC, τ^* is expressed by Eq. 3.30. Since ε has a finite value at the wall, τ^* will approach a finite value at the wall. In EDC, the assumption that the reactions occur at the smallest scales of turbulence is usually employed. The present model (Eq. 3.30) of the residence time is based on this assumption. This assumption may be sufficient for reactions close to a wall since most of (or all of) the reactions take place on the smallest scales here. However, in such regions, one may also have to take slower chemical reactions into account, which e.g. may be a result of intermittent behavior of the turbulent flow, or due to heat transfer from the reactants to a cold wall. Even if finite chemistry effects are calculated through the expression in Eq. 8.1, the residence time may also need modification due to possible change in scales. Thus, the possibility for combustion to take place on larger scales should perhaps not be excluded.

There have been developed models of interest that take such effects into account. A model by Golovitchev and Chomiak [47] was based on the EDC which allows the reaction zone to grow larger than the Kolmogorov eddies (in EDC the reaction zone is quenched if the chemical time scale are larger than the residence time, which is proportional to the Kolmogorov scale). Poinsot [116] outlines several approaches to modify the flame time (proportional to the residence time in EDC) in direct closure methods. Poinsot argues that "there is no reason to assume that only one turbulent scale (large or small) controls the flame time and the turbulent flame structure. A wide range of scales, from Kolmogorov to integral scales, are likely to be involved". According to Poinsot, a more precise approach would be to derive a balance equation for characteristic times of the turbulence-combustion interaction, similar to the approach by Mantel and Borghi [97] based on a balance equation for the scalar dissipation rate.

A detailed investigation of the residence time in EDC, and how the expression in the standard model influences the prediction of local extinction in conjunction with detailed chemical kinetics, was presented in Chapter 6. That work indicated how the residence time controls the prediction of localized extinction (and possible autoignition) in a lifted jet flame. The present model gave a reasonable flame picture. However, the lift-off height was some-

what underpredicted compared to the measured value, and modified expressions for the residence time may have led to improvements. Prior to modifying the expression for the residence time, further investigation is needed. For this reason, the standard model is, so far, kept in its original form.

8.3.3 The mean chemical reaction term, $\overline{R}_i$

By introducing a modification for γ_λ, the mean chemical reaction term in Eq. 8.1 is modified by a factor of γ_λ^2. Even though γ_λ may have a reasonable profile through the boundary layer, this may still not automatically be the case for the mean chemical reaction term since other effects are also introduced through the residence time and the mass fraction expression $(Y_i^\circ - Y_i^*)$.

If it proves difficult to design variables, and hence a reaction term that automatically behaves as desired for both low and high Reynolds numbers, a possible solution might be to introduce several expressions for the reaction term. For example one that take low Reynolds numbers (including the laminar effects very close to the wall) into account and one that is similar to the standard model for high Reynolds numbers. The different terms could then be coupled by Reynolds-number functions similar to those shown in Sec. 8.3.1.

8.4 Summary

- The behavior of EDC close to a wall, where the turbulence Reynolds number is small, has been discussed.
- The standard EDC model for the mass fraction of the fine structure regions, $\gamma_{\lambda\mathrm{STD}}$, increases towards infinity when the turbulence Reynolds number approaches zero.
- It is proposed that $\gamma_\lambda \to 1$, when $Re_\mathrm{T} \to 0$.
- If $\gamma_\lambda \to 1$, the mean and surrounding values in the EDC reactor model will approach the fine-structure values at the wall.
- As the turbulence Reynolds number approaches zero, the EDC mean reaction rate approaches the laminar reaction rate.
- A low-Reynolds-number version of EDC is proposed. By employing Reynolds-number functions, the desired behavior of γ_λ is achieved. This also means that γ_λ approaches $\gamma_{\lambda\mathrm{STD}}$, when $Re_\mathrm{T} > 300$.

- The residence time is kept in its original form.

URN:NBN:no-7265

Chapter 9

Modeling turbulent reacting Couette flow

9.1 Introduction

The present chapter presents the results for a turbulent premixed flame in a lowReynolds-number Couette flow by using Magnussen's Eddy Dissipation Concept (EDC) for turbulent combustion. The configuration from Alshaalan and Rutland [2, 3, 4] was used to predict the turbulent flame which interacts with a wall.

The features that makes this flow attractive for model development are the statistically stationary DNS results produced by Alshaalan and Rutland. The difficulties associated with EDC for this flame are the low Reynolds number which is just above the criteria for fully developed flow, whereas the turbulence Reynolds number approaches zero towards the wall. The present work presents predictions with EDC in conjunction with finite-rate chemistry calculations using a single-step chemical mechanism. The predictions show, as expected, that for the present flow, the standard EDC exhibited unrealistic behavior including numerical instabilities if the mass fraction variable for the reacting fine structures, γ_λ, was not adjusted. However, by introducing limits to γ_λ, or by employing the low-Reynolds-number version of EDC from Chapter 8, the predictions gave a reasonable flame picture. The predictions were in reasonable accordance with the DNS for the adiabatic flame away from the wall, whereas the wall flame was somewhat differently predicted than the DNS. The different predicted wall flame may be resulting from difficulties experienced in the EDC model for low Reynolds numbers, leading to a too fast spreading of the flame towards the wall. Another reason for the discrepancies may be that a constant-density assumption was

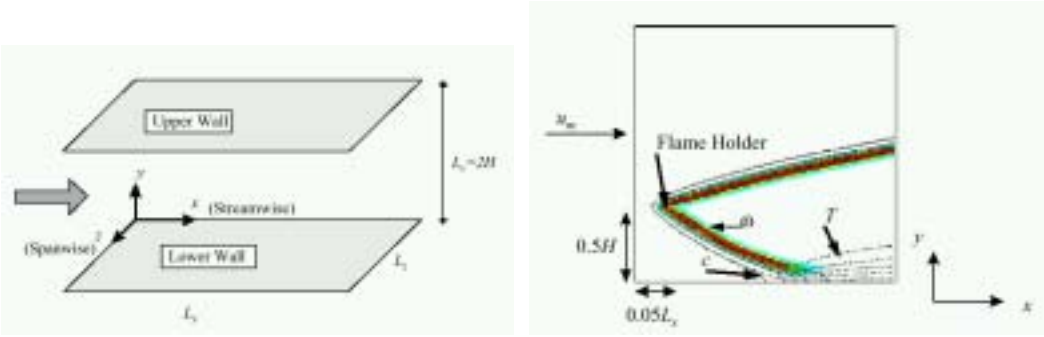

(a) Geometry (b) Laminar Flame

Figure 9.1: Geometry and laminar flame from the DNS work by Alshaalan [2]

applied. Variable-density effects (heat release) might push the flame away from the wall. There were also some uncertainties associated with the inlet conditions that could lead to discrepancies.

9.2 Case description

The flame configuration is shown in Fig. 9.1, where a sketch of the geometry and a contour profile of a predicted laminar flame (the same configuration as the turbulent flame) from the work by Alshaalan [2] are shown. The flame is premixed and similar to a methane-air combustion near the lean flammability limit. It is V shaped and held in position by a flame holder, where one branch of the flame is far away from the wall, and the other branch is interacting with the cold lower stationary wall (like a side-wall configuration). The DNS contour plot (Fig. 9.1(b)) shows contour lines of temperature T (dashed lines) and the progress variable c (solid lines). The chemical reaction term $\dot{\omega}$ is shown by the colors (along the two branches). The lower branch of the flame interacts with the wall and quenches a distance downstream. Due to the cold wall, a thermal boundary layer grows along the lower wall as shown by the temperature contour lines. The top wall moves at a specified velocity, $u_\mathrm{w} = 2.1\,\mathrm{m/s}$. The Reynolds number based on the half channel width and the mean velocity $u_\mathrm{m} = u_\mathrm{w}/2$, was $Re_H = 504$. For turbulent plane Couette flow, the transition criteria from laminar to turbulent flow is about 360 [89, 134], and the criteria for fully developed turbulence is about 500 [7]. Hence, the Reynolds number for the present flow is just above the fully-developed criteria. The channel half width H was 0.023 m and

the channel length L was $4.17H$. The flame was held in place by fixing the temperature at the adiabatic flame temperature ($T_a = 2000\,\mathrm{K}$) at $x = 0.21H$, $y = 0.5H$. The inflow temperature of the fresh gases was $T_F = 600\,\mathrm{K}$. The wall temperatures were constantly fixed at $T_w = 600\,\mathrm{K}$.

9.3 Previous predictions

Alshaalan and Rutland [2, 3, 4] performed three-dimensional direct numerical simulations of the flame described in the previous section. They solved non-dimensionalized equations for overall mass, momentum, energy (normalized temperature), and the normalized reactant mass fraction. The chemical reaction term was solved by a single-step Arrhenius expression, where the parameters for heat release and activation temperature (Zel'dovich number) were 0.7 and 5.24 respectively, and the non-dimensional pre-exponential constant was 50. The ratio of the turbulent velocity fluctuation to the laminar flame speed was of order unity, which results in a moderate (or weak) coupling between chemistry and turbulence. Their calculations were performed using variable density and constant transport properties. Further assumption were low Mach number, unity Lewis number, ideal gas behavior, and in addition, Soret and Dufour effects, and body forces were neglected. The predicted flame shape is shown in Fig. 9.2, where δ_{l0} is the unstrained laminar flame thickness. The figure shows contour lines of the progress variable c and colors along the two branches for the reaction term $\left(\overline{\dot{\omega}}\right)$. The heat flux $\left(\overline{Q}\right)$ shown was a result of the wall flame interacting with the cold isothermal wall. Due to the isothermal wall, the wall flame was quenched at $x/\delta_{l0} \approx 28$.

9.4 Present predictions

9.4.1 Constant-density assumption

Constant density was employed for two reasons. First, since turbulence models generated poor results for the present flow, both far away from, and close to the walls. Similar turbulence model behavior for turbulent plane Couette flow has also been reported by Andersson and Petterson [6]. And second, since detailed initial conditions were not available. Both these conditions led to uncertainties in the calculations. Employing constant density was an attempt to minimize these uncertainties, since it will serve to decouple the fluid dynamics and the flame. The heat released from the flame will then have no effect on the flow. This is so because when transport properties are held constant, only through density changes will

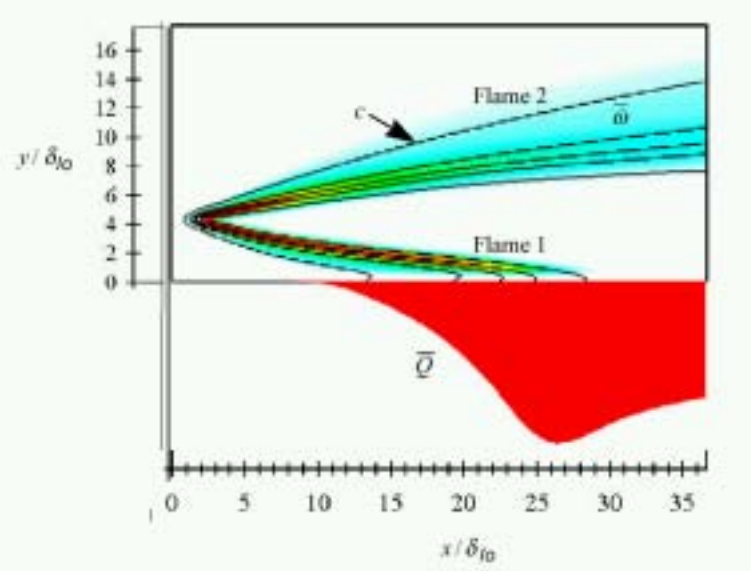

Figure 9.2: The predicted turbulent flame from the DNS work by Alshaalan [3]

changes in the turbulence and momentum equations occur. For this reason, the velocity- and turbulence quantities were held constant and equal to the inlet conditions taken from Alshaalan [2]. This assumption, or simplification, was believed to be reasonable for model investigation, and all predictions made in the present work were investigated having this in mind. With constant density, the result will be somewhat different from Alshaalan and Rutland, although still reasonable for comparison on a qualitative basis. It can also be mentioned that constant density wall-interacting flames were studied by Bruneaux et al. [17]. In their case, the variable-density effects were isolated and they studied only the influence by the flame on the flow through viscosity changes. Later, Bruneaux et al. [18] argued that in addition, for that case, a constant-viscosity assumption allowed a stationary flow field which was more useful for modeling purposes. Alshaalan and Rutland [4] also predicted laminar flame calculations using constant density for isolating the effects of fluid mechanics on the maximum wall heat flux. The same argumentation may also argue in favor of using constant density in the present case, since it eliminates variable-density effects. This isolation of certain effects may lead to clearer understanding of the combustion model at an early stage.

9.4.2 Describing the mixture composition

Similar to the work by Alshaalan [2], the turbulent premixed flame was studied by assuming combustion taking place as a single-step reaction as described by Eq. 3.35. Fuel (F) and Product (P) were defined and given properties equal to methane-air reactants and products respectively (as described in Sec. 2.3). The fuel-to-air ratio was $\Phi = 0.8$. This defined a lean mixture very close to the minimum ignitability limit (near the point of minimum spark energy required for ignition [38]).

9.4.3 Governing equations

Since velocity and turbulence quantities were held constant, the governing equations solved were

$$\frac{\partial}{\partial x_k}(\overline{\rho}\widetilde{h}\bar{u}_k) = \frac{\partial}{\partial x_k}\left(\frac{\mu}{\sigma_h}\frac{\partial \widetilde{h}}{\partial x_k} - \overline{\rho}\widetilde{h''u_k''}\right) + \overline{S}_h, \tag{9.1}$$

$$\frac{\partial}{\partial x_k}(\overline{\rho}\widetilde{Y}_F\widetilde{u}_k) = \frac{\partial}{\partial x_k}\left(\frac{\mu}{\sigma_Y}\frac{\partial \widetilde{Y}_F}{\partial x_k} - \overline{\rho}\widetilde{Y_F''u_k''}\right) + \overline{R}_F, \tag{9.2}$$

where the Prandtl and Schmidt numbers were $\sigma_h = \sigma_Y = 0.7$. The product mass fraction was found from $\widetilde{Y}_P = 1 - \widetilde{Y}_F$.

9.4.4 Modeling

In Eqs. 9.1–9.2 the turbulence fluxes ($-\overline{\rho}\widetilde{h''u_k''}$ and $-\overline{\rho}\widetilde{Y_F''u_k''}$) and the mean chemical reaction term ($\overline{R}_F$) require modeling.

The turbulence fluxes

The turbulence fluxes were modeled by a gradient model (see also Chapter 3) as

$$\overline{\rho}\widetilde{h''u_k''} = \frac{\mu_t}{\sigma_t}\frac{\partial \widetilde{h}}{\partial x_k}, \tag{9.3}$$

$$\overline{\rho}\widetilde{Y_F''u_k''} = \frac{\mu_t}{\sigma_t}\frac{\partial \widetilde{Y}_F}{\partial x_k}, \tag{9.4}$$

where the turbulence viscosity was expressed $\mu_t = \overline{\rho} f_\mu C_\mu \frac{\widetilde{k}^2}{\widetilde{\varepsilon}}$, and the turbulence Prandtl-Schmidt number was chosen $\sigma_t = 0.7$. To adjust the eddy viscosity for the low-Reynolds-number flow, the Reynolds-number function f_μ by Jones and Launder [65] given by Eq. 8.5

was adopted. The similar function proposed by Launder and Sharma [82] given by Eq. 8.6 was also tried out, but gave less satisfying results for the present flow. The constant C_μ was 0.09.

The mean chemical reaction term

The mean chemical reaction term was modeled by employing Magnussen's Eddy Dissipation Concept (see Chapter 3). However, for comparison, an Arrhenius expression, and a simplified version of Spalding's Eddy Breakup Model (EBU), was also employed.

Eddy Dissipation Concept:

For a single-step reaction (Eq. 3.35), the mean chemical reaction term for the fuel mass fraction, can be expressed as

$$-\overline{R}_F = \overline{\rho}\frac{\gamma_\lambda^2}{\tau^*}(Y_F^\circ - Y_F^*). \tag{9.5}$$

By employing finite-rate chemistry calculations, the fine-structure mass fraction Y_F^* was found by integrating the reactor equation,

$$\frac{dY_F^*}{dt} = \omega_F^* + \frac{1}{\tau^*}(Y_F^\circ - Y_F^*), \tag{9.6}$$

to steady state. Here, ω_F^* is the specific fuel reaction rate for the reactor and was found by using the same (laminar) single-step Arrhenius expression, and the same reference variables, as Alshaalan [2]. Hence, ω_F^* was calculated as

$$\omega_F^* = \frac{\widetilde{u}^1}{H}\widehat{\omega}_F^* = \frac{\gamma\widetilde{u}^1}{H}\widehat{\rho}^*\widehat{Y}_F^*\exp\left(-\frac{\beta(1-\widehat{T}^*)}{1-\alpha(1-\widehat{T}^*)}\right), \tag{9.7}$$

where $\widehat{\omega}_F^*$ is the reduced reactor reaction rate and $\gamma\widetilde{u}^1/H$ is the dimensional preexponential constant. $\widehat{\rho}^* = \rho^*/\overline{\rho}^1$ is the non-dimensionalized reactor density and $\widehat{Y}_F^* = Y_F^*/\widetilde{Y}_F^1$ is the reduced reactor fuel mass fraction. The non-dimensional parameters were: $\alpha = 0.7, \beta = 5.24$, and $\gamma = 50$. The reduced reactor temperature was calculated as

$$\widehat{T}^* = \frac{T^* - T^1}{T_\mathrm{a} - T^1}. \tag{9.8}$$

The superscript 1 refers to the conditions in the fresh gases, H is the half channel width, and T_a is the adiabatic flame temperature. The surrounding state (Y_F°) was found by using Eq. 3.31.

An interesting observation can be derived from Eqs. 9.5–9.6. When approaching a wall, as discussed in previous chapter, $\gamma_\lambda \to 1$, which can be interpreted as if all of the flow is fine structure. If the reactor equation is solved for Y_F^* at steady state, that is when $dY_F^*/dt \to 0$, then

$$Y_F^* \to Y_F^\circ + \omega_F^* \tau^*. \tag{9.9}$$

If this expression for Y_F^* is put into Eq. 9.5, then

$$-\overline{R}_F \to -\overline{\rho}\omega_F^* \tag{9.10}$$

when approaching the wall. This shows that the present expression for EDC, in conjunction with finite-rate chemistry, approaches the reactor reaction rate at the wall, which is in accordance with the behavior shown in Sec. 8.2 (Eq. 8.4). This means that the limiting value for EDC at a wall is a laminar reactor.

Arrhenius expression:

For comparison, the mean chemical reaction term was calculated with a similar Arrhenius expression as in Eq. 9.7, assuming that mean values can be used for density and fuel mass fraction. Then the reaction rate is expressed as

$$-\overline{R}_F = A_F \overline{\rho} \widetilde{Y}_F \exp\left(-\frac{\beta(1-\widehat{T})}{1-\alpha(1-\widehat{T})}\right), \tag{9.11}$$

where

$$\widehat{T} = \frac{\widetilde{T} - T^1}{T_\mathrm{a} - T^1}, \tag{9.12}$$

is the reduced temperature, and $A_F = \frac{\gamma \widetilde{u}^1}{H}$ is the dimensional pre-exponential constant. This model is valid for the low-Dahmköhler-number limit only. The Dahmköhler number for the present flame was 0.287, corresponding to the well-stirred reactor regime where reactants mix rapidly and burn slowly. In most turbulent flames the model is completely inadequate, but may be useful for simple analysis [116].

Eddy Breakup Model:

Also, a simplified version of Spalding's Eddy Breakup Model (EBU) [129] was used for comparison [116], where

$$-\overline{R}_F = C_\mathrm{EBU} \overline{\rho} \frac{\widetilde{\varepsilon}}{\widetilde{k}} \widehat{T}(1-\widehat{T}). \tag{9.13}$$

Here, C_EBU is a model constant, and $\widehat{T}$ was calculated by Eq. 9.12.

9.4.5 Computational mesh and boundary conditions

A uniform 42×42 Cartesian grid was employed. The left boundary was placed at the downstream location of the flame holder, and the computational domain was set to $\Delta x = 4.17H, \Delta y = 2H$. The inlet conditions for the mass fraction equation was $\widetilde{Y}_F = 0$ at the location of the flame holder and $\widetilde{Y}_F = 1$ otherwise. Fixing the temperature at $T_\mathrm{a} = 2000\,\mathrm{K}$ held the flame at the selected location (at $x = 0.21H$, $y = 0.5H$). For the enthalpy equation, the inlet conditions were determined from the fixed temperature and species concentration. Except for the flame holder, the inlet temperature was fixed at $\widetilde{T}_F = 600\,\mathrm{K}$. At the lower wall, the boundary condition in the fuel mass fraction equation was zero mass flux across the wall, while for the enthalpy equation, a wall heat flux was modeled according to the fixed wall temperature ($T_\mathrm{w} = 600\,\mathrm{K}$) as [42]

$$S_h = -q_\mathrm{wall} = \frac{\mu}{\sigma}\left(\frac{\partial h}{\partial y}\right)_\mathrm{wall}. \tag{9.14}$$

Here, it has been assumed that the turbulence effects were negligible for the innermost control volume. At the upper wall, the $\widetilde{Y}_F$ equation was treated as for the lower wall, whereas for the enthalpy equation, no heat flux was calculated here, since no flame was interacting with it. However, the temperature for the upper wall was also fixed at 600 K. At the outlet, zero-diffusion boundary conditions were applied.

9.4.6 Numerical method

The general purpose CFD code SPIDER was employed to solve the equations. SPIDER was described in Chapter 5. The reactor equation (Eq. 9.6) was solved to steady state (integrated from 0 to $100 \times \tau^*$) by using an "external" equation solver (LIMEX [37]) for every global iteration.

9.5 Results and discussion

Since EDC is developed for high Reynolds numbers, it was not expected to give a good representation of the present low-Reynolds-number flow. For high-Reynolds-number flows, a certain upper limit $\gamma_\lambda < 0.5$ is normally introduced to avoid excessive reaction rates in the low-Reynolds-number regime (e.g. near walls). For the standard EDC, $\gamma_\lambda > 0.5$ may be considered unrealistic [48]. From these considerations, and since the presumptions of the standard model were broken for the present flow, three modifications were introduced to the mass fraction for the fine-structure region variable, γ_λ. First, an upper limit of 0.5

was applied for γ_λ. Second, an upper limit of 0.8 was introduced since it was found that γ_λ was greater than 0.5 for most of the flow. Third, the modification proposal in Eq. 8.8 was tested. The present wall flame, even though many simplifications have been made in the predictions, was believed to serve as a reasonable case to investigate the behavior of the different EDC variables for low Reynolds numbers and how these features affect the mean chemical reaction term. Figure 9.3–9.5 show contour profiles from the three different calculations with EDC. The figures show the contours of mean fuel mass fraction (a), mean product mass fraction (b), the reduced temperature (c), and the mean chemical reaction term (d). Furthermore, Figs. 9.8–9.9, show the behavior of the EDC variables for the three different cases compared to what the standard EDC "apparently" would have predicted (using no limit on γ_λ was denoted as $\gamma_{\lambda\mathrm{STD}}$ in the figures). These "apparent" values are unphysical close to the wall, and should of course never increase above unity in a calculation when using EDC. However, for comparison, this behavior is still shown here. The predictions by employing the Arrhenius expression and the EBU model are shown in Figs. 9.10–9.12. The Reynolds-number functions in the modified γ_λ for the present flow are shown in Fig. 9.14.

The $\gamma_\lambda < 0.5$ case:

Despite the limitations, the standard model with $\gamma_\lambda < 0.5$ (see Fig. 9.3) actually predicted a reasonable flame picture compared to the DNS flame (Fig. 9.2). However, the flame is too broad in the vicinity of the flame holder and the wall flame was differently predicted from that of the DNS (Fig. 9.2). The wall flame was located at a more upstream location. It seems as if the wall flame was spread too fast towards the wall compared to the DNS flame, where the spreading of the lower branch of the flame was about the same as for the upper branch. For the present model, the upper branch seemed to spread at a reasonable rate. The exclusion of the effects due to heat release will have some effect on this. Since density was held constant in the present computations, the heat released from the flame had no effect on the flow. The expansion from the flame will probably push it away from the wall. This can also be seen in the DNS flame (Fig. 9.2). The deflection of the branches is probably due to the heat release. Also, uncertainties in the inlet conditions may lead to discrepancies. It was investigated if some of the spreading effects might be due to uncertainties in the diffusion modeling. Computations employing the Launder and Sharma (LS) Reynolds-number function f_μ (see Fig. 9.6(b)) led to just noticeable more spreading of both the upper and the lower branch of the flame (therefore contours of this computation are not shown here). This indicates that some of the excessive spreading of the lower branch could be due to the combustion model. This also indicates that even a stronger damping of the turbulence diffusion could have been introduced than the JL f_μ function. However, closer to the wall, the JL and the LS f_μ functions are not very different (Fig. 9.6(b)). Even though there

are some uncertainties due to the diffusion model, this model and the Reynolds-number functions are well-established for non-reactive flows. From the ratio between the molecular and the eddy viscosity (Fig. 9.7), it can be seen that at some distance away from the wall, the eddy viscosity was more than 25 times higher than the molecular viscosity. This also indicates that the standard EDC should predict reasonable behavior of the upper branch and less reasonable behavior of the lower branch. The broadening of the flame, farther from the wall, was somewhat stronger than the other cases, which was probably due to the limitation on γ_λ (see Fig. 9.8(a)). This limit kept the magnitude γ_λ^2/τ^* (see Fig. 9.8(c)) at a lower rate throughout the flow, since γ_λ was greater than 0.5 here. The effects can readily be seen in the radial profiles of the predicted reaction term in Fig. 9.9. For the wall flame (Fig. 9.9(a)), the reaction rate was evidently more underpredicted compared to the other cases. Farther out, it was also underpredicted but not that much. At the other downstream locations (Figs. 9.9(b)–9.9(d)), the wall flame was not that different from the other cases since most of the fuel had already been consumed at these locations.

The $\gamma_\lambda < 0.8$ case:

This approach cut off excessive γ_λ rates towards the wall at a higher level than 0.5. This allowed higher values of γ_λ, and an even faster spreading towards the wall (see Fig. 9.4). The standard model with $\gamma_\lambda < 0.8$ seemed to predict a flame picture in better agreement with the DNS flame except close to the wall, where it seemed worse (faster spreading towards the wall). Around the flame holder, the flame seemed still too broad. The main difference to the previous case was close to the wall, where the present approach overpredicted the reaction rate more (Fig. 9.9(a)). This was due to the higher rate of γ_λ closer to the wall (see Fig. 9.8). From Fig. 9.8(a) it can be seen that for $y/\delta_{l0} < 2$, γ_λ increased much above the 0.5 limit. Therefore, this seemed to be the main reason to the differences close to the wall.

The proposed low-Reynolds-number version:

Figure 9.5 shows that introducing the modified γ_λ expressed in Eq. 8.8, changed the flame picture very little compared to applying the 0.8 limit. The modified γ_λ was close to the standard γ_λ for the outer region $y/\delta_{l0} > 2$, whereas the level was kept below unity close to the wall (see Fig. 9.8(a)). The main differences in the flame picture can be seen close to the wall where, compared to the 0.8 limit, a lower reaction rate, was predicted (see Figs. 9.4–9.5 and Fig. 9.9(a)). The reaction rate was, however, much higher than that obtained when using the 0.5 limit. This indicates that the reaction rate was overestimated also for this case. However, since detailed data for comparison were not available, and since heat-release effects were not calculated, it seems difficult to draw decisive conclusions on this. On the

other hand, it indicates that using the proposed modification improves the predicted reaction rate close to the wall compared to the case using the 0.8 limit. Figure 9.14 shows that the Reynolds-number functions kept γ_λ at a somewhat lower level (closer to the standard γ_λ, see Fig. 9.8), except very close to the wall where it increased towards unity. As long as the innermost control volume was located at a certain distance not too close to the wall, these calculations were possible to perform, even though the value increased above 0.8. It seems as if the modified version held γ_λ at a more reasonable level in the buffer region (the region $1 < y/\delta_{l0} < 2$) compared to the $\gamma_\lambda < 0.8$ case (see Fig. 9.8(a)). The plot of the Reynolds--number functions in the proposed modification of γ_λ (Fig. 9.14), shows that they behave as expected and as discussed in Chapter 8. Thus, this may be a possible path towards an extended EDC capable of predicting turbulent reacting near-wall flows. However, care must be taken when γ_λ approaches unity to obtain a numerically stable solution procedure.

The Arrhenius expression:

The results from applying the Arrhenius expression in Eq. 9.11 are shown in Figs. 9.10–9.11. In this case, two sets of the pre-exponential constant were used since employing $\gamma = 50$ led to excessive spreading and probably too high reaction rates. Alshaalan and Rutland used two different values for the pre-exponential factor. Alshaalan [2] used $\gamma = 50$ in his computations, whereas they have also used $\gamma = 14.58$ [4]. Calculations using $\gamma = 14.58$ predicted a reasonable flame picture and a clearer and definable reaction zone The wall flame was, however, almost not predicted at all. The flame picture was in reasonable accordance with the EDC predictions, and the magnitude of the reaction rate was of the same order.

The EBU model:

Figures 9.12–9.13 show how the EBU expression described in Eq. 9.13 performed for the present flow. The constant C_{EBU} was chosen close to the corresponding values in the EDC ($C_{\mathrm{EBU}} = 10$ was chosen), since predictions using the "universal constant $C_{\mathrm{EBU}} = 0.53$" gave very low reaction rates. The reaction rates using $C_{\mathrm{EBU}} = 10.0$ were excessively over-predicted in the wall regions as evident from the contour profiles in Fig. 9.13. Also, the reaction zone was more broadened for the flame away from the walls. Compared to these predictions one might say that the calculations with EDC gave a more reasonable flame picture.

9.6 Conclusions and recommendations

Conclusions

In the present chapter, the attempt to model a turbulent reacting low-Reynoldsnumber premixed Couette flow by using Magnussen's Eddy Dissipation Concept (EDC) for turbulent combustion was shown and compared to DNS results. It was shown that for calculations employing finite-rate chemistry, when applying a single-step (laminar) expression for the reactor reaction rate, the mean chemical reaction term, reduces to the laminar expression at the wall (when γ_λ approaches unity). This was in accordance with the behavior shown in Sec. 8.2 (Eq. 8.4).

The predictions show that by introducing limits to the mass fraction of fine-structure regions ($\gamma_\lambda < 0.5$ and $\gamma_\lambda < 0.8$), EDC predicted a reasonable flame picture compared to the DNS flame. The proposed low-Reynolds-number version of EDC introduced in Chapter 8 was tested and compared to the cases where $\gamma_\lambda < 0.5$ and $\gamma_\lambda < 0.8$. Introducing $\gamma_\lambda < 0.5$ gave less reasonable results for the flame away from the wall, but predicted a more reasonable wall flame than the other two approaches. For this case, the reaction rate for the rest of the flow was more underpredicted than for the other cases. Previous work has indicated that $\gamma_\lambda > 0.5$ might be unrealistic. However, the present work showed that allowing γ_λ to increase above this value gave more reasonable results for most of the flame. Introducing $\gamma_\lambda < 0.8$ gave more reasonable results for the flame away from the wall, but overpredicted the reaction rate towards the wall. The proposed model kept γ_λ at realistic values and seemed to give more reasonable results for the wall flame compared to $\gamma_\lambda < 0.8$, otherwise these two cases gave almost similar results. Compared to the $\gamma_\lambda < 0.5$ case, the proposed version gave a more reasonable flame away from the wall, but the wall flame was more overpredicted. One of the reasons for the discrepancies for the predictions of the wall flame compared to the DNS predictions may be due to the exclusion of heat release effects. Uncertainties in the inlet conditions may also lead to some discrepancies. The predictions showed that the proposed low-Reynolds-number version of EDC could be a way to extend the model to turbulent reacting flows near walls.

Predictions employing an Arrhenius expression for the mean chemical reaction rate gave reasonable results for $\gamma = 14.58$, but predicted excessive reaction rates for $\gamma = 50$. The EBU model gave in general poor results compared to the EDC calculations.

Recommendations

The objective of the present ongoing work was to develop a combustion model for turbulent reacting near-wall flow. The present work introduced a first attempt to investigate how the existing EDC model behaves close to a wall and showed a possible way to modify it

for low Reynolds numbers. For future work, the following must be in hand: detailed data (DNS or experimental data) for comparison (including inlet and boundary conditions), and turbulence models predicting good behavior for the flow under consideration.

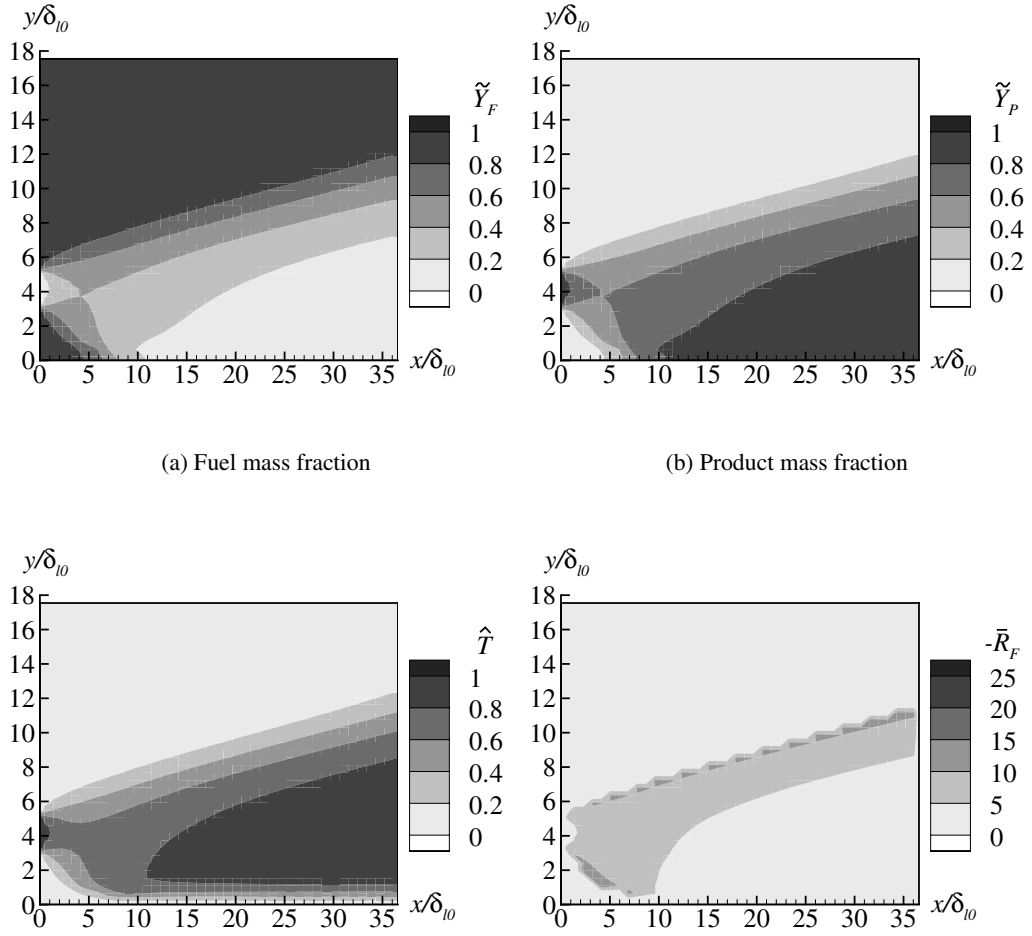

(a) Fuel mass fraction

(b) Product mass fraction

(c) Reduced temperature

(d) Reaction term (kg/m^{3}s)

Figure 9.3: Calculations with standard EDC, $\gamma_\lambda < 0.5$.

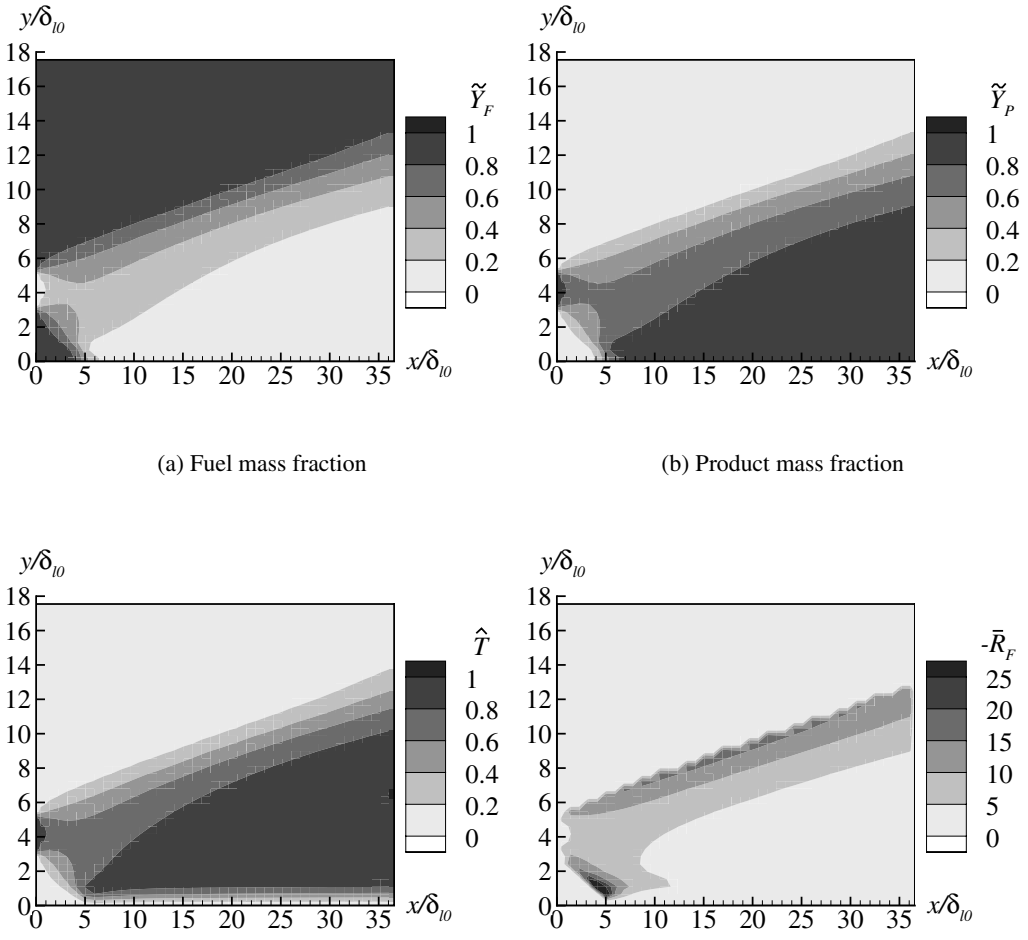

(a) Fuel mass fraction

(b) Product mass fraction

(c) Reduced temperature

(d) Reaction term (kg/m^{3}s)

Figure 9.4: Calculations with standard EDC, $\gamma_\lambda < 0.8$.

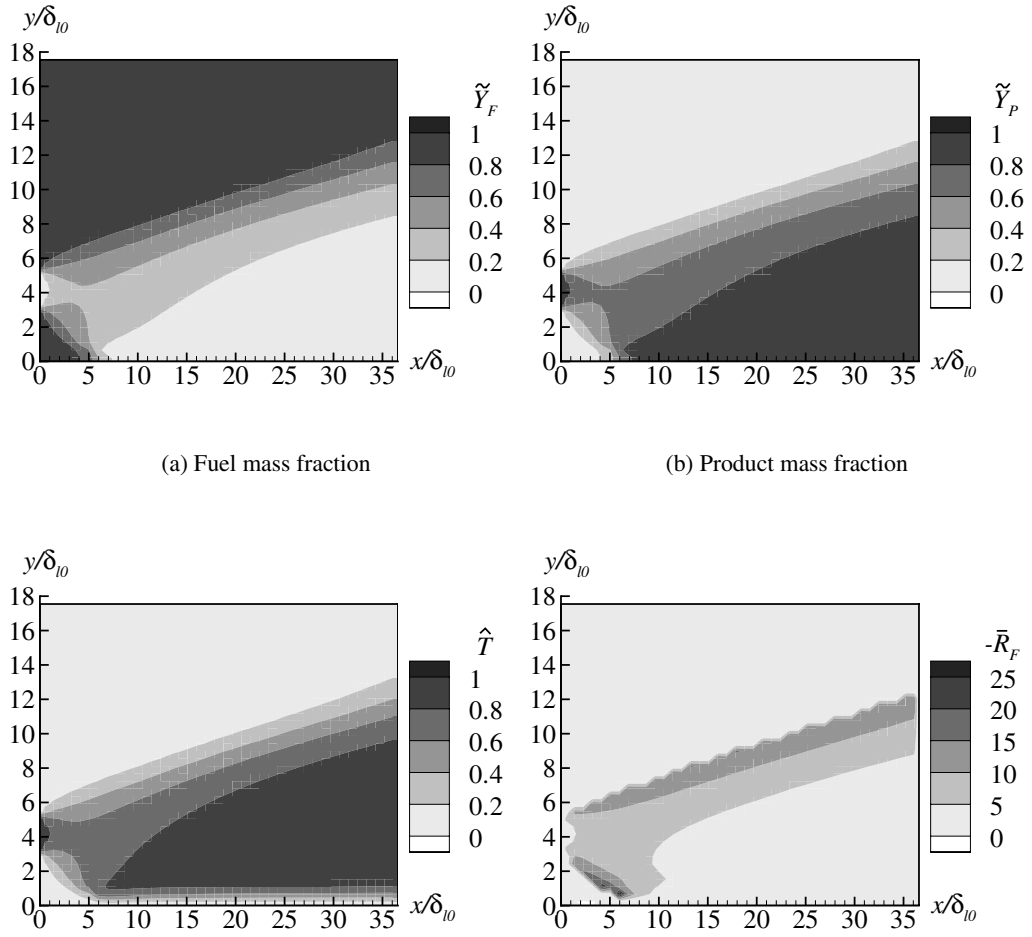

(a) Fuel mass fraction

(b) Product mass fraction

(c) Reduced temperature

(d) Reaction term (kg/m^{3}s)

Figure 9.5: Calculations with the proposed low-Reynolds-number version of EDC.

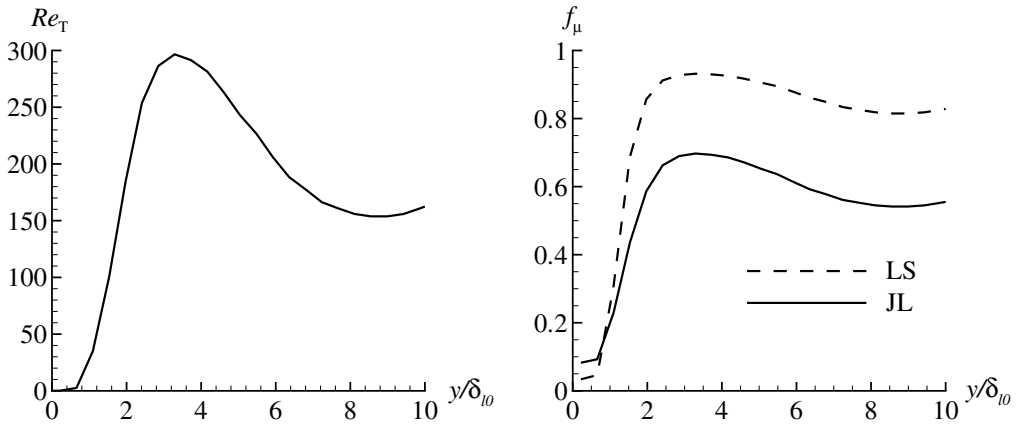

(a) Turbulence Reynolds number (b) Reynolds-number functions

Figure 9.6: The turbulence Reynolds number and the Reynolds-number functions for the present flow.

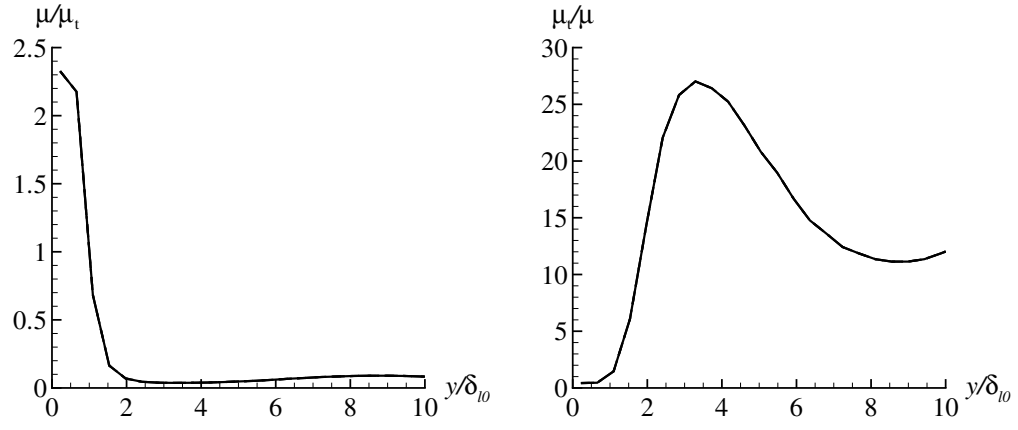

(a) μ/μ_t (b) μ_t/μ

Figure 9.7: Eddy viscosity versus molecular viscosity.

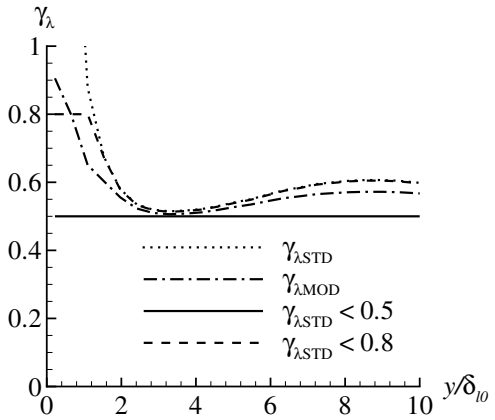

(a) Modified versions of γ_λ versus the standard version.

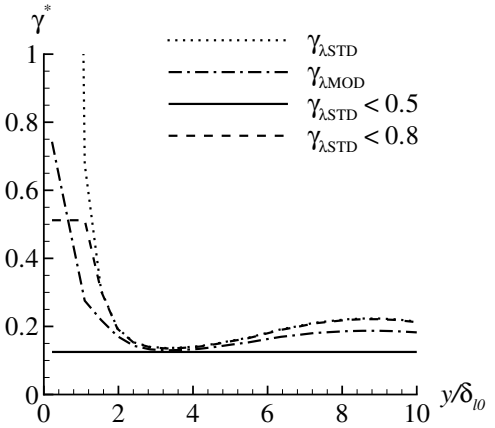

(b) γ^* for modified versions of γ_λ and the standard version.

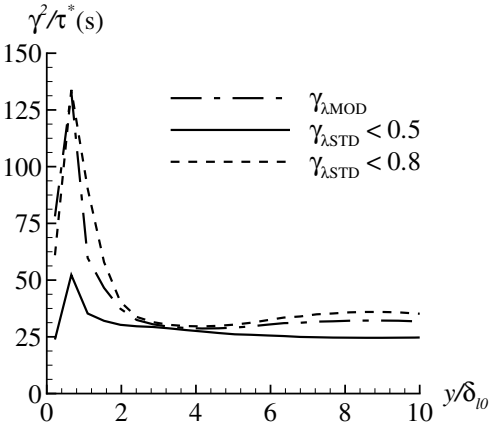

(c) γ_λ^2/τ^* for modified versions of γ_λ.

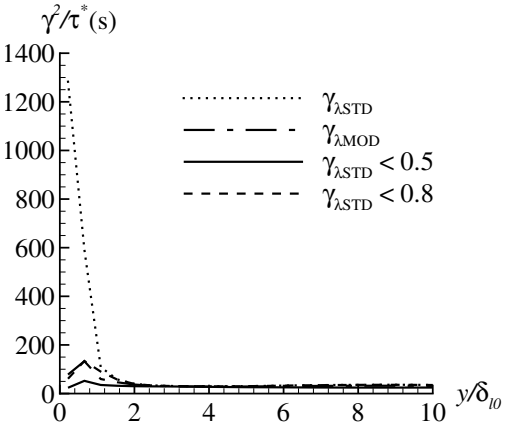

(d) γ_λ^2/τ^* for modified versions of γ_λ and the standard version.

Figure 9.8: Calculations with standard and modified γ_λ.

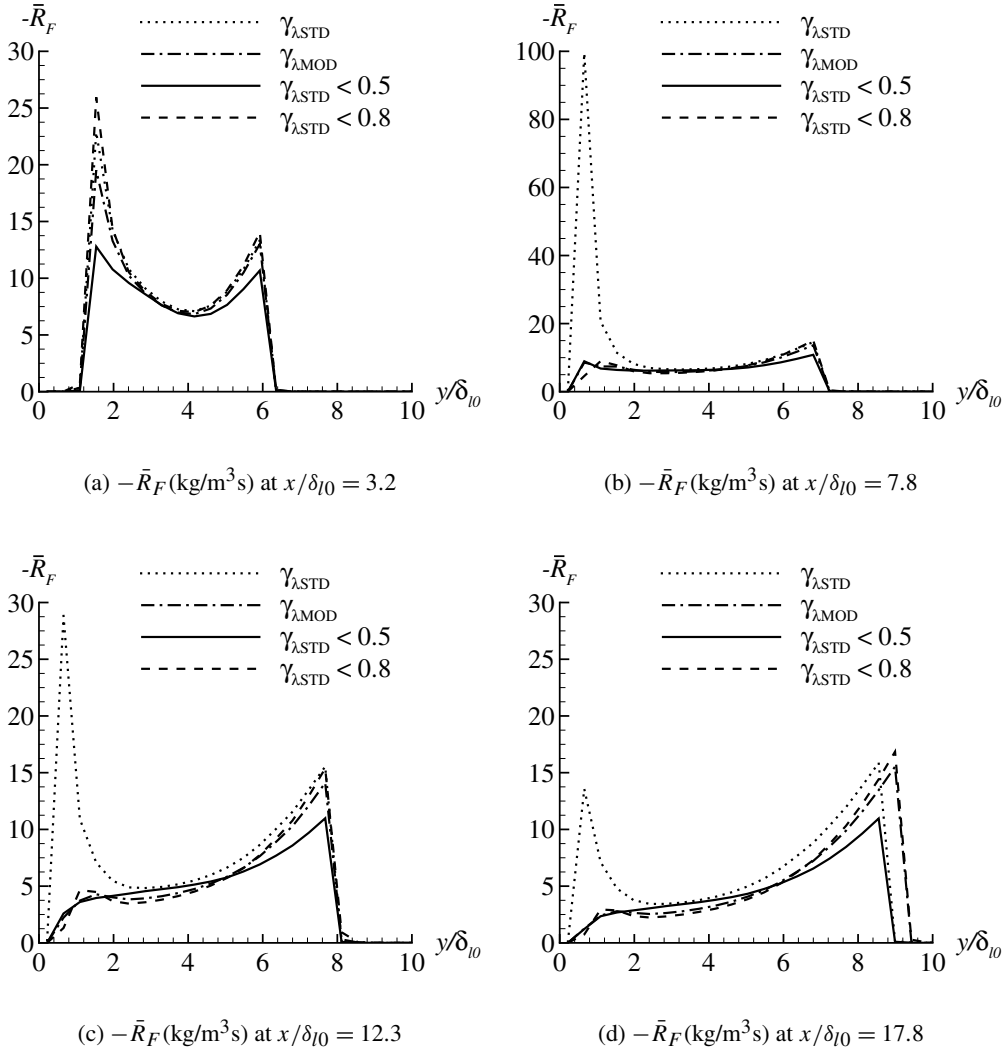

(a) $-\bar{R}_F$(kg/m^{3}s) at $x/\delta_{l0} = 3.2$

(b) $-\bar{R}_F$(kg/m^{3}s) at $x/\delta_{l0} = 7.8$

(c) $-\bar{R}_F$(kg/m^{3}s) at $x/\delta_{l0} = 12.3$

(d) $-\bar{R}_F$(kg/m^{3}s) at $x/\delta_{l0} = 17.8$

Figure 9.9: Radial profiles of the mean chemical reaction term for calculations with standard and modified γ_λ.

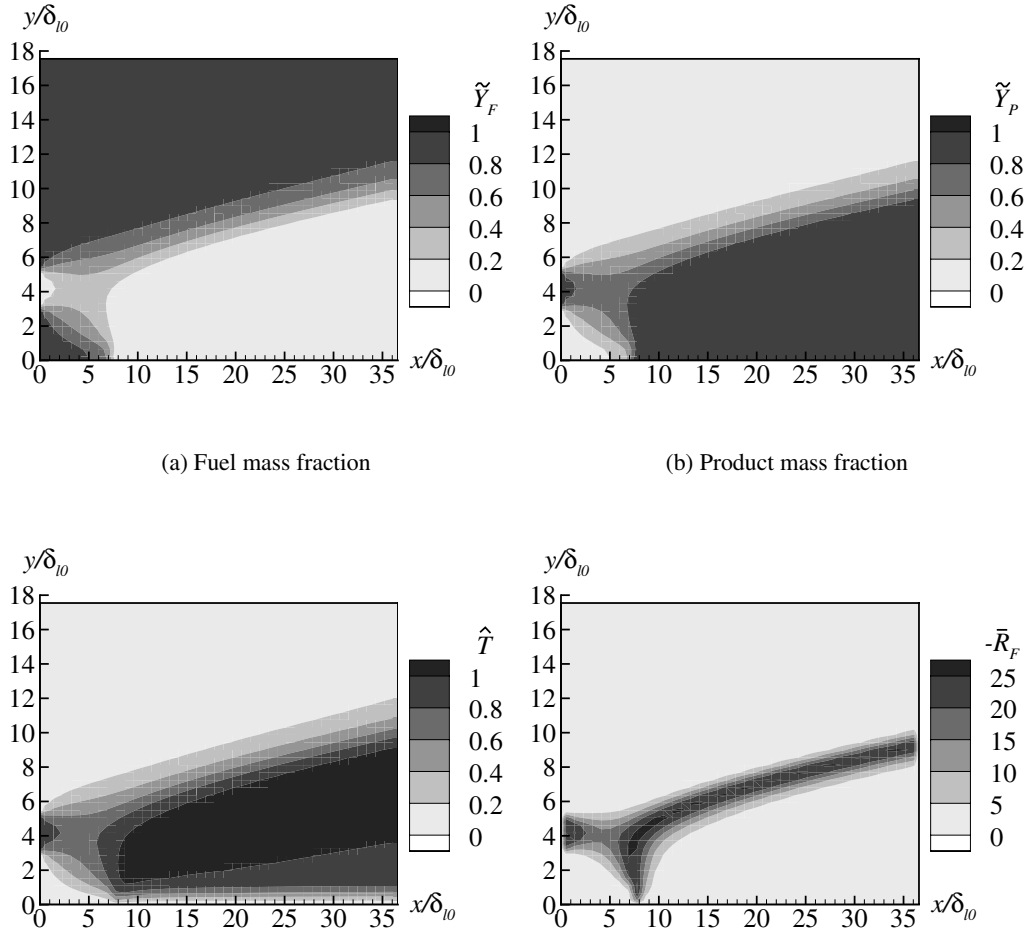

(a) Fuel mass fraction

(b) Product mass fraction

(c) Reduced temperature

(d) Reaction term (kg/m^{3}s)

Figure 9.10: Calculations with Arrhenius expression, $\gamma = 14.58$.

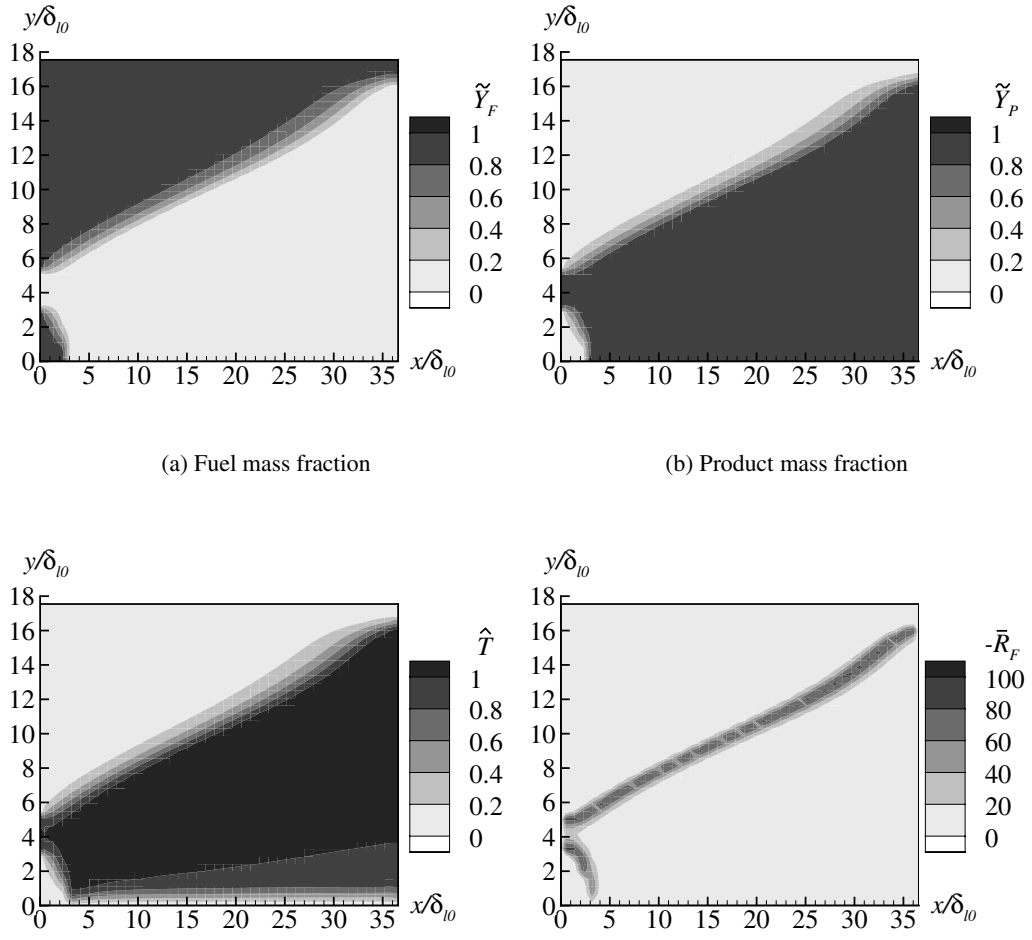

(a) Fuel mass fraction

(b) Product mass fraction

(c) Reduced temperature

(d) Reaction term (kg/m^{3}s)

Figure 9.11: Calculations with Arrhenius expression, $\gamma = 50$.

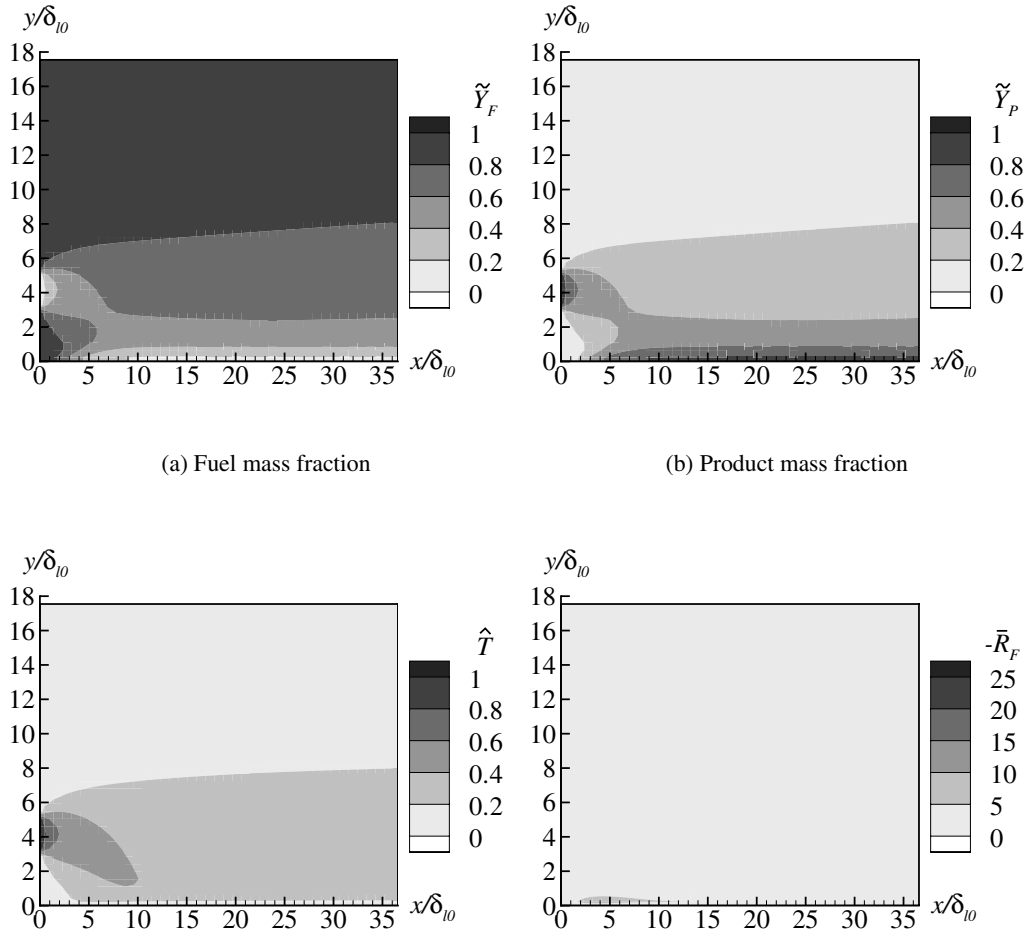

(a) Fuel mass fraction

(b) Product mass fraction

(c) Reduced temperature

(d) Reaction term (kg/m^{3}s)

Figure 9.12: Calculations with EBU model, $C_{\mathrm{EBU}} = 0.53$.

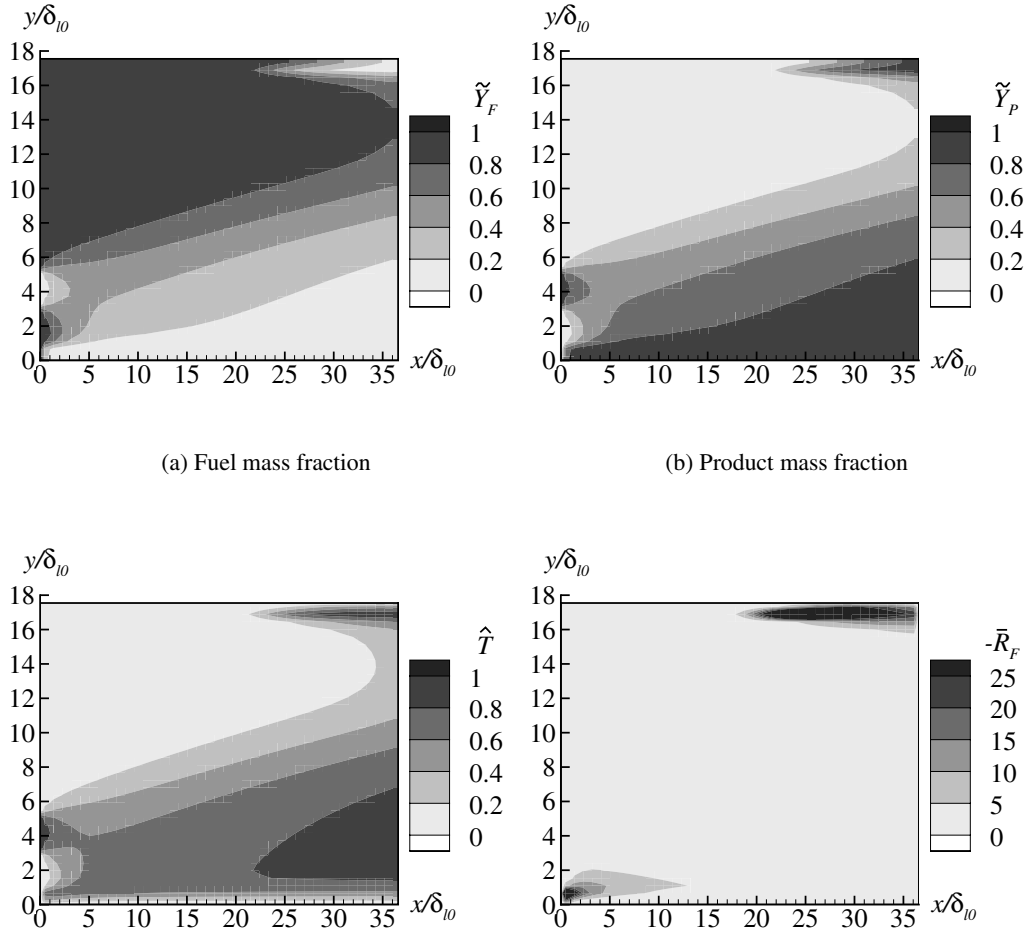

(a) Fuel mass fraction

(b) Product mass fraction

(c) Reduced temperature

(d) Reaction term (kg/m^{3}s)

Figure 9.13: Calculations with EBU model, $C_{\mathrm{EBU}} = 10$.

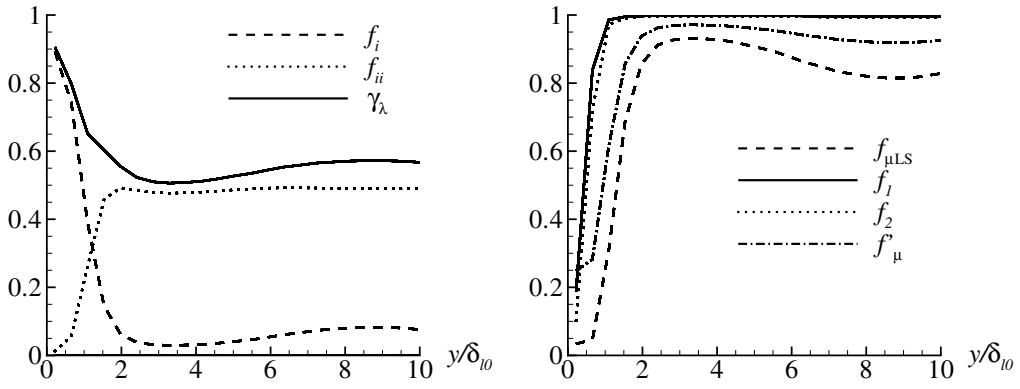

(a) Reynolds-number functions in $\gamma_{\lambda\text{mod}}$

(b) Reynolds-number functions in $\gamma_{\lambda\text{mod}}$

Figure 9.14: The Reynolds-number functions in the modified γ_λ.

Chapter 10

Concluding remarks

The present work dealt with turbulent combustion modeling of boundary-layer flows by using Favre-averaged Navier-Stokes equations. It was focused on turbulence and chemical reactions including local extinction effects. The objective was to investigate these phenomena by using a low-Reynolds-number turbulence model, and a combustion model that employed finite-rate chemistry including detailed chemical mechanisms.

It seems as if the best compromise between computer capabilities and model performance for describing the anisotropic behavior of turbulence in boundary layers, today, is found in the RSE models. Among the closures that take variable-density effects into account, the models of some terms accounting for important effects in combusting flows have not been developed due to the lack of both experimental work and DNS data needed for validation. Since low-Reynolds-number RSE models for constant-density flows are more developed to account for near-wall flows, Favre-averaged versions of such closures seem to be the best choice at the moment. These models are sufficient to calculate combusting flows in many cases.

The review of turbulent reacting near-wall flow revealed that, in general, little is known about the subject, and that there are few experimental- and DNS data. There are no data available on detailed chemistry in turbulent reacting boundary-layer flow, which is, for the moment, only present for laminar flow. The experimental data that is present is mainly concerned with measuring wall heat fluxes, although some are concerned with fluid data such as velocity and Reynolds stresses. The existing DNS data are limited to low-Reynolds-number flows and single-step chemical mechanisms. For these reasons, models are less developed, even if some exist in special cases.

Due to the lack of experimental or DNS data of detailed chemistry for turbulent reacting

URN:NBN:no-7265

near-wall flow, jet flames were used in the present work to study local extinction effects. From the simulations of the syngas jet flame, it was observed that different turbulence models predicted variations in the turbulence-energy dissipation rate, and hence different fields of the fine-structure time scale in the EDC. When the chemical reactions are close to extinction, this may determine whether extinction is predicted or not. Simulations with different chemical mechanisms also indicated that the chemical time scales provided might differ. This may affect the extinction modeling. The predictions of the lifted H_2/N_2 jet flame showed that EDC gave a reasonable flame picture. The predicted flame by EDC was stabilized at an upstream location where turbulent micro mixing and chemical reactions were in balance. The predictions also revealed that by using the k-ε turbulence model, a higher lift-off height was predicted compared to predictions using the RSE model. This was a result of different predicted residence times. The local extinction effects observed by employing different turbulence models for the lifted jet flame were consistent with the findings from the studies of the syngas jet flame.

For the prediction of a turbulent non-reacting boundary-layer flow by using a low-Reynolds-number second-moment closure, the predicted velocity and Reynolds-stress fields were all in reasonable accordance with DNS data, even if there were some discrepancies in a couple of the stresses. These discrepancies may be due to the exclusion of some terms believed to be important for near-wall flow. The implementation of these terms was not completed due to numerical problems at the present stage. The objective of this work was to employ the model for use in the prediction of a reacting near-wall flow.

The behavior of EDC close to a wall, where the turbulence Reynolds number is very low, was also discussed. For the standard EDC, the mass fraction of fine-structure regions, γ_λ, increases towards infinity when the turbulence Reynolds number approaches zero, whereas the residence time approaches a finite value. It was proposed that γ_λ may approach unity when approaching a wall. If $\gamma_\lambda \rightarrow 1$, the mean and surrounding values in the EDC reactor model will approach the fine-structure values. As the turbulence Reynolds number approaches zero, the EDC mean reaction rate approaches the laminar reaction rate. A low-Reynolds-number version of EDC was proposed. In this proposal, by employing Reynolds-number functions, the desired behavior of γ_λ was achieved, which also means that γ_λ approaches $\gamma_{\lambda\mathrm{STD}}$, when $Re_\mathrm{T} > 300$. The residence time was kept in its original form for the prediction of turbulent reacting near-wall flow.

An attempt was also made to model a wall-interacting flame in a turbulent reacting low--Reynolds-number Couette flow by using Magnussen's Eddy Dissipation Concept (EDC) for turbulent combustion. It was shown that for calculations employing finite-rate chemistry, when applying a single-step (laminar) expression for the reactor reaction rate, the mean chemical reaction term, reduces to the laminar expression at the wall (when γ_λ approaches unity). This is in accordance with the indication that the fine-structure values are

the limiting values for EDC at the wall. The predictions show that by introducing limits to γ_λ ($\gamma_\lambda < 0.5$ or $\gamma_\lambda < 0.8$), or by using the proposed low-Reynolds-number version, EDC predicted a reasonable flame picture compared to the DNS flame. Introducing $\gamma_\lambda < 0.5$ gave less reasonable results for the flame away from the wall, but seemed to predict a more reasonable wall flame than the other two approaches. For this case, the reaction rate for the rest of the flow was more underpredicted than for the other cases. Introducing $\gamma_\lambda < 0.8$ gave more reasonable results for the flame away from the wall, but seemed to overpredict the reaction rate towards the wall. The proposed low-Reynolds-number version of EDC seemed to give more reasonable results for the wall flame compared to $\gamma_\lambda < 0.8$, otherwise these two cases gave almost similar results. Compared to the $\gamma_\lambda < 0.5$ case, the proposed version gave a more reasonable flame away from the wall, but the wall flame was more overpredicted. Heat-release effects were not modeled, which may be part of the explanation for the discrepancies in the wall flame compared to the DNS flame. Uncertainties in the inlet conditions may also have led to discrepancies. These predictions indicated that the proposed low-Reynolds-number version of EDC might be a way to extend the model to turbulent reacting flows near walls.

The predictions of the turbulent reacting Couette flow introduced the possibility to investigate the behavior of EDC for a turbulent reacting near-wall flow. The single-step mechanism implemented may be convenient for model building. When detailed chemistry data is available, the detailed mechanisms that already exist can be used as they are well validated in conjunction with EDC.

URN:NBN:no-7265

Bibliography

[1] G. M. Abu-Orf and R. S. Cant. A Turbulent Reaction Rate Model for Premixed Turbulent Combustion in Spark-Ignition Engines. *Combustion and Flame*, 122:233–252, 2000.

[2] T. M. Al-Shaalan. *Studying Reacting Turbulent Couette Flow Using Direct Numerical Simulations*. PhD thesis, University of Wisconsin-Madison, 1997.

[3] T. M. Al-Shaalan and C. J. Rutland. Turbulence, Scalar Transport and Reaction Rates in Flame-Wall Interaction. In *Twenty-Seventh Symposium (International) on Combustion*, pages 793–799. The Combustion Institute, Pittsburgh, 1998.

[4] T. M. Al-Shaalan and C. J. Rutland. Wall Heat Flux in Turbulent Premixed Reacting Flow. *Combustion Science and Technology*, 174:135–165, 2002.

[5] H. I. Andersson. Introduction to turbulence modelling. Lecture Notes, Division of Applied Mechanics, University in Trondheim (NTH), Norway, 1988.

[6] H. I. Andersson and B. A. Petterson. Modeling plane turbulent Couette flow. *International Journal of Heat and Fluid Flow*, 15(6):447–455, 1994.

[7] K. H. Bech, N. Tillmark, P. H. Alfredsson, and H. I. Andersson. An investigation of turbulent plane Couette flow at low Reynolds numbers. *Journal of Fluid Mechanics*, 286:291–325, 1995.

[8] R.W. Bilger. Future progress in turbulent combustion research. *Progress in Energy and Combustion Science*, 26:367–380, 2000.

[9] R. B. Bird, W. E. Stewart, and E. N. Lightfoot. *Transport Phenomena*. Second Edition, John Wiley & Sons Inc., New York, 2002.

[10] R Borghi. Turbulent Combustion Modeling. *Progress in Energy and Combustion Science*, 14:245–292, 1988.

URN:NBN:no-7265

[11] C. T. Bowman, R. K. Hanson, D. F. Davidson, W. C. Gardiner Jr., V. Lissianski, G. P. Smith, D. M. Golden, M. Goldenberg, and M. Frenklach. Gri-Mech 2.11. http://www.me.berkeley.edu/gri_mech/, 2003.

[12] D. Bradley, P. H. Gaskell, and X. J. Gu. The mathematical modeling of liftoff and blowoff of turbulent non-premixed methane jet flames at high strain rates. In *Twenty-Seventh Symposium (International) on Combustion*, pages 1199–1206. The Combustion Institute, Pittsburgh, 1998.

[13] P. Bradshaw. *An Introduction to Turbulence and its Measurement*. Pergamon Press Ltd, Oxford, 1971.

[14] P. Bradshaw. Understanding and prediction of turbulent flow–1996. *International Journal of Heat and Fluid Flow*, 18:45–54, 1997.

[15] K. N. C. Bray, M. Champion, and P. A. Libby. Premixed Flames in Stagnating Turbulence Part IV: A New Theory for the Reynolds Stresses and Reynolds Fluxes Applied to Impinging Flows. *Combustion and Flame*, 120:1–18, 2000.

[16] K. N. C. Bray, M. Champion, and P. A. Libby. Pre-Mixed Flames in Stagnating Turbulence Part V–Evaluation of Models for the Chemical Source Term. *Combustion and Flame*, 127:2023–2040, 2001.

[17] G. Bruneaux, K. Akselvoll, T. Poinsot, and J. H. Ferziger. Flame-Wall Interaction Simulation in a Turbulent Channel Flow. *Combustion and Flame*, 107:27–44, 1996.

[18] G. Bruneaux, T. Poinsot, and J. H. Ferziger. Premixed flame-wall interaction simulation in a turbulent channel flow: budget for the flame surface density evolution and modelling. *Journal of Fluid Mechanics*, 349:191–219, 1997.

[19] S. Byggstøyl and B. F. Magnussen. A Model for Flame Extinction in Turbulent Flow. In *Fourth International Symposium on Turbulent Shear Flows*, pages 381–385, Springer, Berlin, 1983.

[20] R. Cabra, T. Myhrvold, J.-Y. Chen, R. W. Dibble, A. N. Karpetis, and R. S. Barlow. Simultaneous Laser Raman-Rayleigh-LIF Measurements and Numerical Modeling Results of a Lifted Turbulent H_2/N_2 Jet Flame in a Vitiated Coflow. To appear in: *Proceedings of the Combustion Institute*, 29, 2003.

[21] S. Candel, D. Thévenin, N. Darabiha, and D. Veynante. Progress in Numerical Combustion. *Combustion Science and Technology*, 149:297–337, 1999.

[22] J.-Y. Chen and W. Kollmann. PDF modeling of chemical nonequilibrium effects in turbulent nonpremixed hydrocarbon flames. In *Twenty-Second Symposium (International) on Combustion*, pages 645–653. The Combustion Institute, Pittsburgh, 1988.

[23] M. Chen, M. Herrmann, and N. Peters. Flamelet modeling of lifted turbulent methane/air and propane/air jet diffusion flames. *Proceedings of the Combustion Institute*, 28:167–174, 2000.

[24] R. K. Cheng, R. G. Bill JR., and F. Robben. Experimental study of combustion in a turbulent boundary layer. In *Eightteenth Symposium (International) on Combustion*, pages 1021–1029. The Combustion Institute, Pittsburgh, 1981.

[25] K.-Y. Chien. Predictions of Channel and Boundary-Layer Flows with a Low-Reynolds-Number Turbulence Model. *AIAA Journal*, 20(1):33–38, 1982.

[26] J. Chomiak. *Combustion: A Study in Theory, Fact and Application*. Abacus Press/Gordon & Breach Science Publishers, Montreux, Switzerland, 1990.

[27] P. Y. Chou. On an extension of Reynolds' method of finding apparent stress and the nature of turbulence. *Chinese Journal of Physics*, 4:1–33, 1940.

[28] P. Y. Chou. On velocity correlations and the solutions of the equations of turbulent fluctuation. *Quarterly of Applied Mathematics*, 3:38–54, 1945.

[29] D. E. Cormack, L. G. Leal, and J. H. Seinfeld. An Evaluation of Mean Reynolds Stress Turbulence Models: The Triple Velocity Correlation. *Journal of Fluids Engineering*, 100:47–54, 1978.

[30] T. J. Craft. Developments in a low-Reynolds-number second-moment closure and its application to separating and reattaching flows. *International Journal of Heat and Fluid Flow*, 19:541–548, 1998.

[31] T. J. Craft, J. W. Kidger, and B. E. Launder. Second-moment modelling of developing and self-similar 3D turbulent free-surface jets . *International Journal of Heat and Fluid Flow*, 21:338–344, 2000.

[32] T. J. Craft and B. E. Launder. Computation of Impinging Flows using Second-Moment Closures. In *Eighth Symposium on Turbulent Shear Flows*, pages 8.5.1–8.5.6. Munich, Germany, 1991.

[33] T. J. Craft and B. E. Launder. New wall-reflection model applied to the turbulent impinging jet. *AIAA Journal*, 30(12):2970–2972, 1992.

[34] T. J. Craft and B. E. Launder. A Reynolds stress closure designed for complex geometries. *International Journal of Heat and Fluid Flow*, 17:245–254, 1996.

[35] B. J. Daly and F. H. Harlow. Transport equations in turbulence. *Physiscs of Fluids*, 13(11):2634–2649, 1970.

[36] B. I. Davydov. On statistical dynamics of an incompressible turbulent fluid. *Soviet Physics - Doklady*, 6(1):10–12, 1961.

[37] P. Deuflhard, E. Hairer, and J. Zugck. One-step and Extrapolation Methods for Differential-Algebraic Systems. *Numerische Mathematik*, 51:501–516, 1987.

[38] D. Drysdale. *An Introduction to Fire Dynamics*. John Wiley and Sons, Chichester, England, 1985.

[39] P. A. Durbin. A Reynolds stress model for near-wall turbulence. *Journal of Fluid Mechanics*, 249:465–498, 1993.

[40] I. S. Ertesvåg. Private communication.

[41] I. S. Ertesvåg. *Utvikling av turbulensmodell for låge reynoldstal med likning for reynoldsspenningane og likning for karakteristisk frekvens*. Dr. ing. thesis, University of Trondheim, Norway, Norway, 1991. (In Norwegian).

[42] I. S. Ertesvåg. *Turbulent strøyming og forbrenning (Turbulent Flow and Combustion)*. (In Norwegian). Tapir akademisk forlag, Trondheim, Norway, 2000.

[43] I. S. Ertesvåg and B. F. Magnussen. The Eddy Dissipation turbulence energy cascade model. *Combustion Science and Technology*, 159:213–236, 2000.

[44] D. Escudié and E. Haddar. Experimental Study of a Premixed Turbulent Stagnating Flame. *Combustion and Flame*, 95:433–435, 1993.

[45] J. H. Ferziger and M. Perić. *Computational Methods for Fluid Dynamics*. Springer, Berlin, 1996.

[46] M. M. Gibson and B. E. Launder. Ground effects on pressure fluctuations in the atmospheric boundary layer. *Journal of Fluid Mechanics*, 86(3):491–511, 1978.

[47] V. I. Golovitchev and J. Chomiak. Analysis of main assumptions underlying the revised EDC approach for combustion modeling. Seminar on Mathematical Modelling of Turbulence-Combustion Interaction, Trondheim, Norway, 10-11 September 2002.

[48] I. R. Gran. Numerical simulation of fluid flow and combustion in gas turbine combustors. Master's thesis, University of Trondheim (NTH), Norway, 1990.

[49] I. R. Gran. *Mathematical modeling and numerical simulation of chemical kinetics in turbulent combustion*. Dr. ing. thesis, University of Trondheim (NTH), Norway, 1994.

[50] I. R. Gran and B. F. Magnussen. A Numerical Study of a Bluff-body Stabilized Diffusion Flame. Part 1. Influence of Turbulence Modeling and Boundary Conditions. *Combustion Science and Technology*, 119:171–190, 1996.

[51] I. R. Gran and B. F. Magnussen. A Numerical Study of a Bluff-Body Stabilized Diffusion Flame. Part 2. Influence of Combustion Modeling and Finite-Rate Chemistry. *Combustion Science and Technology*, 119:191–217, 1996.

[52] I. R. Gran, M. C. Melaaen, and B. F. Magnussen. Numerical simulation of local extinction effects in turbulent combustor flows of methane and air. In *Twenty-Fifth Symposium (International) on Combustion*, pages 1283–1291. The Combustion Institute, Pittsburgh, 1994.

[53] D. Han and M. G. Mungal. Direct Measurement of Entrainment in Reacting/Nonreacting Turbulent Jets. *Combustion and Flame*, 124:370–386, 2001.

[54] K Hanjalić. Advanced turbulence closure models: a view of current status and future prospects. *International Journal of Heat and Fluid Flow*, 15(3):178–203, 1994.

[55] K Hanjalić and S. Jakirlić. Contribution towards the second-moment closure modelling of separating turbulent flows. *Computers and Fluids*, 27(2):137–156, 1998.

[56] K Hanjalić and B. E. Launder. A Reynolds stress model of turbulence and its application to thin shear flows. *Journal of Fluid Mechanics*, 52:609–638, 1972.

[57] K Hanjalić and B. E. Launder. Contribution towards a Reynolds-stress closure for low-Reynolds number turbulence. *Journal of Fluid Mechanics*, 74:593–610, 1976.

[58] J. O. Hinze. *Turbulence*. Second Edition, McGraw-Hill, New York, 1975.

[59] F. P. Incropera and D. P. De Witt. *Fundamentals of Heat and Mass Transfer*. Third Edition, John Wiley & Sons, New York, 1990.

[60] F. Irgens. *Kontinuumsmekanikk (Continuum Mechanics)*. Institutt for mekanikk, termo- og fluiddynamikk, NTNU, Trondheim, Norway, 1997. (In Norwegian).

[61] A. Iserles. *A First Course in the Numerical Analysis of Differential Equations*. Cambridge University Press, Cambridge, 1996.

[62] S. Jakirlić. *Reynolds-Spannungs-Modellierung komplexer turbulenter Strömungen*. Dr.-Ing. thesis, Der Technischen Fakultät der Universität Erlangen-Nürnberg. Herbert Utz Verlag, München (In German), 1997.

[63] W. P. Jones. Private communication.

[64] W. P Jones. Turbulence modelling and numerical solution methods for variable density and combusting flows. In P. A. Libby and F. A. Williams, editors, *Turbulent Reacting Flows*, pages 309–374. Academic Press Ltd, London, 1994.

[65] W. P. Jones and B. E. Launder. The prediction of laminarization with a two-equation model of turbulence. *International Journal of Heat and Mass Transfer*, 15:301–314, 1972.

[66] W. P. Jones and B. E. Launder. The calculation of low-reynolds-number phenomena with a two-equation model of turbulence. *International Journal of Heat and Mass Transfer*, 16:1119–1130, 1973.

[67] W. P. Jones and P. Musonge. Closure of the Reynolds stress and scalar flux equations. *Physics of Fluids*, 31(12):3589–3604, 1988.

[68] W. P. Jones and J. H. Whitelaw. Calculation Methods for Reacting Turbulent Flows: A Review. *Combustion and Flame*, 48:1–26, 1982.

[69] W. P. Jones and J. H. Whitelaw. Modelling and measurements in turbulent combustion. In *Twentieth Symposium (International) on Combustion*, pages 233–249. The Combustion Institute, Pittsburgh, 1984.

[70] W. M. Kays and M. E. Crawford. *Convective Heat and Mass Transfer*. Third Edition, McGraw-Hill, New York, 1993.

[71] R. J. Kee, F. M. Rupley, and J. A. Miller. CHEMKIN-II, A Fortran chemical kinetics package for the analysis of gas-phase chemical kinetics. Technical report, SAND89-8009, Sandia National Laboratories, Livermore, CA, 1989.

[72] L. A. Kennedy and O. A. Plumb. Prediction of buoancy controlled turbulent wall diffusion flames. In *Sixteenth Symposium (International) on Combustion*, pages 1699–1707. The Combustion Institute, Pittsburgh, 1976.

[73] A. R. Kerstein. Turbulence in Combustion Processes: Modeling Challenges. To appear in: *Proceedings of the Combustion Institute*, 29, 2003.

[74] J. Kim, P. Moin, and R. Moser. Turbulence statistics in fully developed channel flow at low Reynolds number. *Journal of Fluid Mechanics*, 177:133–166, 1987.

[75] S. H. Kim, K. Y. Huh, and R. W. Bilger. Second-order Conditional Moment Closure Modeling of Local Extinction and Reignition in Turbulent Non-Premixed Hydrocarbon Flames. To appear in: *Proceedings of the Combustion Institute*, 29, 2003.

[76] T. Kojima and K. Nishiwaki. Modeling of flame-wall interaction for combustion and heat transfer in s.i. engines. *Society of Automotive Engineers of Japan Review*, 18:11–17, 1997.

[77] K. K. Kuo. *Principles of Combustion*. John Wiley & Sons, New York, 1986.

[78] B. E. Launder. Second-moment closure: present... and future? *International Journal of Heat and Fluid Flow*, 10(4):282–300, 1989.

[79] B. E. Launder. An Introduction to Single-Point Closure Methodology. In *Computational Fluid Dynamics*, pages 257–323. Elsevier Science, 1996.

[80] B. E. Launder and S.-P. Li. On the elimination of wall-topography parameters from second-moment closure. *Physics of Fluids*, 6(2):999–1006, 1994.

[81] B. E. Launder, G. J. Reece, and W. Rodi. Progress in the development of a Reynolds-stress turbulence closure. *Journal of Fluid Mechanics*, 68(3):537–566, 1975.

[82] B. E. Launder and B. I. Sharma. Application of the energy-dissipation model of turbulence to the calculation of flow near a spinning disc. *Letters in heat and mass-transfer*, 1:131–138, 1974.

[83] B. E. Launder and D. B. Spalding. The numerical computation of turbulent flows. 3:269–289, 1974.

[84] B. E. Launder and D. P. Tselepidakis. Progress and Paradoxes in Modelling Near-Wall Turbulence. In *Eighth Symposium on Turbulent Shear Flows*, pages 29.1.1–29.1.6. Munich, Germany, 1991.

[85] B. E. Launder and D. P. Tselepidakis. Contribution to the Modelling of Near-Wall Turbulence. *Turbulent Shear Flows*, 8:81–96, 1993.

[86] S. C. Li, P. A. Libby, and F. A. Williams. Experimental investigation of a premixed flame in an impinging turbulent stream. In *Twenty-fifth Symposium (International) on Combustion*, pages 1207–1214. The Combustion Institute, Pittsburgh, 1994.

[87] F. C. Lockwood. The Modelling of Turbulent Premixed and Diffusion Combustion in the Computation of Engineering Flows. *Combustion and Flame*, 29:111–122, 1977.

[88] J. L. Lumley. Computational Modeling of Turbulent Flows. *Advances in Applied Mechanics*, 18:123–176, 1978.

[89] A. Lundbladh and A. V. Johansson. Direct simulation of turbulent spots in plane Couette flow. *Journal of Fluid Mechanics*, 229:499–516, 1991.

[90] B. F. Magnussen. On the Structure of Turbulence and a Generalized Eddy Dissipation Concept for Chemical Reaction in Turbulent Flow. In *Nineteenth AIAA Aerospace Meeting*, St. Louis, January 1981.

[91] B. F. Magnussen. Modeling of NO_x and soot formation by the Eddy Dissipation Concept. International Flame Research Foundation, First Topic Oriented Technical Meeting, Amsterdam, 17-19 October 1989.

[92] B. F. Magnussen. The Eddy Dissipation Concept (EDC) for Turbulent Combustion Modeling. Seminar on Mathematical Modeling of Turbulence-Combustion Interaction, The Scandinavian-Nordic Section of the Combusiton Institute, Trondheim, Norway, 10-11 September 2002.

[93] B. F. Magnussen and B. H. Hjertager. On mathematical modeling of turbulent combustion with special emphasis on soot formation and combustion. In *Sixteenth Symposium (International) on Combustion*, pages 719–729. The Combustion Institute, Pittsburgh, 1976.

[94] B. F. Magnussen, B. H. Hjertager, J. G. Olsen, and D. Bhaduri. Effects of Turbulent Structure and Local Concentration on Soot Formation and Combustion in C_2H_2 Flames. In *Seventeenth Symposium (International) on Combustion*, pages 1383–1393. The Combustion Institute, Pittsburgh, 1978.

[95] R. R. Maly. State of the art and future needs in S.I. engine combustion. In *Twenty-fifth Symposium (International) on Combustion*, pages 111–124. The Combustion Institute, Pittsburgh, 1994.

[96] R. Manceau and K. Hanjalić. A new form of the elliptic relaxation equation to account for wall effects in RANS modeling. *Physics of Fluids*, 12(9):2345–2351, 2000.

[97] T. Mantel and R. Borghi. A New Model of Premixed Wrinkled Flame Propagation Based on a Scalar Dissipation Equation. *Combustion and Flame*, 96:443–457, 1994.

[98] M. C. Melaaen. *Analysis of curvilinear non-orthogonal coordinates for numerical calculation of fluid flow in complex geometries*. Dr. ing. thesis, University of Trondheim (NTH), Norway, 1990.

[99] M. C. Melaaen. Calculation of fluid flows with staggered and nonstaggered curvilinear nonorthogonal grids–a comparison. *Numerical Heat Transfer, Part B*, 21:21–39, 1992.

[100] M. C. Melaaen. Calculation of fluid flows with staggered and nonstaggered curvilinear nonorthogonal grids–the theory. *Numerical Heat Transfer, Part B*, 21:1–19, 1992.

[101] Y. Mizobuchi, S. Tachibana, J. Shinjo, S. Ogawa, and T. Takeno. A Numerical Analysis on Structure of Turbulent Hydrogen Jet Liefted Flame. To appear in: *Proceedings of the Combustion Institute*, 29, 2003.

[102] C. J. Montgomery, C.R. Kaplan, and E.S. Oran. The Effect of Coflow Velocity on a Lifted Methane-Air Jet Diffusion Flame. In *Twenty-Seventh Symposium (International) on Combustion*, pages 1175–1182. The Combustion Institute, Pittsburgh, 1998.

[103] M. J. Moran and H. N. Shapiro. *Fundamentals of Engineering Thermodynamics*. Second Edition, John Wiley and Sons, New York, 1993.

[104] C. M. Müller, H. Breitbach, and N. Peters. Partially premixed turbulent flame propagation in jet flames. In *Twenty-Fifth Symposium (International) on Combustion*, pages 1099–1106. The Combustion Institute, Pittsburgh, 1994.

[105] T. Myhrvold, T. Weydahl, and I. S. Ertesvåg. Investigation of the Eddy Dissipation Extinction Model for Turbulent-Flame Simulations with Chemical Kinetcis. In *First Biennal Meeting*, pages 1–6. The Scandinavian-Nordic Section of the Combustion Institute, 2001.

[106] D. Naot, A. Shavit, and M. Wolfshtein. Interactions between components of the turbulent velovity correlation tensor due to pressure fluctuations. *Israel Journal of Technology*, 8(3):259–269, 1970.

[107] T. T. Ng, R. K. Cheng, and F. Robben. Combustion-turbulence interaction in the turbulent boundary layer over a hot surface. In *Nineteenth Symposium (International) on Combustion*, pages 359–366. The Combustion Institute, Pittsburgh, 1982.

[108] S. V. Patankar. *Numerical Heat Transfer and Fluid Flow*. Hemisphere, Washington, 1980.

[109] V. C. Patel, W. Rodi, and G. Scheuerer. Turbulence Models for Near-Wall and Low Reynolds Number Flows: A Rewiew. *AIAA Journal*, 23(9):1308–1319, 1985.

[110] R. H. Perry and C. H. Chilton. *Chemical Enginners' Handbook*. Fifth Edition, McGraw-Hill, New York, 1973.

[111] N. Peters. *Turbulent Combustion*. Cambridge University Press, Cambridge, 2000.

[112] W. M. Pitts. Assessment of theories for the behaviour and blowout of lifted turbulent jet diffusion flames. In *Twenty-Second Symposium (International) on Combustion*, pages 809–816. The Combustion Institute, Pittsburgh, 1988.

[113] T. Poinsot. Using direct numerical simulations to understand premixed turbulent combustion. In *Twenty-Sixth Symposium (International) on Combustion*, pages 219–232. The Combustion Institute, Pittsburgh, 1996.

[114] T. Poinsot, S. Candel, and A. Trouve. Applications of direct numerical simulation to premixed turbulent combustion. *Progress in Energy and Combustion Science*, 21:531–576, 1996.

[115] T. Poinsot, D. C. Haworth, and G. Bruneaux. Direct Simulations and Modeling of Flame-Wall Interaction for Premixed Turbulent Combustion. *Combustion and Flame*, 95:118–132, 1993.

[116] T. Poinsot and D. Veynante. *Theoretical and Numerical Combustion*. R.T. Edwards, Philadelphia, 2001.

[117] S. Pope. Computations of turbulent combustion, progress and challenges. In *Twenty-Third Symposium (International) on Combustion*, pages 591–612. The Combustion Institute, Pittsburgh, 1990.

[118] S. Pope. *Turbulent Flows*. Cambridge University Press, Cambridge, 2000.

[119] P. Popp and M. Baum. Analysis of wall heat fluxes, reaction mechanisms, and unburnt hydrocarbons during the head-on quenching of a laminar methane flame. *Combustion and Flame*, 108:327–348, 1997.

[120] M. K. Razdan and K. K. Kuo. Erosive Burning studies of Composite Solid Propellants by Turbulent Boundary-Layer Approach. *AIAA Journal*, 17(11):1225–1233, 1979.

[121] O. Reynolds. On the Dynamical Theory of Incompressible Viscous Fluids and the Determination of the Criterion. *Philosofical Transactions of the Royal Society of London, Series A*, 186:123–164, 1895.

[122] C. M. Rhie and W. L. Chow. Numerical Study of the Turbubulent Flow Past an Airfoil with Trailing Edge Separation, 1983.

[123] J. Rotta. Statistischer theorie nichthomogener turbulenz - 1. mitteilung. *Zeitschrift für Physik*, 129:547–572, 1951.

[124] H. Schlichting. *Boundary-Layer Theory*. Seventh Edition, McGraw-Hill, New York, 1979.

[125] T. Shih and J. L. Lumley. Critical Comparison of Second-Order Closures with Direct Numerical Simulations of Homogeneous Turbulence. *AIAA Journal*, 31(4), 1993.

[126] C. C. Shir. A Preliminary Numerical Study of Atmospheric Turbulent Flows in the Idealized Planetary Boundary Layer. *Journal of Atmospheric Science*, 30:1327–1339, 1973.

[127] N. S. A. Smith, R. W. Bilger, C. D. Carter, R. S. Barlow, and J.-Y. Chen. A Comparison of CMC and PDF Modeling Predictions with Experimental Nitric Oxide LIF/Raman Measurements in a Turbulent H_2 Jet Flame. *Combustion Science and Technology*, 105:357–375, 1995.

[128] R. M. C. So, Y. G. Lai, H. S. Zhang, and B. C. Hwang. Second-Order Near-Wall Turbulence Closures: A Review. *AIAA Journal*, 29(11):1819–1835, 1991.

[129] D. B. Spalding. Mixing and chemical reaction in steady confined turbulent flames. In *Thirteenth Symposium (International) on Combustion*, pages 649–657. The Combustion Institute, Pittsburgh, 1971.

[130] D. B. Spalding. Development of the Eddy-Breakup model of turbulent combustion. In *Sixteenth Symposium (International) on Combustion*, pages 1657–1663. The Combustion Institute, Pittsburgh, 1976.

[131] D. B. Spalding. Mathematical Models of Turbulent Flames; A Review. *Combustion Science and Technology*, 13:3–25, 1976.

[132] C. G. Speziale, S. Sarkar, and T. B. Gatski. Modelling the pressure-strain correlation of turbulence: an invariant dynamical systems approach. *Journal of Fluid Mechanics*, 227:245–272, 1991.

[133] H. Tennekes and J. L. Lumley. *A First Course in Turbulence*. Sixteenth printing, 1997, MIT Press, Cambridge, 1972.

[134] N. Tillmark and P. H. Alfredsson. Experiments on transition in plane Couette flow. *Journal of Fluid Mechanics*, 235:89–102, 1992.

[135] E. R. van Driest. On Turbulent Flow Near a Wall. *Journal of the Aeronautical Sciences*, 23:1007–1011, 1956.

[136] B. E. Vembe. *A Generic Preprocessor for Computational Fluid Dynamics*. Dr. ing. thesis, University in Trondheim (NTH), Norway, 1993.

[137] L. Vervisch. Using numerics to help the understanding of non-premixed turbulent flames. *Proceedings of the Combustion Institute*, 28:11–24, 2000.

[138] H. Y. Wang and P. Joulain. Three-Dimensional Modeling for Prediction of Wall Fires with Buoancy-Induced Flow along a Vertical Rectangular Channel. *Combustion and Flame*, 105:391–406, 1996.

[139] J. Warnatz, U. Maas, and R. W. Dibble. *Combustion*. Springer, Berlin, 1999.

[140] F. M. White. *Fluid Mechanics*. Third edition, McGraw-Hill, New York, 1994.

[141] F. A. Williams. *Combustion Theory*. Second Edition, Benjamin/Cummings, Menlo Park, California, 1985.

[142] B. A. Younis, T. B. Gatski, and C. G. Speziale. Towards a rational model for the triple velocity correlations of turbulence. *Proceedings of the Royal Society of London, Series A: Mathematical and Physical Sciences*, 456:909–920, 2000.

[143] Y. Zhang and K. N. C. Bray. Brief Communication: Characterization of Impinging Jet Flames. *Combustion and Flame*, 116:671–674, 1999.

Appendix A

Simultaneous Laser Raman-Rayleigh-LIF Measurements and Numerical Modeling Results of a Lifted Turbulent H_2/N_2 Jet Flame in a Vitiated Coflow

Presented at the International Symposium on Combustion, June 2002, Sapporo, Japan. To appear in the Proceedings of the Combustion Institute, volume 29, 2003.

URN:NBN:no-7265

URN:NBN:no-7265

Simultaneous Laser Raman-Rayleigh-LIF Measurements and Numerical Modeling Results of a Lifted Turbulent H_2/N_2 Jet Flame in a Vitiated Coflow

R. Cabra, T. Myhrvold[+] [1], J.Y. Chen, and R.W. Dibble
Department of Mechanical Engineering
University of California at Berkeley, CA 94720, USA

A.N. Karpetis and R.S. Barlow
Combustion Research Facility
Sandia National Laboratories
Livermore, CA 94550, USA

Twenty-Ninth International Symposium on Combustion

Keywords: TURBULENT, NON-PREMIXED, PARTIALLY-PREMIXED

Colloquium: Turbulent Combustion

Publications Number: 1A03

Corresponding Author: Ricardo Cabra Tel: (510) 642-9158
50-B Hesse Hall Fax: (510) 642-1850
University of California E-mail: ricardo@me.berkeley.edu
Berkeley, CA 94720, USA

[1] + Norwegian University of Science and Technology, Trondheim, Norway

URN:NBN:no-7265

Simultaneous Laser Raman-Rayleigh-LIF Measurements and Numerical Modeling Results of a Lifted Turbulent H_2/N_2 Jet Flame in a Vitiated Coflow

R. Cabra, T. Myhrvold[+ 2], J.Y. Chen, and R.W. Dibble
Department of Mechanical Engineering
University of California
Berkeley, CA 94720, USA
and
A.N. Karpetis and R.S. Barlow
Combustion Research Facility
Sandia National Laboratories
Livermore, CA 94550, USA

ABSTRACT

An experimental and numerical investigation is presented of a lifted turbulent H_2/N_2 jet flame in a coflow of hot, vitiated gases. The vitiated coflow burner emulates the coupling of turbulent mixing and chemical kinetics exemplary of the reacting flow in the recirculation region of advanced combustors. It also simplifies numerical investigation of this coupled problem by removing the complexity of recirculating flow. Scalar measurements are reported for a lifted turbulent jet flame of H_2/N_2 (Re=23,600, H/d=10) in a coflow of hot combustion products from a lean H_2/Air flame (ϕ=0.25, T=1,045K). The combination of Rayleigh scattering, Raman scattering, and laser-induced fluorescence is used to obtain simultaneous measurements of temperature and concentrations of the major species, OH, and NO. The data attest to the success of the experimental design in providing a uniform vitiated coflow throughout the entire test region. Two combustion models (PDF: joint scalar Probability Density Function and EDC: Eddy Dissipation Concept) are used in conjunction with various turbulence models to predict the lift-off height (H_{PDF}/d=7, H_{EDC}/d=8.5). Kalghatgi's classic phenomenological theory, which is based on scaling arguments, yields a reasonably accurate prediction (H_K/d=11.4) of the lift-off height for the present flame. The vitiated coflow admits the possibility of auto-ignition of mixed fluid, and the success of the present parabolic implementation of the PDF model in predicting a stable lifted flame is attributable to such ignition. The measurements indicate a thickened turbulent reaction zone

[2] + Norwegian University of Science and Technology, Trondheim, Norway

at the flame base. Experimental results and numerical investigations support the plausibility of turbulent premixed flame propagation by small scale (on the order of the flame thickness) recirculation and mixing of hot products into reactants and subsequent rapid ignition of the mixture.

INTRODUCTION

Clear understanding of turbulent flame stabilization in an environment of hot combustion products will aid the advancement of combustion technology. Practical combustor designs employ the recirculation of hot combustion products to achieve flame stabilization in their intensely turbulent flows. Numerical investigations of these flows are difficult to execute because of the detailed, fully coupled, turbulent fluid mechanics and chemical kinetics. A challenge for combustion researchers is to design experiments that address flame stabilization in combustion products, while decoupling the chemical kinetics from the complex recirculating flow.

The simplified flow of the vitiated coflow burner provides experimental and numerical access to fundamental combustion features of recirculation burners. The design (Fig. 1) consists of a jet flame in a coaxial flow of hot combustion products from a lean premixed flame (vitiated coflow). The reacting flow associated with the central jet exhibits similar chemical kinetics, heat transfer, and molecular transport as recirculation burners without the recirculating fluid mechanics. The well-defined, uniform boundary conditions and simplified flow associated with the coaxial jet design are attractive features for numerical modeling. Additionally, the open design facilitates the use of optical diagnostics.

The vitiated coflow burner enables investigation of stabilization mechanisms for lifted turbulent jet flames in environments that are relevant to combustion applications but have not been studied systematically. Typically, lifted turbulent jet flame experiments are conducted on fuel jets in cool air, where the air is either quiescent or a low velocity coflow. The range of flows that can be studied is limited because a relatively small increase in air coflow velocity can result in flame blow-off. In turbulent jet flame research, this limitation of flame stability is often circumvented with the use of pilots [1,2], which introduce the complexity of a third stream (jet, pilot, and coflow) and non-uniformity of fluid entrained by the jet. The vitiated coflow is a large pilot that provides a uniform environment for the investigation of highly turbulent jet flames with low Damköhler numbers. Such turbulent flow characteristics are exemplary of practical combustors.

Lifted turbulent jet flames have received significant attention in the combustion literature, and competing theories of flame stabilization have been proposed [e.g., 3-5]. A recent review in the text by Peters [6] presents the view that stabilization of a lifted flame involves the propagation of a turbulent partially premixed flame at a speed that balances the local streamwise convective velocity. This description consolidates ideas involving turbulent premixed flame propagation and triple flame (or edge flame) propagation, and computations based upon this concept have yielded successful predictions of liftoff height [7]. It has also been proposed [8,9] that hot, product containing eddies rotate upstream, entrain preheated reactants, and facilitate reaction. Recent studies using scalar field imaging [10] and PIV

URN:NBN:no-7265

[11] showed evidence of the importance of such recirculation at the stabilization region.

In the present study, multiscalar laser diagnostics and numerical models are used to investigate a lifted turbulent H_2/N_2 jet flame in a coflow of lean H_2/air combustion products. This lifted flame has some features consistent with the theory of stabilization by propagation of a turbulent partially premixed flame. However, the conditions of the vitiated coflow admit the interesting possibility that mixtures can autoignite as they convect downstream. In addition, there are features in the laser measurements that suggest the reaction zone in the stabilization region is thickened (thicker than the smallest estimated scales of turbulence) or may include localized ignition events. Experimental and computational results are discussed in the context of these novel conditions.

EXPERIMENTAL METHODS

Experiments were conducted on a lifted turbulent H_2/N_2 jet flame in a vitiated coflow (Table 1). The combustor consists of a central H_2/N_2 turbulent jet with a coaxial flow of hot combustion products from a lean premixed H_2/Air flame (Fig. 1). The design is an adaptation of the design by Chen et al. [2]. The central jet exit diameter is d =4.57 mm and the coflow flame is stabilized on a perforated disk with 87% blockage and an outer diameter of 210 mm. The central jet extends 70 mm above the surface of the perforated disk. For the conditions listed in Table 1, the observed lift-off height was $H/d \cong 10$, and the total flame length was H_F/d=30.

Simultaneous, temporally and spatially resolved measurements of temperature and species mass fractions were obtained using laser diagnostic systems of the Turbulent Diffusion Flame laboratory at the Combustion Research Facility of Sandia National Laboratories. Details of the experimental setup and calibration techniques have been previously presented [12-15]. Spontaneous Raman scattering and Rayleigh scattering, using two frequency-doubled Nd:YAG lasers, were combined to measure temperature and the concentrations of N_2, O_2, H_2O, and H_2. Concentrations of OH and NO were measured using laser-induced fluorescence (LIF). The LIF systems were operated in the linear fluorescence regime, and corrections were applied on a shot-to-shot basis to account for local variation in Boltzmann fraction and collisional quenching rates for OH and NO. These multiscalar measurements were virtually simultaneous, with delays of about 100ns between the different laser pulses. The spatial resolution of the system is 750μm. NO concentrations were consistently very low in this flame (Y_{NO}<3ppm), and they will not be presented here.

The precision and accuracy of the Raman-Rayleigh-LIF system is determined from calibration flame measurements [15]. The precision of single-shot measurements of an H_2 flame with no fluorescence interferences is limited by the photoelectron shot noise [16], and it is indicated by the standard deviations (RMS) of the flat (Hencken) flame measurements: temperature 1.2%, N_2 3.2%, H_2O 5.4%, OH 12% and NO 10%. Experimental uncertainties

in averaged scalar values were estimated from the repeatability of calibration results and uncertainties in reference quantities. Representative uncertainties for the present results are: temperature 3%, N_2 3%, H_2O 4%, and OH 10%. Uncertainty in the O_2 is best represented as an absolute error in mass fraction of about ± 0.005, regardless of the local value of Y_{O2}.

NUMERICAL METHODS

Presented are two turbulent combustion models, the Eddy Dissipation Concept (EDC) and the Probability Density Function (PDF). These models are coupled with either the standard k-ε or Reynolds stress fluid dynamic model for turbulent flow.

Eddy Dissipation Concept (EDC) Numerical Method

The general-purpose CFD code *Spider* [17] with EDC was developed at the Norwegian University of Science and Technology division of Thermodynamics in Trondheim. The turbulent reacting flow is modeled by the density-weighted Reynolds-averaged conservation equations for momentum components, energy, and mass fractions of species. Turbulence was modeled either by the standard k-ε model or by two versions of Reynolds-stress models by Launder, Reese and Rodi (LRR) [18] or by Jones and Musonge (JM) [19,20]. In the present calculations *Spider* employs a 2-D axisymmetric geometry.

The mean reaction rate of chemical species j is modeled by EDC [21,22] as

$$\overline{R}_j = -\frac{\overline{\rho}\gamma^* \dot{m}^*}{(\gamma^*)^{1/3}} \left(Y_j^0 - Y_j^*\right),$$

where γ^* is the mass fraction of turbulence in fine structures and $\dot{m}^*$ is the reciprocal of the fine-structure residence time ($\tau^* = 1/\dot{m}^*$). These two quantities are expressed as functions of the turbulence energy and the turbulence energy dissipation rate [21,23]. Specifically, the fine-structure residence time is assumed proportional to the Kolmogorov time scale. Y_j^0 and Y_j^* are the mass fractions of species j in the surrounding fluid state and the fine structure state. The fine structure is regarded as a perfectly stirred reactor and the mass balance for species j in the reactor is modeled as

$$\frac{dY_j^*}{dt} = \frac{R_j^*}{\rho^*} + \frac{1}{\tau^*}\left(Y_j^0 - Y_j^*\right)$$

These species mass balances, together with equations for energy and momentum, are integrated in time until steady state is reached. A detailed H_2 mechanism taken from GRI-Mech 2.11 [24] is used (carbon species and reactions excluded).

Probability Density Function (PDF) Numerical Method

The model utilizes the joint scalar PDF for composition only and the k-ε turbulence model for a parabolic flow [25]. The turbulent flux and scalar dissipative terms appearing in the PDF transport equation are modeled by a gradient diffusion model and the Curl mixing model [26], respectively. Monte Carlo simulation is used to compute the transport equation for the PDF [27]. Four hundred stochastic particles per grid are used. A 7-step reduced chemistry (6 steps for combustion and 1 for NO formation) is integrated directly in time for each particle. The reduced chemistry model has been thoroughly tested and performs well in calculations of laminar opposed-flow nonpremixed flames, laminar premixed flames, perfectly stirred reactors, and ignition. Therefore, we expect satisfactory performance here.

RESULTS AND DISCUSSION

The structure of the lifted turbulent H_2/N_2 jet flame is investigated by examining the measured temperature and species concentrations profiles. Centerline measurements were taken from z/d=1 to 34 downstream of the nozzle exit. Radial profiles were obtained at several axial locations (z/d=1, 8, 9, 10, 11, 14 and 26). The radial domain covered by these profiles was -3mm to 50mm with spacing typically between 1 and 3mm. The single-shot data was processed and the Favre averages and RMS fluctuations were generated. The following formulation, modified for the current H_2/N_2 system, determines the mixture fraction [28].

$$f = \frac{\left(1/2M_H\right)\left(Y_H - Y_{H,2}\right) - \left(1/M_O\right)\left(Y_O - Y_{O,2}\right)}{\left(1/2M_H\right)\left(Y_{H,1} - Y_{H,2}\right) - \left(1/M_O\right)\left(Y_{O,1} - Y_{O,2}\right)}$$

The stoichiometric mixture fraction for the present fuel composition is f_s=0.474.

Inlet and Far-Field Boundary Conditions

Radial profiles of Favre averaged temperature at z/d=1, 14 and 26 are plotted in Fig 2. The measured mean temperature in the coflow at z/d=1 is uniform (2% RMS), indicating a well-mixed mixture. Also, the far-field (coflow) measurements of temperature do not change with axial distance. Thus, the integrity of the coflow is maintained in the entire test region. The same well-defined boundary conditions are observed for the species measurements. These results demonstrate that the flame can be modeled as a jet flame issuing into an infinite hot coflow, and they attest to the success of the experimental design.

Flame Structure and Lift-Off Height

The OH mass fraction, Y_{OH}, is used as a marker of the average flame lift-off height in both measured and modeled results. Fig. 3a shows a contour map generated using an aggregate of the point measurements (white dots). Several points were taken in the flame stabilization

region to provide adequate resolution for determination of the lift-off height, $H/d \cong 10$, which was taken to be the location where the Favre average Y_{OH} reaches 600 ppm.

The numerical models each predict a lifted flame structure, which is a significant result in itself, regardless of the accuracy of the predicted lift-off height. It is was not obvious, *a priori*, that the PDF model would predict a lifted flame because the present calculation proceeds in a downstream marching solution and includes no mechanism for propagation of a turbulent premixed or partially premixed flame into the convecting flow. However, it is apparent from Fig. 3b that there is reaction progress for some fraction of the PDF particles well upstream of the flame stabilization location at the Y_{OH}=600 ppm contour. This result is associated with auto-ignition of mixed fluid, a process that would not occur with a cold air coflow. There were no visually obvious auto-ignition events well below the lift-off height; perhaps they would have been revealed by radial profiles taken at intermediate locations ($1<z/d<8$). However, the flame does spontaneously ignite in the laboratory, starting at a far downstream location, when the coflow is operating and jet flow is turned on. This possibility for auto-ignition leading to flame stabilization in the vitiated burner and the PDF calculation are worthy of further exploration.

Results from three numerical simulations are shown. Fig. 3b shows the OH contours from the PDF combustion model and the standard k-ε model, which yields a lift-off height of H_{PDF}/d=7. Using the same k-ε model, the EDC model predicts H_{EDC}/d=8.5, as shown in Fig. 3c. The standard k-ε model is known to over-estimate the turbulent diffusivity and, consequently, over predict the spreading rate of round jets. This may account for the wide flame predictions in these two calculations (Figs. 3b and 3c) relative to the experimental results (Fig. 3a). The third simulation, using the EDC model and the LRR Reynolds stress model, predicted a shorter lift-off height of H_{LRR}/d=5 (Fig. 3d). The overall flame shape is narrower than that predicted by the standard k-ε model and in better agreement with the measured flame width, even though the lift-off height is under predicted.

Using the present EDC model, a parametric study was conducted to explore the sensitivity of the predicted lift-off height to boundary conditions, turbulence models, and grid resolution. The base case employed the standard k-ε model, and the boundary conditions consisted of a fully developed turbulent pipe flow ($\hat{u}_j$=107m/s) for the jet and a uniform flow field ($\hat{u}_c$=3.5m/s) for the coflow. The inlet coflow turbulence variables k and ε were determined using rough estimates of the integral length scale and turbulence intensity (λ_o=1mm and u'/u_c=5%). Most cases were calculated with a mesh of 60x55 (axial x radial) with grids clustered near the jet exit. The predicted lift-off height was found to be insensitive to changes in the coflow turbulence parameters (increased to λ_o=3mm and u'/u_c=10%) and unaffected by the use of detailed modeling of the nozzle wall turbulence. Increases in the jet velocity to $\hat{u}_j$=120m/s and the coflow velocity to $\hat{u}_c$=10m/s caused the predicted lift-off height to increase by roughly 25% and 50%, respectively. Refinement of the grid revealed a

sensitivity of the calculated lift-off height to grid resolution, confirming that fine grids in the near field region are needed for adequate accuracy. The mesh was refined to 150x55, while keeping the computational domain for all EDC simulations fixed (z/d=40 x r/d=12). However, further increases in grid resolution (beyond 150x55) produce insignificant changes in model results. The fine grid resolution was also used for the computational domain of Reynolds stress models. The results in Figs. 3 and 4 were calculated using the fine grid. Predictions of lift-off height by the Reynolds stress turbulence models were consistently lower than those by the k-ε model.

Figure 4 compares centerline profiles of mixture fraction and oxygen mass fraction and shows the sensitivity of predicted mixing rates to the turbulence model. The peak in oxygen seen near $z/d \approx$14 (Fig 4b) illustrates the upstream penetration (increased with lift-off height) and subsequent consumption of oxygen by the flame. By presenting an entrainment rate profile similar to the Y_{O2} centerline profile, Han and Mungal [29] observed a similar correlation between mixing and lift-off height. Since the standard k-ε model over-predicts turbulent diffusion for round jets, the predicted oxygen penetration is higher than the data, as evident by the early (PDF) or high (EDC) centerline Y_{O2} peaks and the rapid decay in mixture fraction. While the lift-off height predicted by the EDC with the Reynolds stress model is low, both predicted centerline profiles agree well with the data.

Combustion Statistics at Flame Stabilization

Scatter data of temperature vs. mixture fraction are shown in Fig. 5. Approximately 4,000 point measurements from different radial positions were grouped together to form a probability density map for three axial positions (z/d=8,11,14). There is a clear progression from a predominantly mixing condition (z/d=8) to vigorous flame burning (z/d=14) that corresponds to the transition from mixing only to mixing combined with ignition and flame stabilization. Since the flame is not attached to the nozzle, the central fuel jet entrains hot oxidizer from the coflow, evolving into a partially premixed flow with fluid temperatures corresponding to the mixing line between the jet and coflow boundary conditions in Fig. 5c. Beyond the potential core of the jet there is progressive dilution of the richest samples, such that the fuel-rich boundary condition for combustion at z/d=14 has decreased from f=1.0 to values between f$\sim$0.9 and f$\sim$0.6. Also plotted in Fig. 5a are the results from a series of laminar opposed flow flame calculations with equal molecular and thermal diffusivities. Corresponding calculations with full transport (i.e. with differential diffusion included) poorly matched the data, suggesting that turbulent stirring is more important than differential molecular diffusion in determining the relative mass fractions of major species in the measured flame. The fuel side boundary condition for the laminar flame calculations was set at f=0.8, to represent this measured departure from the pure jet composition.

The range of scalar dissipation rates in the turbulent flame above the stabilization region can be estimated by determining the strain rates whose corresponding opposed flow laminar flame solutions match the upper and lower bounds of the laser shot measurements [30], particularly on the fuel-lean side. In Fig. 5a, the laser shot data is approximately bounded by solutions with strain rates of $100s^{-1}$ and $5{,}000s^{-1}$. The computed strain rate prior to laminar flame extinction was $13{,}000s^{-1}$, and a number of data points are below the $5{,}000s^{-1}$ solution. It should be noted that the low strain rate calculation adequately describes the lean side results as expected, since these results correspond to the hot co-flow where low strain should prevail and where viscosity is still relatively high. The rich-side experimental results cannot be adequately represented by this limited set of laminar flame calculations because of the broad range of fuel-side boundary conditions produced by mixing upstream of the reaction zone.

Perhaps the most interesting condition can be seen in Fig. 5b, where the data is scattered throughout the zone between the mixing (lower) and fast chemistry (upper) limits on temperature. This axial position (z/d=11) is one diameter above the observed lift-off height. The behavior of the scatter data in Fig. 5b is qualitatively different from that reported for lifted H_2 jet flames in air [31,32], where there is clear bimodality between unreacted and reacted samples in the region of flame stabilization. Results for the present burner suggest the existence of a thickened turbulent flame in the stabilization region. A laminar premixed flame simulation predicts an unstrained flame thickness of δ_L=2.5mm, while the turbulence models suggest a Kolmogorov scale of roughly 50-500 microns in the stabilization region. Therefore, it may be argued that there are turbulent eddies of order 1mm within a thickened reaction zone. The observed scatter could also result from a process of small-scale mixing and ignition at the flame base, as outlined below.

Flame Stabilization

The experimental and numerical results present an opportunity to discuss possible flame stabilization mechanisms for the vitiated coflow burner. The presented EDC and k-ε model results (Fig. 3c) indicate an average flow velocity of 10m/s at the flame base, while the maximum laminar premixed flame speed was calculated to be S_L=3m/s for reactants at f=0.4 along the mixing line. A factor of 3 increase in velocity for a propagating turbulent premixed or partially premixed flame is plausible [6,33,34]. Interestingly, the correlation by Kalghatgi [4], which is based upon scaling arguments:

$$H_K = 50\left(\frac{\nu_{jet}U_{jet}}{S_{L,\max}^2}\right)\left(\frac{T_{coflow}M_{jet}}{T_{jet}M_{coflow}}\right)^{1.5},$$

yields a relatively accurately prediction of our measured lift-off height. For the present flame the jet mixture viscosity is ν_{jet}=2x10^{-5} m^2/s, and molar mass of the jet and coflow mixtures are M$_{jet}$=21.5 and M$_{coflow}$=27.6. For the given conditions, this engineering correlation predicts a lift-off height of H_K/d=11.4, indicating the robustness of the correlation and suggesting that stabilization of the present flame may be controlled by the same mechanisms that control lifted flames in cold air. However, the potential for auto-ignition of mixed fluid and the behavior of the temperature scatter data noted above both allow for speculation on variations or additional mechanisms that may contribute to stabilization of the present flame.

It is possible that auto-ignition of mixed fluid is only important for the transient startup of the laboratory flame and that, once ignited, a propagating partially premixed flame advances upstream to a lift-off height for which convective times from the nozzle are shorter than ignition delay times for any fluid sample along the mixing line. It is also possible that auto-ignition in the stabilization region serves to augment or anchor the propagating flame. A specific mode of ignition-enhanced turbulent flame propagation is illustrated in Figs. 5d,e and is based on the observation that the ignition delay for mixtures of products and reactants can be short compared to the timescale of small eddies in the stabilization region. The illustration shows mixing of product and reactant samples (Fig. 5d), each at f=0.4. Such mixing could occur around an auto-ignition kernel or by eddy turnover in the thickened partially premixed flame. After rapid ignition of the mixed fluid, a reaction front propagates through neighboring mixtures (Fig. 5e). This sort of mixing/ignition/propagation mechanism would be consistent with the measured distribution of temperature scatter data in Fig. 5b. However, multiscalar imaging measurements would be needed to detect such events.

CONCLUSIONS

The vitiated coflow burner provides a simplified flow with well-defined boundary conditions. Measurements confirm that the coflow properties are uniform throughout the test region. The configuration enables the examination of turbulent mixing and chemical kinetics relevant to the modeling of advanced combustors without the complex recirculating fluid mechanics.

Simultaneous multiscalar measurements of a lifted H_2/N_2 jet ($H/d \cong 10$) were presented and compared to a series of numerical simulations with various combustion and turbulence models. Numerical results from a PDF and an EDC combustion model reasonably predict the lift-off height (H_{PDF}/d=7, H_{EDC}/d=8.5).

Features of the instantaneous scalar measurements in the stabilization region, together with information on laminar flame thickness and turbulence quantities from calculations, suggest that a thickened turbulent partially premixed flame exists at the flame stabilization location.

The vitiated coflow admits the possibility of auto-ignition of mixed samples. Such ignition is the only possible stabilization mechanism in the PDF calculation, which proceeds by a parabolic marching solution. While there is no clear experimental evidence of auto-ignition events below the lift-off height, it is plausible that auto-ignition or turbulent mixing of products and reactants in the stabilization, followed by rapid ignition, may augment the stability of the present flame.

ACKNOWLEDGEMENTS

The research is part of a project supported by NASA Glenn Research Center Contract NAG3-2103. Research conducted at Sandia was supported by the United States Department of Energy, Office of Basic Energy Sciences. T. Myhrvold worked in close collaboration with I.S. Ertesvåg and I.R. Gran at the Norwegian University of Science and Technology and was supported by the Research Council of Norway.

REFERENCES

Masri, A. R., Dibble, R. W., and Barlow, R. S., *Prog. Energy Combust. Sci*. 22:307 (1996).

Chen, Y.G., Peters, N., Schneemann, G.A., Wruck, N., Renz, U., & Mansour, M.S., *Combust. Flame* 107:223 (1996)

Vanquickenborne, L. & Van Tiggelen, A., *Combust. Flame* 10:59 (1966).

Kalghatgi, G.T., *Comb. Sci. Tech*. 41:17 (1984).

Pitts, W.M., *Proc. Comb. Inst*. 22:809 (1988).

Peters, N., Turbulent Combustion, Cambridge University Press, 2000 p.237-261.

Chen, M., Herrmann, M., and Peters, N., *Proc. Comb. Inst*. 28:167 (2000).

Broadwell, J.E., Dahm W.J.A., & Mungal, M.G., *Proc. Comb. Inst*. 20:303 (1984).

Dahm, W.J.A., & Dibble, R.W., *Proc. Comb. Inst*. 22:801 (1988).

Tacke, M.M., Geyer, D., Hassel, E.P., & Janicka J., *Proc. Comb. Inst*. 27:1157 (1998).

Upatnieks, A. Driscoll, J. F., Ceccio, S. L., *Proc. Comb. Inst*. 29:?? (2002).

Nooren, P. A., Versluis, M., van der Meer, T. H., Barlow, R. S., and Frank, J. H., *Appl. Phys. B* 71:95 (2000).

Barlow, R.S., Karpetis, A.N., Frank, J.H. & Chen, J.Y., *Combust. Flame* 127:2102 (2001).

Nguyen, Q.V., Dibble, R.W., Carter, C.D., Fiechtner, G.J., & Barlow, R.S., *Combust. Flame* 105:499 (1996).

Barlow, R.S., Fiechtner, G.J., Carter, C.D., & Chen, J.-Y., *Combust. Flame* 120:549 (2000).

Dibble, R.W., Masri, A.R., & Bilger, R.W., *Combust. Flame* 67:167 (1987).

Melaaen, M.C., Ph.D. Dissertation, University in Trondheim, 1990.

Launder, B. E., Reece, G. J., & Rodi, W., *J. Fluid. Mech*. 68(3):537 (1975).

Jones, W. P., Turbulent Reacting Flows, Academic Press Ltd., 1994 p.171-189.

Jones, W. P., Musonge, P., *Phys. Fluids* 31(12):3589 (1988).

Ertesvåg, I. S., Turbulent Flow & Combustion (in Norwegian), Tapir Academic Publisher, 2000 p.309-372.

Gran, I. R., Magnussen B. F., *Comb. Sci. Tech*. 119:191 (1996).

URN:NBN:no-7265

Ertesvåg, I. S., Magnussen, B. F., *Comb. Sci. Tech*. 159:213 (2000).

Bowman, C.T., Hanson R. K., Davidson, D. F., Gardiner Jr., W. C., Lissianski V., Smith, G. P., Golden, D. M., Goldenberg, M., Frenklach, M., Gri-Mech 2.11, http://www/me.berkeley.-edu/gri_mech/ (1999).

Smith, N.S.A., Bilger, R.W., Carter, C.D., Barlow R.S., & Chen, J.Y., *Comb. Sci. Tech*. 105:357 (1995).

Pope, S.B., *Proc. Comb. Inst*. 23:591 (1990).

Chen, J.-Y. & Kollmann W., *Proc. Comb. Inst*. 22:645 (1988).

Bilger, R.W., Stårner, S.H., & Kee, R.J., *Combust. Flame* 80:135 (1990).

Han, D.H. & Mungal, M.G., *Combust. Flame* 124:370 (2001)

Warnatz, J., Maas, U., & Dibble, R.W., Combustion, Physical & Chemical Fundamentals, Modeling & Simulation, Experiments, Pollutant Formation, 3^{rd} Edition, Springer-Verlag, 2000 p.195

Cheng, T. S., Wehrmeyer, J. A., and Pitz, R. W., *Combust. Flame* 91:323 (1992).

Brockhinke, A., Andresen, P., Kohse-Höinghaus, K., *Appl. Phys. B* 61:533 (1995).

Liñán, A., & Williams, F.A., Fundamental Aspects of Combustion, Oxford University Press, 1993 p.120

Ruetsch, G.R., Vervisch, L., & Liñán, A., *Phys. Fluids* 7:1447 (1995)

URN:NBN:no-7265

FIGURE CAPTIONS

Fig 1.

Vitiated coflow burner: a lifted H_2/N_2 jet flame in a coflow of hot combustion products from a lean premixed H_2/Air flame.

Fig 2.

Radial profile of Favre averages for temperature at axial locations z/d=1, 14, 26. Well-defined boundary conditions are shown by the z/d=1 profile and the matching far-field measurements.

Fig 3.

The flame structure is represented by the averaged OH mass fraction fields. Presented are experimental results (a), PDF combustion with standard k-ε turbulence model (b), EDC combustion with k-ε turbulence model (c) and EDC combustion with LRR Reynolds stress model (d). The white dots in plot (a) denote the locations of the laser based multiscalar measurements.

Fig 4.

Axial profiles of the mixture fraction (a) and oxygen mass fraction (b). Presented are experimental results (solid circles), PDF combustion with k-ε turbulence model (dotted line), EDC combustion with k-ε turbulence model (solid line), and EDC combustion with LRR Reynolds stress model (dashed line).

Fig 5.

Scatter plots of temperature vs. mixture fraction from three axial positions (z/d =14,11,8) showing the progress from mixing (c) to fully burning (a). Data from complete radial profiles were grouped together to form each plot. Lines in (a) show the results of steady strained opposed-flow nonpremixed laminar flame calculations with equal species and thermal diffusivities. Schematic of the fastest possible auto-ignition (f=0.4) and flame-holding (d). Schematic of the classic ignition scenario [6, p. 219], starting at f=0.4 and propagating in time and space (e).

Table 1 Flame and flow conditions.

Central Jet		**Coflow**	
Q_{H2} (slm)	25	Q_{H2} (slm)	225
Q_{N2} (slm)	75	Q_{AIR} (slm)	2,100
T_{JET} (K)	305	T_{COFLOW} (K)	1,045
V_{JET} (m/s)	107	V_{COFLOW} (m/s)	3.5
Re_{JET}	23,600	Re_{COFLOW}	18,600
d_{JET} (mm)	4.57	D_{COFLOW} (mm)	210
		ϕ	0.25
X_{H2}	0.2537	X_{O2}	0.1474
X_{N2}	0.7427	X_{H2O}	0.0989
		X_{N2}	0.7534

Q: volumetric flow rate; X: mole fraction; Re: Reynolds number; d and D: diameter.

ϕ :equivalence ratio.

URN:NBN:no-7265

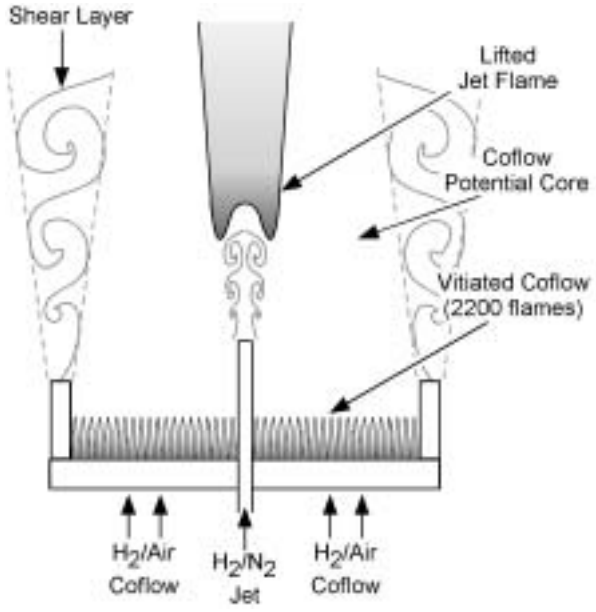

Fig 1. (single column)

URN:NBN:no-7265

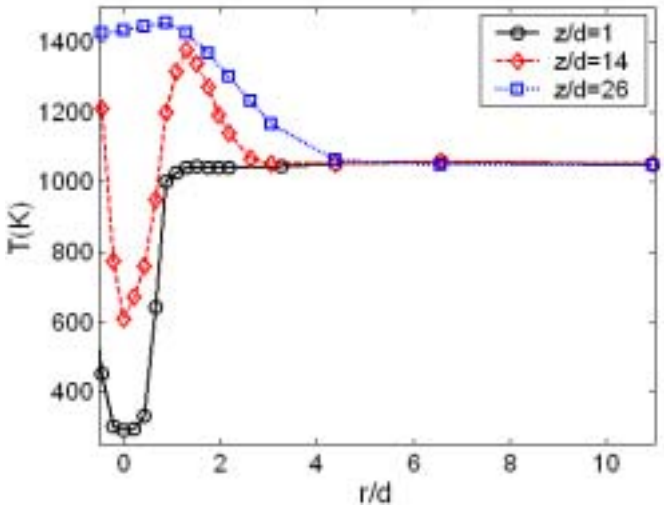

Fig 2. (single column)

URN:NBN:no-7265

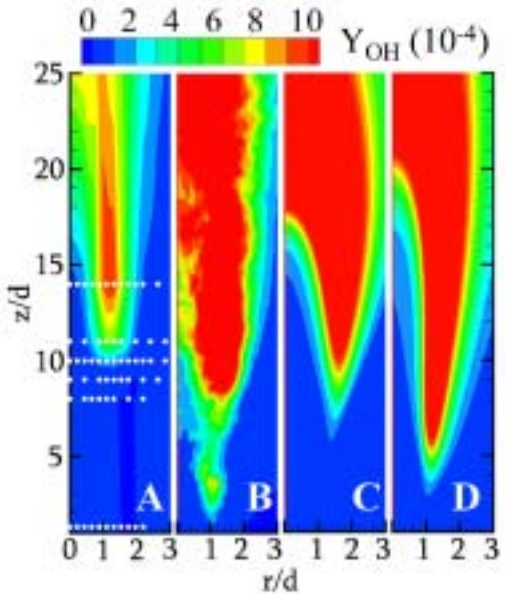

Fig 3. (single column)

URN:NBN:no-7265

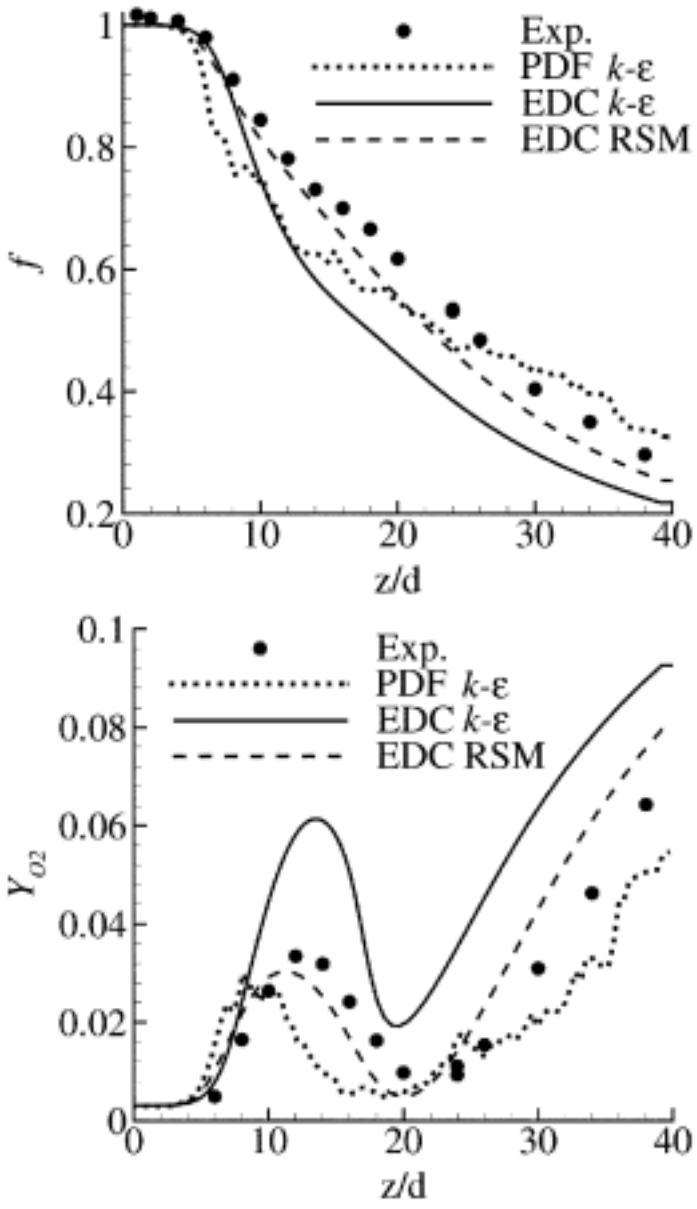

Fig 4. (single column)

URN:NBN:no-7265

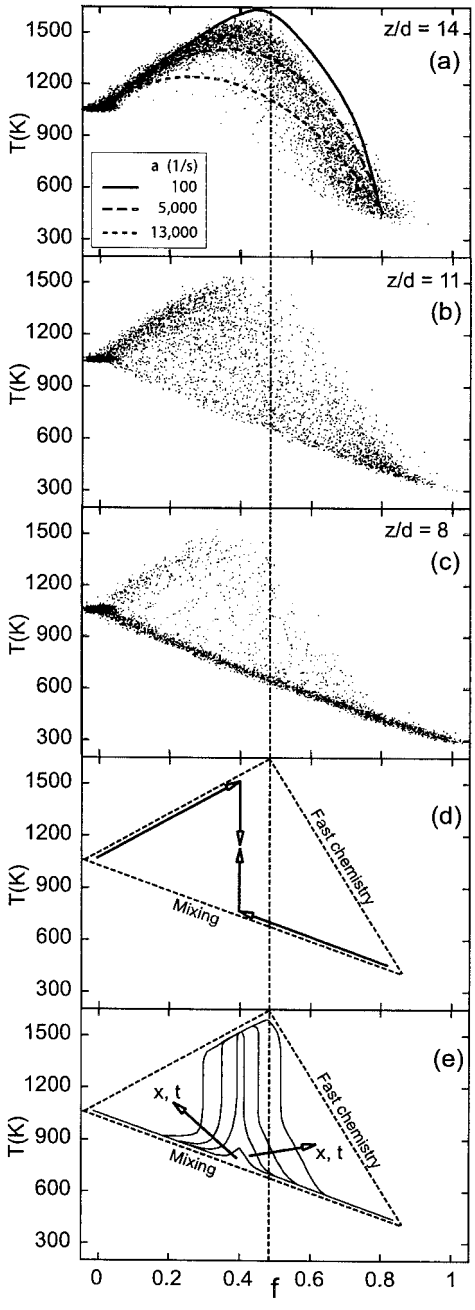

Fig 5. (single column)

Appendix B

Investigation of the Eddy Dissipation Extinction Model for Turbulent-Flame Simulations with Chemical Kinetics

In: Proceedings of The Scandinavian-Nordic Section of the Combustion Institute, First Biennal Meeting, 18th to 20th April 2001, Göteborg, Sweden, pages 1-6.

URN:NBN:no-7265

URN:NBN:no-7265

Investigation of the Eddy Dissipation Extinction Model for Turbulent-Flame Simulations with Chemical Kinetics

Tore Myhrvold, Torleif Weydahl, and Ivar S. Ertesvåg(*)

Department of Applied Mechanics, Thermodynamics, and Fluid Dynamics
Norwegian University of Science and Technology
N-7491 Trondheim, Norway

(*)Author for correspondence: ivar.s.ertesvag@mtf.ntnu.no

The influence of turbulence modeling on the extinction model of Magnussen's Eddy Dissipation Concept was studied. A syngas jet flame was simulated with detailed chemistry and various turbulence models. The models compared were variants of the k-ε model and Reynolds-stress-equation models. It was observed that the different models gave different fields of the important turbulence quantities.

Motivation, Background

In this study, the extinction model used in Magnussen's Eddy Dissipation Concept (EDC) [1, 2] for turbulent combustion was investigated. This was motivated by some observations that in certain cases, extinction was predicted contrary to experimental data. This seems to depend on the turbulence model used. Moreover, it also seems to depend on the chemical mechanism that is used for detailed chemistry calculations. The aim of this study was mainly to investigate the influence of turbulence modeling on the extinction.

Test case

The calculations are designed to simulate a non-premixed turbulent jet flame in a co-flowing low-turbulence wind tunnel [3, 4]. The fuel is syngas containing 30% H_2, 40% CO, and 30% N_2, with and without small amounts of CH_4 and NH_3. The same case is simulated in Ref. [5] and further described there.

Models for turbulence and combustion

The EDC [1] is used to model the interaction between turbulence and combustion. The implementation of chemical kinetics is described in Ref. [2]. The EDC provides a time scale for the reacting fine structure of the flame: $\tau^* = 0.4(\nu/\varepsilon)^{1/2}$, where ν and ε are the kinematic viscosity and the dissipation rate of turbulence kinetic energy, respectively.

This fluid-dynamics time scale is the residence time of the chemical reactor in the EDC (see [2]). It balances against a chemical time scale which is expressed for each species by EDC from chemical-kinetics data. The reaction will be extinguished if the residence time is too short. Detailed chemistry was modeled with data from GRI-Mech 2.11.

URN:NBN:no-7265

The time scale τ^* depends on the modeled dissipation rate ε. We used the standard k-ε model [6], the "Basic" Reynolds-Stress-Equation (RSE) model [7] and some newer RSE models, here Ref. [8]. These models were used with and without the simple modifications usually made to overcome the round-jet anomaly, *i.e.* to reduce the spreading of the round jet in accordance with experimental data.

The mass-weighted Reynolds-averaged equations were solved for momentum components, energy, and all involved species. For diffusion of energy and mass, the general gradient model was used with a turbulence diffusivity modeled by a constant turbulence Prandtl or Schmidt number, $\sigma_h = \sigma_Y$.

It is well known that with the standard values of the model constants in the k-ε model, and in the RSE models using the same ε equation, the spreading of the round jet is too large. Thus, quantities like temperature and fuel concentration are underestimated near the center of the jet, and accordingly, e.g. thermal NO-formation is also underestimated. This is remedied either by reducing the constant $C_{\varepsilon 2}$ or by increasing $C_{\varepsilon 1}$ to give a more representative velocity field.

The predictions were made using the general-purpose CFD code Spider, which is based on finite volumes and non-orthogonal curvilinear computational mesh. In this case, a 2-dimensional rectangular mesh with axial symmetry was used. The calculations presented here were made with 50×28 control-volume grid. The upstream boundary coincide with the nozzle outlet. However, this case has been compared to simulations where the fuel-jet tube was simulated by blocking out a corresponding area in the calculation domain where only the energy equation was solved. The results from these two approaches were very close to each other.

Results and discussion

Initially, a fast-chemistry assumption was applied. The flame was simulated with the k-ε model using standard constants $C_{\varepsilon 1}$ and $C_{\varepsilon 2}$ equal to 1.44 and 1.92, respectively. It was also simulated with values 1.44 and 1.79, 1.44 and 1.83, and with 1.60 and 1.92. From this and other simulations, it seems that the combination of 1.44 and 1.83, together with turbulence Prandtl and Schmidt numbers of 0.5 gives the best representation of the reacting turbulent round-jet flow. Similarly, the flame was simulated with the RSE models with the same variants of the ε equation.

When a detailed chemistry model was applied together with the k-ε model, extinction of the flame was predicted. This can be avoided in two ways: Either by replacing the k-ε model by a better model; or by increasing the residence time of the fine-structure reactor.

In the simulations with the k-ε model, the residence time of the fine-structure reactor was increased by multiplying the reactor mixing rate ($1/\tau^*$) by a factor (actually 0.7 here). Then, the extinction was avoided in the k-ε predictions with detailed chemistry. When RSE models were applied, the flame was stable without modifying the reactor mixing rate.

URN:NBN:no-7265

The figures presented here indicate a reason for this difference. It should be noted that all calculations were made from the same initial and boundary conditions for velocities, turbulence energy and dissipation, temperature and species concentrations. In addition, the RSE models require initial and boundary conditions for the individual Reynolds stresses.

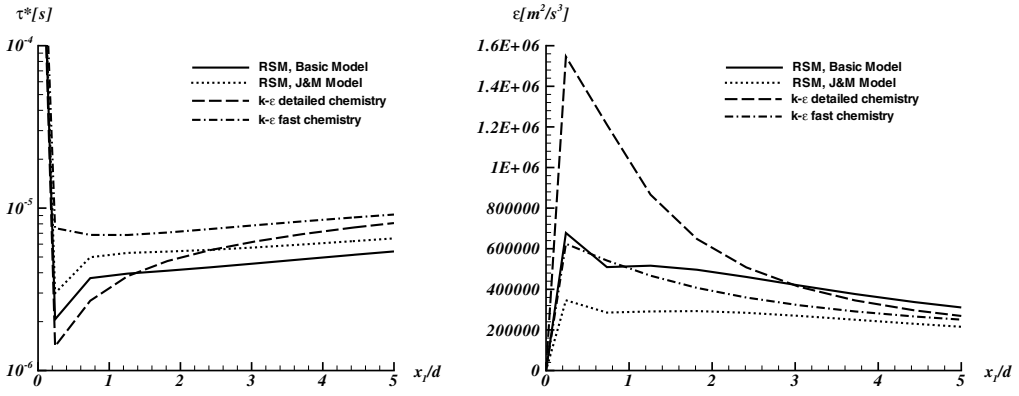

(a) Fine-structure timescale in EDC

(b) Turbulence energy dissipation rate

Figure B.1: Timescale and dissipation rate along $x_2/d = 0.56$

Figure B.1(a) shows the fine-structure time scale τ^* along the line $x_2/d = 0.56$. Here, x_1 and x_2 are the axial and the transverse (radial) coordinates, respectively, and d is the nozzle internal diameter. The corresponding profile of the dissipation rate ε is shown in Fig. B.1(b). The upstream edge of the flame was positioned at this line and close to the nozzle. Figures B.2(a) and B.2(b) show τ^* and ε profiles at $x_1/d = 0.24$.

In these figures, results are shown for two RSE models ("Basic Model" and Jones and Musonge's model) with detailed chemistry and for the k-ε model with fast chemistry and with detailed chemistry. All models were used with the round-jet modifications (*i.e.* $C_{\varepsilon 2} = 1.83$, $\sigma_h = \sigma_Y = 0.5$) when the presented results were obtained. However, the standard versions provided similar differences.

When detailed-chemistry simulations are compared, it is seen that the k-ε model predicts a higher dissipation rate and, correspondingly, a lower timescale than the RSE models. When the timescale of the k-ε model was divided by the factor 0.7 used in the modified reactor mixing rate, the result was close to the timescale from the "Basic" RSE model, and the reaction was not extinguished.

A possible explanation for this difference can be found in the modeling of the turbulence-energy production. The production term of the dissipation-rate equation is proportional to that of the turbulence energy. In a k-ε model, this is proportional to the turbulence viscos-

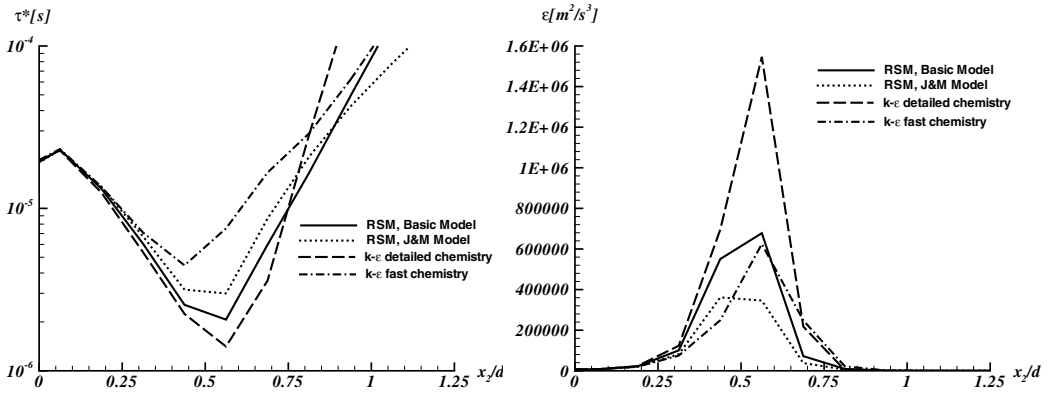

(a) Fine-structure timescale in EDC

(b) Turbulence energy dissipation rate

Figure B.2: Timescale and dissipation rate along $x_1/d = 0.24$

ity, whereas in an RSE model, the production is expressed from the individual Reynolds stresses. Therefore, as the flow close to the nozzle has strong gradients in two directions, an RSE model is expected to give a better representation of the flow than a turbulence-viscosity model.

For the k-ε model, the figures show a considerable larger fine-structure timescale for fast chemistry than for detailed chemistry. An explanation can be deduced from the velocity profiles in Figs. B.3(a) and B.3(b). In the fast-chemistry calculations, the jet expands radially and axially due to intense combustion close to the nozzle. This leads to a smoother profile of the axial velocity. In the detailed-chemistry calculations, the reactions are somewhat delayed, and the expansion is considerably smaller. Then, the sharp gradient of the inlet is less smoothed, and the production of turbulence energy and dissipation is larger. This contributes to the larger τ^* for detailed chemistry compared to fast chemistry shown in Fig. B.1(a).

In a preliminary simulation, the flame was also calculated with the k-ε-model and EDC with chemical kinetics from the Warnatz mechanism (see Ref. [2]). In this case, the reactor mixing rate ($1/\tau^*$) had to be multiplied by a smaller factor than described for the GRI-Mech 2.11 simulations above (typically 0.35, compared to 0.7 above). This indicates that the different mechanisms provide different chemical timescales, and that one mechanism may require a larger reactor timescale for a specific case.

In the simulations presented here, radiation was not included. Further work is carried out on the implementation of a radiation model. As this flame can be approximated as an optically thin flame, a simple model for radiative emission from major species can be applied.

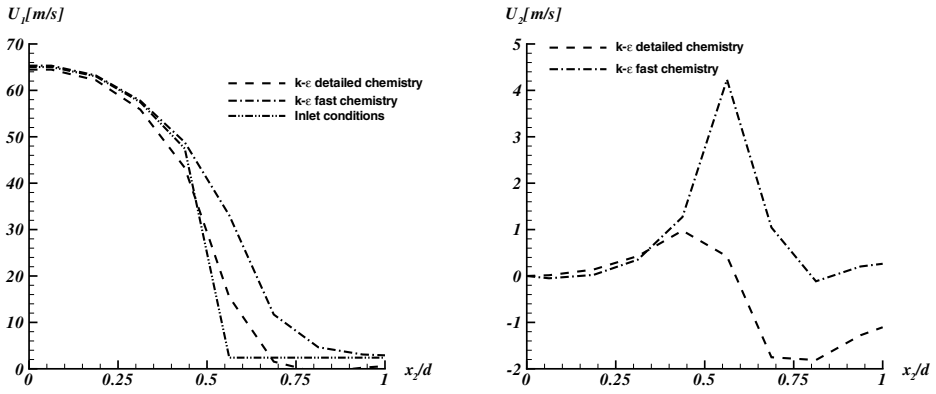

(a) Axial mean velocity

(b) Transverse (radial)mean velocity

Figure B.3: Velocity profiles along $x_1/d = 0.24$

Preliminary calculations were made with a radiation model, a k-ε turbulence model, and detailed chemistry without the mixing-rate modification. This resulted in a stable flame, which was lifted to about $x_1/d = 1.25$. The timescale at the upstream edge of the flame gave a reactor mixing rate ($1/\tau^*$) similar to the modified mixing rate described above (*i.e.* $0.7/\tau^*$) used with the k-ε calculations without radiation.

Further work will also investigate the influence of spatial resolution. As can be seen from the figures, this appears to be coarse relative to the phenomena studied.

Concluding Remarks

It has been observed that different turbulence models provide different fields of the turbulence-energy dissipation rate, and hence different fields of the fine-structure timescale of the Eddy Dissipation Concept for turbulent combustion. When the chemical reactions are close to extinction, this may determine whether extinction is predicted or not.

In the presented predictions with detailed chemistry, the k-ε model gave a lower fine-structure timescale than the Reynolds-stress-equation (RSE) models. In the case of simulations with detailed chemistry and the k-ε model, this lead to blowoff, whereas the RSE models predicted a stable flame. This may be caused by the ability of the latter type of models to represent the turbulent flow close to the nozzle outlet.

Preliminary simulations with another chemical mechanism also indicated that the chemical time scales provided may differ. This may affect the extinction modeling.

URN:NBN:no-7265

Bibliography

[1] Magnussen, Bjørn F. 1989 Modeling of NO_x and soot formation by the Eddy Dissipation Concept. *Int. Flame Research Foundation, 1st Topic Oriented Technical Meeting.* 17-19 Oct., Amsterdam, Holland.

[2] Gran, Inge R., Bjørn F. Magnussen 1996 A numerical study of a bluff-body stabilized diffusion flame. Part 2. Influence of combustion modeling and finite-rate chemistry. *Comb. Sci. Technol. 119:* 191-217.

[3] Lapp, M., M.C. Drake, C.M. Penney, R.W. Pitz, S. Correa 1983 *Turbulent Combustion Experiments and Modeling.* Final Report prepared for Power Systems Division, U.S. Dept. Energy, Washington D.C.

[4] Drake, M.C., R.W. Pitz, S.M. Correa, M. Lapp. 1984 Nitric oxide formation from thermal and fuel-bound nitrogen sources in a turbulent nonpremixed syngas flame. *20th Symp. (Int.) Comb.:* 1983-1990

[5] Weydahl, Torleif, Inge R. Gran, Ivar S. Ertesvåg 2001 Prediction of nitric oxide formation in ammonia-doped turbulent syngas jet flames. *1st Biennal Meeting, Scand.-Nord. Sect. Comb. Inst.*, 18-20 April 2001, Göteborg, Sweden.

[6] Launder, B.E. , D.B. Spalding 1974 The numerical computation of turbulent flows. *Computer Methods in Appl. Mech. and Eng. 3:* 269-289.

[7] Launder, Brian E. 1989b Second-moment closure: present... and future?. *Int. J. Heat and Fluid Flow 10:* 282-300.

[8] Jones, W.P., P. Musonge 1988 Closure of the Reynolds stress and scalar flux equations. *Phys. Fluids 31:* 3589-3604.

URN:NBN:no-7265